Silica-based functional materials: Recognition and detection of viruses

Inauguraldissertation
zur
Erlangung der Würde eines Doktors der Philosophie
vorgelegt der
Philosophisch-Naturwissenschaftlichen Fakultät
der Universität Basel

von

Sabine Sykora

aus

Österreich

Basel, 2019

Genehmigt von der Philosophisch-Naturwissenschaftlichen Fakultät
auf Antrag von
Prof. Dr. Wolfgang Meier
Prof. Dr. Patrick Shahgaldian
Prof. Dr. Uwe Pieles

Basel, den 26.06.2018

Prof. Dr. Martin Spiess
Dekan

Acknowledgements

The work presented here would not have been possible without the support of many people and it is my pleasure to express my gratitude towards them here.

Above all, I would like to thank my supervisor Professor Patrick Shahgaldian for accepting me as a PhD student in his group and for giving me the opportunity to work with him. His logical way of thinking and critical discussion has been of great value for me. I want to thank him for his patience during a long series of failures and the not less long publication processes.

I would like to express my sincere gratitude to my close group members: Rito Correro, Alessandro Cumbo, Carolina Giunta, Mohamed Elridis, Negar Moradi, Mina Moridi, Federica Richina, Vanessa Rullaud and Ludovico Tulli.
They were all great colleagues, who shared their scientific expertise with me and created an enjoyable atmosphere with pleasant conversations in the group. At that point, I want thank Mohamed furthermore for providing the modified fluorescence dyes for my work.
Also outside the lab we enjoyed many different events together, including the weddings in case of Negar and Ludovico. I am grateful for inviting me to their weddings, which were both nice experiences for me.

This thesis could not have been written without the preliminary work of Alessandro Cumbo. On one hand he initially provided the protocol for synthesizing the virus-imprinted particles, the protagonists of this thesis, during his PhD thesis. On the other hand he supported me during my first years with his expertise and good spirit.

Last but not least, I owe my loving thanks to my fiancé and my family who have lost a lot due to my PhD study abroad. Without their continuous encouragement and understanding, it would have been impossible for me to finish this work.

I am grateful for the financial support from the European Union through the ENVIRUS project.

Table of Contents

Abbreviations

AA	Amino acid
Ab	Antibody
Ag	Antigen
AP	Acid phosphatase
APTES	3-aminopropyltriethoxysilane
APTMS	3-aminopropyltrimethoxysilane
bgal	β-galactosidase
BSA	Bovine serum albumine
CA	Citrate
DMAP	4-(dimethylamino)pyridine
EDTA	Ethylenediaminetetraacetic acid
ELISA	Enzyme-linked immunosorbent assay
FDA	Fluorescein-diacetate
FDA-APTES	APTES-conjugated fluorescein-diacetate
FESEM	Field emission scanning electron microscopy
FITC	Fluorescein isothiocyanate
HAV	Hepatitis A virus
HEPES	2-(4-(2-Hydroxyethyl)-1-piperazinyl)-ethansulfonic acid
IEP	Isoelectric point
KM	Michaelis constant
MES	2-(N-morpholino)ethanesulfonic acid
MIPs	Molecularly imprinted polymers
MUB	4-methylumbelliferone
MUG	4-methyl-umbelliferone b-D-galactopyranoside
NIP	Non-imprinted particle
NorV	Norovirus
NorVLP	Norovirus-like particle
ONPG	o-nitrophenyl-β-D-galactopyranoside
PLE	Porcine liver esterase
pNPA	p-nitrophenyl acetate
pNPP	p-nitrophenyl phosphate
QCM	Quartz crystal microbalance
QQ	Quenching quotient
RFU	Relative fluorescence units
RLG	Recognition layer growth
RT	Room temperature
SEB	Staphylococcal enterotoxin B
SEM	Standard error
SNP	Silica nanoparticle
SNPcat	Biocatalytic active silica particles
SPR	Surface plasmon resonance
TBSV	Tomato bushy stunt virus
TEOS	Tetraethoxysilane
TMB	3,3´,5,5´-tetra-methylbenzidine
TMOS	Tetramethoxysilane
TMPS	Trimethoxypropylsilane
TYMV	Turnip yellow mosaic virus
U	Unit of enzymatic activity
VIP	Virus-imprinted particle
VIPco	Control VIP_FDA
VIPest	Esterase-treated VIP_FDA
VIP_F*	Virus-imprinted particle containing Fluorescein
VIP_FDA	Virus-imprinted particle containing Fluorescein diacetate
VLP	Virus like particles
vmax	Velocity at substrate saturation
WHO	World Health Organization

Abstract

Millions of people falling ill annually due to viral infections caused after the consumption of contaminated water or food. The fact that industrialized countries with high hygienic standards are also affected by water- and food-borne viral diseases indicates that the water purification and food control systems that are implemented are not sufficient to combat all viruses or do not cover all transmitting pathways. The advancing globalization and increased exchange of goods has further elevated the risk of contamination. For instance, there was a huge outbreak of norovirus in German schools due to infected strawberries imported from China. Food vehicles that were earlier in contact with contaminated water suppliers transmit most of the Norovirus. Considering this transmission pathway, there is a high interest for such materials or systems that can efficiently bind viruses with high affinity directly from environmental water or from the food vehicle. Besides the removal of the virus from water and food, the detection of viruses during the food preparation or in the water source will help determine the source of contamination, leading to an improvement in safety. For both the removal and detection, binding of the viruses is required. The best known way to bind viruses is using antibodies. However, their application is limited due to their fragility. Therefore, the solution would be to use materials with the binding properties of antibodies based on organically functional groups and the stability of inorganic materials. Such a material can be acquired from the so-called organic-inorganic hybrid materials.

Organic-inorganic hybrid materials are most suitable to provide a system for rapid and specific detection of viral contaminants directly in the environment. They are provided with a surface that has the properties of (bio)-organic molecules for specific binding, while their core substance is inorganic, providing the required stability to resist environmental factors over a long period of time. Among the large number of hybrid materials, silica, with organic functional groups, is one of the few that come closest to having the properties of antibodies in terms of binding. Furthermore, there are a number of ways to modify silica. On the one side, silica can be easily synthesized in different forms. On the other side, silica can be easily equipped with a broad range of compounds, from organic molecules to complete biomolecules. These modifications in silica are possible by controlled building-up of silica at the molecular level. The desired building blocks can be linked like Lego blocks to form various sophisticated and functionalized silica structures. This principle allows us to synthesize multi-functional silica that specifically binds viral contaminants as well as generates a signal that visualizes the binding directly. Such multi-functional silica was prepared in the frame of this work.

By applying different well-known techniques for functionalizing silica, such as molecular imprinting and entrapment, it was demonstrated the preparation of an artificial virus-recognition material with an integrated detection system, allowing the direct visualization of the virus binding. Molecular imprinting is suited to generate artificial recognition surfaces that overtake antibodies in terms of stability. By combining surface imprinting with nanoparticles, the high surface-area-to-volume ratio of nanoparticles provides a high number of recognition sites, also called imprints, for the specific binding of the previously imprinted virus. In the frame of this work,

norovirus-like particles as safe replacement for the human pathogen norovirus were successfully imprinted and thereby, also provided crucial information for further development of silica-based molecular imprinting in general.

To use these imprinted particles for detection as well, they were equipped with two different detection systems that were integrated with the binding site, generating a visible signal accordingly to target concentration.

First, silica particles were equipped with a biocatalytic layer that contained a signal-generating enzyme, which was covered by a recognition layer. It was assumed that covering the biocatalytic layer with the recognition layer would form a connection between the enzymatic activity and the virus binding. This connection was based on the concept that the recognition layer limits the transport of substrate to the enzyme except where the imprints are. As a result of this, occupation of the imprints causes a decrease in the enzymatic activity. This concept was demonstrated using acid phosphatase as the signal-generating enzyme and norovirus-like particles for imprinting. The activity of the biocatalytic layer could be followed via colorimetric assay and depended on the amount of bound norovirus-like particles. This result proves this read-out system over steric inhibition of the substrate uptake, which represents a straightforward detection system for viruses.

The second detection system was based on a fluorescence signal emitted by a dye that was site-specifically integrated in the binding site. The relation between the fluorescence intensity and virus binding was based on the concept that the bound viruses quench the signal of the fluorescent dye, allowing a direct display of the virus binding over the quenching intensity. To enable sufficient quenching, an inactive version of the dye was first integrated and then activated site-selectively, mainly in the imprints. This concept was demonstrated using fluorescein and its inactivated version, fluorescein diacetate, as the signal-generating dye and norovirus-like particles for imprinting. The so-prepared imprinted fluorescent particles showed a fluorescent signal depending on the amount of bound norovirus-like particles. This result proves this read-out system over fluorescent without the addition of external compounds, such as substrate, which represents another straightforward detection system for viruses.

In summary, the application of different tools was demonstrated to prepare multi-functional silica for detection, and which is not limited to silica particles but could be used to functionalize different surfaces for the purpose of detection and in water-purification systems.

1 Overview and scope of thesis

1.1 Background

Water- or food-borne diseases are often associated with bacteria such as salmonella, campylobacter or cholera. However, the advancement in detecting pathogens in water and food revealed that viruses cause an increasing number of these diseases. The recent estimate from the World Health Organization (WHO) has concluded that viruses contribute substantially to the global burden of food-borne diseases. Recognized as priority above all food-borne pathogens are noroviruses (NorV) in industrialized countries and hepatitis A virus (HAV) in developing countries.[1-3]

In the case of both viruses, only a small number of virus particles are required to spread an infection, leading to huge outbreaks due to their easy transfection from person-to-person. However, the primary source of such outbreaks has often been the consumption of contaminated food or water. Outbreaks associated with NorV have been linked to the consumption of contaminated food vehicles[4-6] such as seafood (*e.g.*, oysters[7,8]) and fruits (*e.g.*, raspberries[9] and strawberries).

Most of the NorV-transmitting food vehicles have at some point been in contact with contaminated water supplies. For instance, fruits are contaminated during fruit production, while oysters accumulate NorVs from the sea as they filtrate the water for nutrients and oxygen. Purification treatments after harvest have not been efficient enough to prevent the occurrence of NorV outbreaks. Therefore, the path of NorV from the environment water to the plantations or the sea is one crucial aspect to be considered for an efficient risk management.

Considering this virus transmission through water supplies, there is a high interest to remove or detect virus particles in environmental water for disease prevention. In this context, the ultimate goal is to develop a material or system that specifically binds and differentiates various pathogens, and is inexpensive, quick and simple to use so as to encourage widespread application.

In terms of specificity and sensitivity, biological receptors such as antibodies are very attractive recognition elements. But they are usually high priced, have low stability and are intolerant to environmental conditions. Therefore, they cannot be used at a wider scale or directly in environmental water, limiting the coverage of virus monitoring.

Alternatively, similar binding properties can be obtained with antibody-like synthetic materials such as molecularly imprinted polymers (MIPs). MIPs have been considered as potential alternatives to antibodies for a variety of applications such as purification, separation and sensing. In contrast to their biological counterparts, molecularly imprinted materials comprise high mechanical and chemical stability, ease of preparation and potential re-usability.

Among the different MIPs, silica-based MIPs feature many advantages for building artificial antibodies for protein and virus binding. Silica, as an inorganic material, provides a stable carrier that is known to be highly biocompatible due to its hydrophilic surface. Furthermore, it can be equipped with functional groups, mimicking the binding properties of antibodies.

In 2012, Cumbo and Shahgaldian demonstrated the synthesis of silica particles as artificial material for binding viruses with high affinity and specificity.[10] However, for detecting the virus binding, they still depended on reference methods to find the concentration of non-bound viruses in the solution.

To transduce the binding event to a visible signal, the imprinted silica particles need to be combined with a transduction system. The different approaches to form and modify silica allow us to equip the particles with an intrinsic transduction system that allows one-step detection and does not require the addition of external components. Therefore, such intrinsic transduction systems open up new applications for virus binding materials.

1.2 Main objective of this work

The research work carried out in the frame of this PhD thesis aimed at developing novel detection systems that are constructed at the nanometer scale. These systems were based on virus-imprinting on the surface of silica particles and was demonstrated on plant viruses.[10] The plant virus-imprinted particles showed artificial binding sites that were proven to be highly affine and specific to the template virus.

In this work, silica particles were functionalized with the binding site for virus recognition as well as with two different transduction systems that were directly integrated in the particles. The study focused on the following three aims:

1. Providing a standard protocol for imprinting human pathogen viruses;
2. Building two intrinsic transduction systems;
3. Providing the proof of concept for the correlation between virus quantity and signal change.

The virus detection systems based on artificial binding sites are of particular interest in medical diagnostics for point-of-care diagnostics or mobile detection devices. Therefore, these detection systems should be applicable for human pathogen viruses. To overcome the challenges associated with the utilization of human pathogen viruses, because such viruses cause health hazards, the possibility to replace native viruses with virus-like particles (VLP) that possess the same structure as the original virus but deprived of genetic material was investigated. The model virus in this thesis was the human pathogen, Norovirus, replaced by virus-like particles (VLP). So, the first aim of this research was to adjust the protocol to synthesize virus-imprinted particles based on the properties of the Norovirus-like particle (NorVLP).

At this point, it should be mentioned that due to the lack of standard protocols for imprinting, especially in case of protein imprinting, application of the protocols has been limited to a few molecules that could resist the imprinting conditions. However, our silica-based imprinting protocol uses the interactions of simple functional groups - hydroxyl (OH-) and amine (NH_2-) groups - which are basis of hydrogen bonds that are commonly found in biomolecules. These hydrogen bonds allow binding of any biomolecule, including viruses.

Therefore, the protocol offers high potential to prepare artificial binding sites for a broad variety of viruses.

Another aim of the thesis was to develop nanoparticles with an intrinsic transduction, allowing detection of the virus binding in one step. Detection without any further separation steps is a significant improvement for immunoassays and has been nearly exclusively possible only for biosensors with more complex transduction systems that are not commonly in use. In this work, two different strategies were followed to provide the transduction.

A transduction system converts an invisible process (here, the binding of the virus) into a measureable signal. To achieve this conversion, various methods have been developed. In our transduction systems, the model in principle was the routinely used enzyme-linked immunosorbent assay (ELISA). Its high throughput and easy detection system is based on an enzymatic reaction that generates an optical signal. In other immunoassays similar to ELISA, the enzyme is replaced with a fluorescent dye for improved sensitivity. Accordingly, both transduction systems are based on optical signal-generating components: enzymatic reaction and fluorescent dye, respectively. The respective signal-generating component was integrated into the binding site to obtain a relation between the signal intensity and the virus concentration. The final aim of this work was to demonstrate that the presence of viruses in the imprints induces, directly or indirectly, a change in signal.

The development of these two transduction systems provides new concepts for virus detection and imprinting. It also offers a broader knowledge of the functionalizing of silica at the nanometer scale, improving the attraction of the use of silica.

1.3 References

1 EFSA (2015) Shaping the Future of Food Safety, Together: Proceedings of the 2nd EFSA Scientific Conference. *EFSA Journal* **13**

2 WHO (2015) Estimates of the global burden of foodborne diseases. *WHO - Report*

3 Ahmed, S. M. *et al.* (2014) Global prevalence of norovirus in cases of gastroenteritis: a systematic review and meta-analysis. *The Lancet Infectious Diseases* **14**, 725-730

4 El-Senousy, W. M., Costafreda, M. I., Pinto, R. M. and Bosch A. (2013) Method validation for norovirus detection in naturally contaminated irrigation water and fresh produce. *Int J Food Microbiol* **167**, 74-79

5 EFSA (2015) The European Union summary report on trends and sources of zoonoses, zoonotic agents and food-borne outbreaks in 2014. *EFSA Journal* **13**

6 Verhoef, L. et al. (2015) Norovirus genotype profiles associated with foodborne transmission, 1999-2012. *Emerg Infect Dis* **21**, 592-599

7 Dowell, S. F. *et al.* (1995) A Multistate Outbreak of Oyster-Associated Gastroenteritis: Implications for Interstate Tracing of Contaminated Shellfish. *JID* **171**, 1497-1503

8 Carol Shieh, Y.-S. *et al.* (2000) Detection of Norwalk-like Virus in Shellfish Implicated in Illness. *JID* **181** (Suppl 2), S360-S366

9 Le Guyader, F. S. *et al.* (2004) Detection of noroviruses in raspberries associated with a gastroenteritis outbreak. *Int J Food Microbiol* **97**, 179-186

10 Cumbo, A., Lorber, B., Corvini, P. F., Meier, W. and Shahgaldian, P. (2013) A synthetic nanomaterial for virus recognition produced by surface imprinting. *Nat Commun* **4**, 1503-1509

2 Synthesis of functional materials with silica

2.1 Innovative functional materials

2.1.1 Learning from nature

Living organisms consist of "functional materials" built from small building blocks; for *e.g.*, amino acids forming a functional protein, fatty acids forming a membrane or multiple cells forming an organ or tissue. Likewise organisms synthesize minerals, so-called biominerals, by polymerizing inorganic building blocks with biomolecules. Almost all of these biominerals are composite materials comprised of both mineral and organic components, forming an organic-inorganic hybrid material for a desired function. Biominerals are formed for a variety of functions such as providing mechanical support (*e.g.*, skeleton), protection (*e.g.*, bones, shells), orientation (*e.g.*, otolith) and visual perception (*e.g.*, eye lens).[1]

The formation of biominerals, also called biomineralization, can be described as a bottom-up process in which inorganic building blocks are polymerized under the regulation of an organic matrix including specific biomolecules. The remarkable feature of biomineralization is its exceptional control over the composition, structure, size and morphology, which gives the biomineral its functionality. The functional structures of biominerals are significantly more elaborate than their geological and synthetic counterparts, illustrating the superiority of the biomineralization process over abiotic mineral formation.[2]

For decades, the formation of materials in nature has inspired scientists to study biomineralization processes and to mimic the process to engineer novel functional materials. In 1992, Philip Ball and Laura Garwin proposed that chemists have only to learn the basic mechanisms from nature and combine them with novel creative concepts.[3] This has been implemented, for instance, in the form of so-called bioinspired approaches, which, among others, apply condensation of building blocks as well as self-assembly mechanism involving weak intermolecular forces.[4-13]

2.1.2 Hybrid materials

Inspired by nature, an increasing number of innovative functional materials are created through the association between organic components (i.e.: molecules, polymers) and inorganic components (i.e.: transition metals) at the molecular level. The resulting organic-inorganic hybrid materials comprise properties that arise from the synergistic cooperation between the organic and inorganic components, which has found promising applications in several industrial fields.[14-18]

The organic-inorganic hybrid materials that can be found in the industry are significantly different from biominerals. Biominerals are formed due to the cooperation of biomolecules with minerals such as calcium carbonate, calcium phosphate and silica, while most of the hybrid materials in the industry are made of organic molecules with an amorphous network built up by transition metals (such as Sn, Ti, and Zr) or silicon (Si).

A straightforward method to prepare these networks is the sol-gel process, which is a simple bottom-up approach that yields amorphous networks through polymerization of alkoxides at low temperature. The resulting amorphous network can easily result in a wide variety of complex architectures due to the high density of crosslinks in variable direction.

Depending on the direction of the polymerization, two overall structures[19] can be distinguished:

- Sol: A stable suspension of colloidal particles that are formed through radially orientated polymerization.
- Gel: A porous three-dimensionally interconnected network that expands throughout a solvent due to linearly orientated polymerization.

Among the components used for the preparation of sol-gels, silica has been of particular interest for scientists because it comprises some attractive features required for the generation of hybrid materials. First of all, the formation of silica networks can be easily controlled through synthesis conditions. Second, organic molecules, polymers and biomolecules, as well as whole cells, can be easily incorporated into the silica network. Because of these features, silica-based hybrid materials have found application in various fields, including chemical and biological sensors, separation technology, optical devices, and catalysis. Due to the high biocompatibility of silica, there is also a particular interest in the use of silica in biomedical engineering to integrate the engineered components into the biological environment.

2.2 Silane-based sol-gel chemistry

In this section, the basics about the formation of silane networks and the sol-gel process are described. Some general methods to control the structure of silica are presented as well.

2.2.1 Silica

Silicon (Si) is the second most abundant element on earth. In the form of silicon dioxide or silica (SiO_2), which is the main element of sand and quartz, it is the main component of the earth's crust. Silica is made up of SiO_4 tetrahedral units that form a network through linkages in up to four directions. Amorphous silica is a SiO_2 network with variable Si–O–Si bond angles and Si–O bond distances.[20, 21]

Amorphous silica is also produced through biomineralization by some living organisms, especially when transparency is needed for instance for photosynthesis. The outstanding feature of biosilica is their incredible variety of sophisticated shapes, in which structure and function are optimized at different length scales. The formation of biosilica has been intensely studied in diatoms, which are unicellular algae with a porous silica shell. Their shell exhibits regularly arranged slits or pores in the size range between 10 nm and 1000 nm (Fig. 2.1).[22, 23] The building of diatom silica from silicic acid is promoted by special biomolecules such as silaffins[24-27], long-chain polyamines[28,29] and silacidins[30].

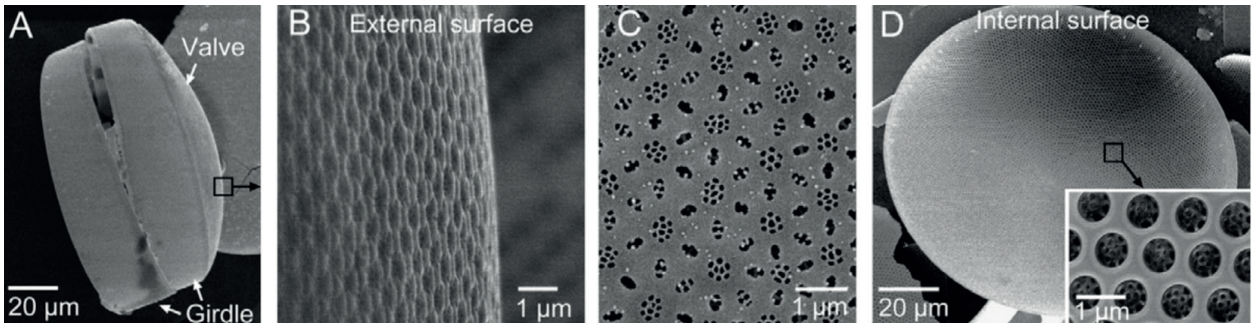

Figure 2.1: Scanning electron microscopy images of the diatom *Coscinodiscus sp.*: A) complete frustule, (B) external surface, (C) sieve pores on external surface and (D) internal surface and pattern of large pores. [Reproduced with permission from ref. 23; Copyright by Elsevier.]

These biomolecules fulfil two crucial functions[9,10] for the silica formation:

1) They induce or accelerate silica precipitation.
2) They participate in pattern formation as structure-directing template.

The function of these biomolecules has been mimicked to generate silica with specific structural and chemical compositions.[31] For instance, a synthetic derivative of a naturally occurring silaffin protein is the silica-precipitating peptide R5. It can rapidly form a network of fused silica nanospheres with a diameter of up to 500 nm.[31,32]

Alternatively, silica can be formed via enzymes such as silicatein[32] from a marine sponge, which are characterized through a high number of cationic amines. Accordingly, silica-formation can be catalysed by a wide range of amine-rich polypeptides such as polyethyleneimine[34] and poly-L-lysine[35-37] as well as amine-rich proteins such as lysozyme[38-40]. For instance, cysteine-lysine block co-polypeptides were showed to self-assemble into structured aggregates that catalysed the formation of silica, while simultaneously directing the building of ordered morphologies.[41]

2.2.2 Condensation of alkoxysilanes

Silicon-based hybrid materials are made from alkoxysilanes such as tetramethoxysilane (TMOS) and tetraethoxysilane (TEOS). In these compounds, the central silicon atom is attached covalently via ester linkages between the silicic acid and the alkoxy-group. These compounds are used as molecular precursors that lead to an amorphous silica via the sol-gel process.

The sol-gel process for silica involves two initial reaction steps (Fig. 2.2). The first step is the hydrolysis of the alkoxy-groups releasing the corresponding alcohol. The resulting hydroxyl-groups then undergo the condensation reactions, linking two SiO_4 tetrahedral units. Continuation of the hydrolysis and condensation reaction with the remaining hydroxyl-groups results in the formation of a silica network.[19]

The shape and properties of the final silica network depend on the reaction conditions applied that affect the rate of the hydrolysis and condensation reaction as well as the position on which the reactions occur.

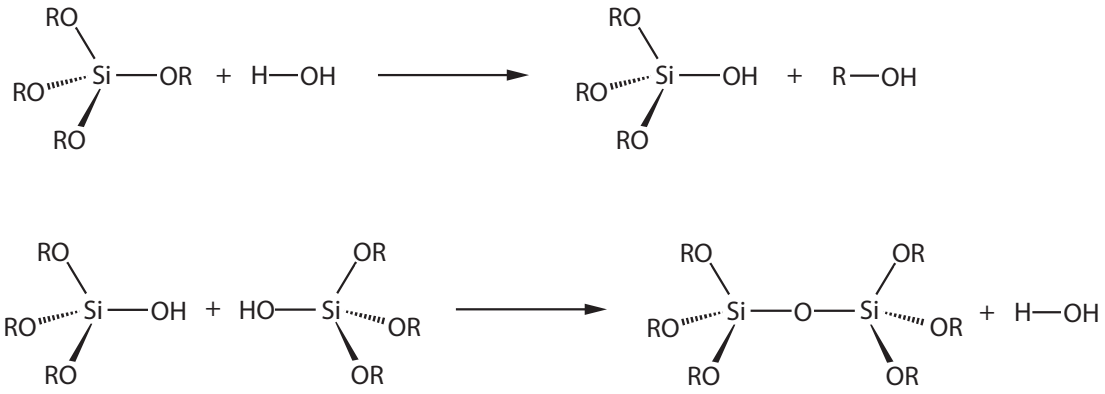

Figure 2.2: Initial reaction steps in siliane condensation based on tetra-alkoxysilane

The hydrolysis of alkoxysilanes requires a catalyst, which can be acidic, basic or nucleophilic.[42] As these catalysts have different mechanisms and reaction rates, the choice of the catalyst is decisive in the structure of the resulting silica. In acid-catalysed processes, the reaction rate decreases as more alkoxy-groups are replaced with hydroxyl groups because the positively charged transition state becomes less stabilized as the hydroxyl groups are less electron donating than the alkoxy-groups. Conversely, for the negatively charged transition state in the basic and nucleophilic-catalyzed reaction, more hydroxyl groups mean more stabilization of the transition state. Therefore, the hydrolysis occurs faster, leading to the successive hydrolyses of all four alkoxy-groups. As a result of the deprotonating rate, acid hydrolysis leads to largely linear structures, while base/nucleophilic hydrolysis leads to branched structures.[42-44]

2.2.3 Formation of structured silica

An important requirement in the fabrication of advanced inorganic materials is control over the condensation direction to give the material its functional shape. Many factors affect the condensation from the molecular level upwards, including concentration and properties of precursors, temperature, pressure, pH, and the presence of ions or other molecules.

For instance, in basic conditions, silanes form cyclic oligomers early in the condensation process. Other silane molecules condensate preferentially with these cyclic oligomers as they have a higher density of dissociated silanol groups. The cyclic oligomers thus become the core in the formation of spherical particles. In salt-free conditions, these particles can continue growing isolated from each other due to their negatively charged surface, repelling other particles forming a sol. If salts or other charge species are added, then the repulsing surface charge is reduced, allowing interconnections among particles to form a dense network.[20]

There are an increasing number of approaches that combine different factors to spatially control silane polycondensation at the nano- and meso-scale. Some of these approaches allow the formation of silica particles with a functional and highly reproducible shape, such as Stöber particles, mesoporous particles or hollow particles as illustrated in Fig. 2.3.[45]

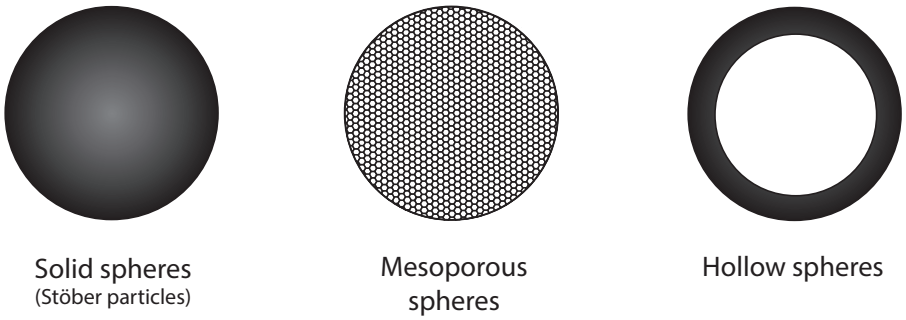

Figure 2.3: Schematic representations of four kinds of spherical silica

The first approach to synthesize highly monodispersed silica nanoparticles was introduced by Stöber *et al.* in 1968. This approach involves the hydrolysis of TEOS in a mixture of alcohol and water using ammonia as a catalyst.[46] Further investigation of this approach led to the preparation of particles with diameters ranging from tens of nanometers to a few microns.[47-50]

A significant breakthrough in the development of sophistically structured silica has been achieved with the emergence of ordered mesoporous silica with uniform pore sizes. The key issue in the synthesis of porous silica is the interaction with a template, which guides the growth of the silica network, as illustrated in Fig. 2.4.[51] The templates are often ordered structures formed through self-assembling, such as block copolymers[52-54], micellar systems made by surfactants[55,56] or amphiphilic peptides[57] as well as biological macromolecules,[58-60] and complex biological systems[61] such as bacteriophages[62]. Alternatively, the use of latex particles as hard templates has also been investigated.[63,64]

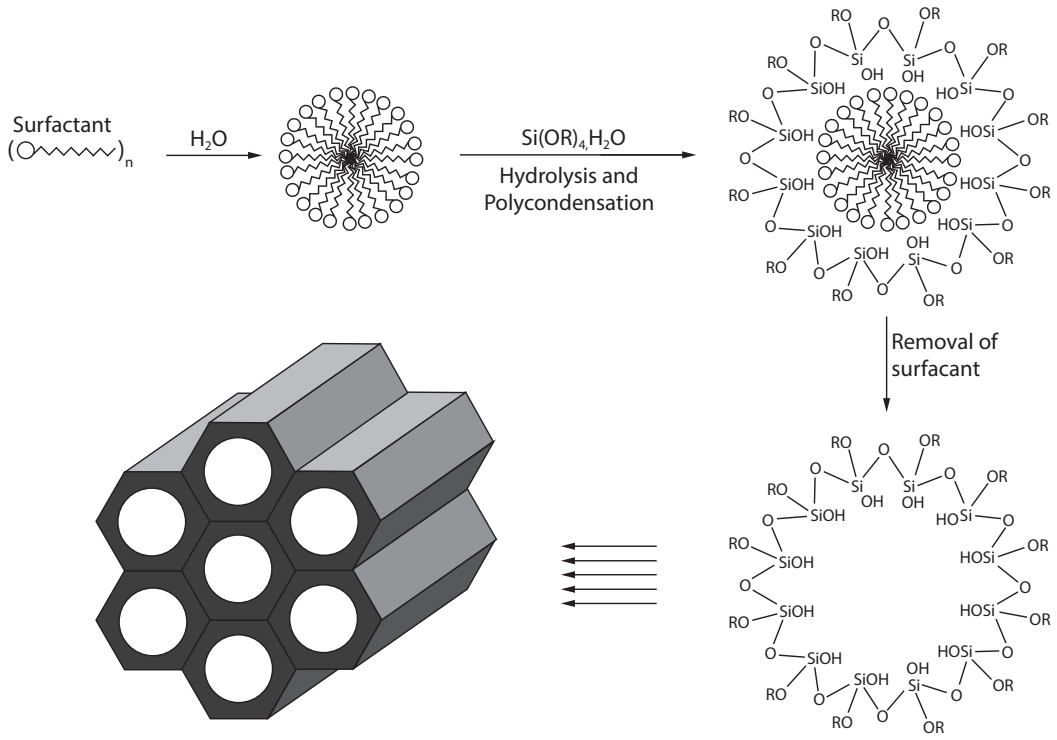

Figure 2.4: Synthesis of mesoporous particles via templating surfactants.

2.3 Functionalization of silica

Pure amorphous silica nanomaterials have limited applications and are therefore hybridized with organically functional groups or components to extend their applications. Moreover, they can be designed with more than one function to accomplish complex tasks.[65-67]

In this section, two different concepts to functionalize silica are given:

1) Integration of a functional component into the silica network.
2) Use of alkoxysilanes with organic functional groups to synthesize the silica network.

The section then provides an overview explaining how this functionalized silica can be used in detection systems to complete this state-of-the-art research work.

2.3.1 Silica with functional components

Silica nanomaterials are often equipped with functional components to provide the resulting material with new properties, such as fluorescence[68-70], magnetism[71], therapeutic ability[72,73] and catalytic function[74-77]. Conversely, the silica matrix provides a chemically and mechanically stable vehicle, which serves as a protective shell around the components. In the form of a shell, silica protects the encapsulated component from external influences, while exposing a biocompatible and chemically modifiable surface. The resulting silica hybrids thus combine the properties and advantages of both silica and the functional component, overcoming some of their individual limitations.[78]

Examples of functional components that have been integrated into silica are fluorescent dyes[68], chemiluminescent molecules[70], quantum dots[69], drug molecules[72], gold nanomaterials[79] and magnetic nanoparticles[71]. Even biomolecules were brought into the silica network, forming biohybrids.[74] The integration of biomolecules as well as fluorescent dyes will be discussed here in more detail due its relevance to the presented work (see also chapter 3).

Biomolecules such as enzymes, antibodies or whole cells have remarkable functions such as selectivity, efficiency, and environment-friendliness that exceed the performances of their artificial counterparts. However, biomolecules suffer from limited lifetime and resistance against environmental stress. Therefore, the entrapment of biomolecules in silica is an attractive option since it improves their operational stability and, in turn, their application. Other advantages of entrapped biomolecules as compared to free ones are the possibility to separate them from the reaction mixture and to co-entrap multi-enzyme systems, enhancing the efficiency of catalysis.[80-84]

Fluorescent dyes are a very important tool in the field of fluorescence microscopy visualization processes in living organisms due to their high sensitivity.[85-93] However, they have limited photostability against continuous light exposure and are affected by the complex environment inside living cells, inducing chemical degradation. In order to create more robust dyes, researchers

have synthesized, among others, nanoparticles from dye molecules and amorphous silica. These nanoparticles contain a large quantity of dye molecules entrapped inside the silica network. They emit an intense fluorescence signal that is up to 10,000 times more intense than that of single fluorescent dyes. Their extreme brightness combined with the improved biocompatibility and stability makes them interesting for ultrasensitive analysis in biological samples.[68,69,94]

In general, there are three different strategies to combine a component with silica:

a) Components are attached either through electrostatic interaction or covalently on the surface and in the pores of the silica particles.

b) Components are integrated into the silica network during the silane condensation.

c) Silica is built up at the surface of a component as outer shell.

Ad a – Example 1: Attachment of biomolecule on silica

The simplest way to prepare biohybrids is to attach the biomolecule through electrostatic interaction or covalently on the surface of silica particles such as Stöber particles, mesoporous particles or hollow particles. Here, it is noteworthy that a high variety of enzymes are already immobilized, in particular, on mesoporous particles. The immobilization of these particles reduces the interaction with the external media, preventing aggregation, proteolysis by proteases, and the contact with hydrophobic interface, such as air bubbles.[95,96] Furthermore, the environment inside the pores protects the entrapped enzymes against harsh pH values and thus broadens the usage of the enzymatic reaction.[97]

To improve this system, different approaches have been intensively studied to increase the capacity and reduce the leakage of the enzyme. In this context, Ortac *et al.* recently published the following approach: They used template-derived hollow particles with mesoporous (5-50nm) openings that allow the passage of the enzyme into the particles. Their system, as a whole, can be interpreted as a "bottle" that is first filled with enzyme before the pores are sealed with a nanoporous (< 2nm) silica layer. The latter allows the passage of only the substrate, but not the enzyme, as illustrated in Fig. 2.5.[64] These hollow particles feature a significantly higher concentration of the enzyme than mesoporous particles.

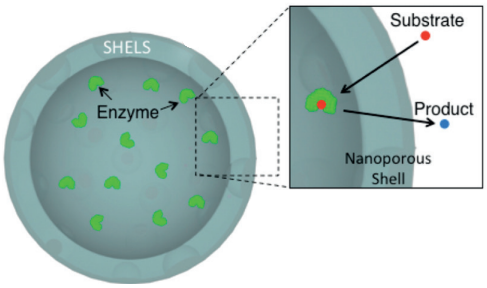

Figure 2.5: Schematic illustration of the enzyme-filled hollow particles, the SHELS: As depicted in the inset showing the scale-up of a section of SHELS, enzymes that were entrapped within the hollow core cannot escape, while the small substrate molecule (red dot) can diffuse through the nanoporous shell, interact with the enzyme and diffuse out of SHELS after modification by the enzyme (blue dot). [Reproduced with permission from ref. 64; further permissions related to the material excerpted should be directed to the ACS.]

Ad b – Example 1: Entrapment of fluorescent dyes

The second strategy to combine a component with silica is to entrap it into the silica network during the silane condensation. Most of the common fluorescent dyes are hydrophobic and are, therefore, soluble in the solvents that are used for the synthesis of silica nanoparticles. To prepare dye-doped silica nanoparticles, two general synthetic routes have been used: the Stöber process and the microemulsion process.

The Stöber process was previously introduced as a method for synthesizing fairly monodisperse silica nanoparticles. It has been further optimized to covalently entrap fluorescent dye molecules to the silica matrix.[49,98] The procedure involves two steps: At first, the dye is chemically attached to an amine-containing silanes (such as 3-aminopropyltriethoxysilane, APTES). Then both TEOS and the dye-modified APTES are allowed to hydrolyse and condensate in a mixture of water, ammonia, and ethanol, resulting in dye-doped silica nanoparticles.

Alternatively, dye-doped silica nanoparticles can also be synthesized by forming silica in a reverse-micelle or water-in-oil (w/o) microemulsion system.[99-101] In a typical w/o microemulsion system, water droplets are stabilized by surfactant molecules and remain dispersed in bulk oil. The formation of silica is highly regulated in the water droplets, while the dye molecules are entrapped in the silica network.[99,102] The entrapment via the w/o microemulsion system is particularly interesting for polar dyes and water-soluble inorganic dyes. These dyes can be entrapped without covalent attachment to silanes because of the strong electrostatic attraction between the dye molecules and the negatively charged silica.

Ad b – Example 2: Entrapment of biomolecules in silica

Similar to the fluorescent dyes, biomolecules can be entrapped into the silica network during the silane condensation. But in contrast to the dyes, the encapsulation of biomolecules requires such conditions for the condensation that do not denature the sensitive biomolecules.

One crucial point in the formation of silica is the release of high amount of alcohol, which can lead to denaturation, and thus, inactivation of the biomolecules. Therefore, in most described encapsulations of biomolecules, the hydrolysis of organosilanes releasing alcohol is separated from the silane condensation in presence of biomolecules. By using this approach, silica encapsulation of different biomolecules can be achieved in various shapes, including monoliths, microparticles and films.[103,104] To obtain thin films for instance, biomolecules are firstly immobilized on a solid material before silane condensation is induced.[104] Thereby, the thickness of the silica can be easily controlled. Such thin layers of biohybrids have been applied particularly in biosensors because the silica film directly forms on the transducer and allows target molecules to diffuse into the binding biomolecule.

Based on this method, the research group of Shahgaldian demonstrated the encapsulation of biomolecules even without separation of hydrolysis and condensation.[105-107] In their approach, biomolecules were firstly immobilized on silica nanoparticles in a buffered solution and silica for-

mation was induced subsequently by mixing TEOS and APTES in the same medium. Because of the stabilizing effect of the immobilization and the dilution of the released alcohol in the buffered solution, the denaturation and inactivation were negligible.

Natural processes such as the silane biomineralization in diatoms give inspiration for new approaches that allow the polymerization at neutral pH and the present of salts. For instance, Luckarift et al. demonstrated the entrapment of butyrylcholinesterase in silica nanoparticles. In their approach, silaffin polypeptide from diatom polymerized TMOS in the presence of the enzyme in the solution, resulting in enzyme-containing silica spheres. The entrapped enzyme retained all of its activity and was substantially more stable than the free enzyme.[32]

The biohybrids that are finally obtained from the silica encapsulation feature nano- or micro-structured oxygen-bridged frameworks in which the biomolecules are physically confined. Till date, studies indicate that proteins with molecular weights above 10,000 (~1.3–1.7 nm ellipsoids) can be irreversibly encapsulated in this framework. Absorbance and fluorescence studies also showed that proteins are entrapped in their native conformations, which is operative and functional within the rigid silica network. The network is like a cage that restricts global movements (*e.g.*, unfolding, rotation), while segmental motions that are required, for instance, for substrate binding and catalysis, are largely unaffected. At the same time, small compounds (*e.g.*, substrates) with molecular weights below 1000 can easily penetrate and transit the silica network through three-dimensional pore connectivity.[81,108-115]

Ad b – Example 3: Silica as outer shell around nanostructures

To complete the overview of the different ways to functionalize silica, the possibility to grow a thin silica layer around other nanostructures also deserves a brief mention.

Different nanostructures, such as quantum dots, magnetic nanoparticles[71] or carbon nanotubes, are covered with silica to increase their biocompatibility and allow their application in medicine. The covering with a silica matrix can also prevent nanoparticles from self-aggregation and from reacting with environmental species. The silica layer also serves as a medium for subsequent functionalization of these nanostructures. Typically, the thin silica layer is post-coated on the surface of the nanostructures using the previously mentioned three methods: hydrolysis of silicate in acidic solutions, the Stöber method, or the reverse microemulsion method.[78,116-121]

2.3.2 Silica with functional groups

Instead of integrating a component, silica can be functionalized through the use of organically modified alkoxysilane (also called organosilanes) as building blocks for the silica formation. In these organosilanes, the organic groups are covalently attached to the silicon atom directly. This Si-R covalent bond does not react in the course of silane condensation, and therefore remains in the final material.

The final silica resulting from the polycondensation of organosilanes is a hybrid material that combines the structural stability of the siloxane bonds and the features of the organic R groups, modifying the properties of the formed silica.

Here the possibility of mimicking the functional properties of enzymes and antibodies (catalysis and binding, respectively) is of particular interest. These functions are achieved by functional groups that are in a specific position to each other and have a specific composition. Binding of a substrate or an antigen is achieved through shape complementarity combined with a high number of non-covalent interactions, such as hydrogen bonding, ionic interactions, π-π interactions, van der Waals forces and hydrophobic effects. These interactions are known to be fairly weak, but synergistically induce high affinity.

The increasing variety of commercially available organosilanes in functional groups makes it possible to impart hydrophobicity, hydrophilicity and even ionic charge to silica. With this broad spectrum of functional groups, silica can be engineered to suit the target molecule. Therefore, these molecules are excellent candidates to build a silica layer with interaction properties similar to that of biomolecules.

To provide silica with high affinity for target-specific recognition, the three-dimensional positioning of the functional groups is generated artificially by using the target itself as template that instructs the construction of the recognition site, as illustrated in Fig. 2.6. This technique is similar to the previously described technique of synthesis of mesoporous silica with uniform pore sizes. The interaction with the template does not influence only the final structure of the silica, but also the position of the functional groups. Thus, the final silica is tailored with structures and functional groups complementary to that of the template molecules for rebinding. Because the template seems to imprint its structural and chemical information into the silica network, this technique is better known as molecular imprinting.[104]

Molecular imprinting is the best-known method to form specific artificial binding sites, with either organic or inorganic polymers as carriers of the imprints/binding sites.[122-124] During the last three decades, there has been immense advancement in synthesis approaches and application of molecular imprinted polymers (MIPs) in various fields.[125]

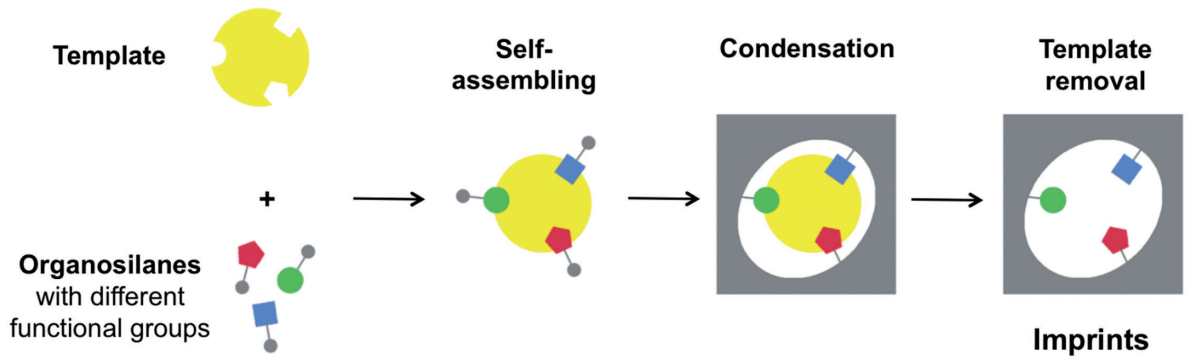

Figure 2.6: Schematic representation of the principle of molecular imprinting

Today, MIPs can be prepared for a wide range of target molecules, including biomolecules such as proteins[126-128], viruses,[105,129-131] microorganisms[132-135] and cells[136]. They find broad applications as separation matrices in chromatography,[137-141] as catalyst mimicking enzymes,[142-145] and as selective binding interface for detection systems[146-152].

Owing to the biocompatibility of silica and its condensation reaction, silica is commonly used for imprinting biomolecules.[153] Because of the large size and thus associated low diffusion of biomolecules, the preferred approach for imprinting of biomolecules is generally surface imprinting. In this approach, the template is immobilized on a surface before silica formation is induced to fabricate thin silicate films that ease the template release and recognition. To increase the finite number of recognition sites, imprinting has often been applied on carriers with a high surface-to-volume ratio area, such as nanostructures and nanoparticles, resulting in the synthesis of nanostructured MIPs.[146,154-158]

For instance, Shiomi et al. prepared haemoglobin-specific silica particles using a surface imprinting approach. They covalently immobilized the template protein (haemoglobin) on porous silica nanoparticles before inducing polycondensation of 3-aminopropyltrimethoxysilane (APTMS) and trimethoxypropylsilane (TMPS). The resulting imprinted particles bound the haemoglobin with high affinity due to the characteristics of the binding sites (imprints).[155]

A similar surface imprinting approach was employed by Cumbo et al., demonstrating the possibility to imprint virus particles as well as to improve the specificity of the binding sites by using up to four different organosilanes, mimicking the function of amino acids.[105]

2.3.3 Functionalized Silica for detection

Different functionalized silica materials have already been used as carriers of the recognition site in detection systems. The recognition site is either a biomolecule entrapped in silica or the imprinted silica surface itself. In both cases, the functionalized silica has been incorporated in different kinds of detection systems, such as immunoassays and sensor systems.

A detection system consists of two crucial parts: the recognition site and the transducer. The recognition site is able to selectively bind a target molecule (analyte) with high affinity in the required analytical concentration range.[159] When a target molecule binds to the recognition site, the resulting physical and chemical changes can be exploited to transform the event into a measurable signal, which is enabled by the transducer, which can be:

a) An external component added to the system;

b) A physical change in the surface;

c) A component integrated as part of the recognition site

Immunoassays with functionalized silica

Immunoassays are one of the broadly used detection systems and are commonly used in routine laboratory due to their high precision and high throughput. In immunoassays, the selective affinity of an antibody for its antigen is used to form an antibody-antigen complex that is detected via signal-generating labelled probes, which are added to the system after binding. Since MIPs possess binding characteristics in terms of affinity and specificity similar to those of antibodies, MIPs have been successfully used as direct replacement for antibodies in immunoassays.[160-166] However, while there are various approaches to detect the antigen-antibody complex, the detection of the imprint-antigen complex is limited to mostly competition assay, requiring a signal-generating labelled target molecule. The supply of labelled targets can be cost-intensive, making MIP-based assays unaffordable.

Sensor systems with functionalized silica

Sensor systems such as chemical sensors or biosensors provide highly sensitive real-time detection with short response times. They are made of a recognition unit that is intimately associated with or integrated within a physicochemical transducer unit. When a target molecule binds to the recognition unit, the resulting physical and chemical changes are converted to an electronic signal for quantification.

In contrast to immunoassays, sensor systems can provide a quick analysis directly in the original place where the analyst is found without the need to transport samples to a laboratory. To achieve this, the recognition unit needs to be resistant to a variety of chemical environments and microbial spoilage. In case of biosensors, the recognition unit is based on biological receptors (such as antibodies and enzymes) to obtain the required specificity and selectivity. The required resistance for sensors have been obtained through either stabilizing the receptor or replacing the biological receptor with artificial ones.

Among methods for stabilizing biological receptors, the entrapment of these receptors in silica provides a number of advantages such as long-term storage stability, potential re-usability and resistance to microbial spoilage. The resulting silica-based biohybrids have found application in biosensors.[167-170] However, small target molecules that can easily diffuse through the silica network to the recognition unit have mainly limited the application of this type of biosensor, for instance, to drug discovery.[171-173]

Alternatively, biosensors are equipped with molecularly imprinted receptor, rather than a biomolecule. MIPs are of particular interest for sensors since they combine selective recognition and high robustness.[174] Among the several examples of using MIP-based sensors, different approaches that provide a surface-imprinted silica films on transducer surfaces have also been reported.[175-177] Most of these approaches depend on specific chemical functionalities of the target molecule for signal transduction. These transduction techniques include: electro-chemical, fluorescence quenching, IR and Raman spectroscopy.

For instance, Lulka et al. used surface-imprinted silica for the detection of fluorescein. Addition of quencher to the sample solution suggests that the MIP-bound fluorescein was protected from the quencher allowing quantification based on the quenching intensity.[178]

In case of target molecules without any electro-active moiety, light-absorbing metal complex, or an intrinsic fluorescence - which is the case in most proteins - optical and acoustic sensors have been developed. These methods essentially measure changes in the refractive index (*e.g.*, surface plasmon resonance, SPR) or changes in the mass of the sensing layer (*e.g.*, quartz crystal microbalance, QCM). For instance, Liu et al. prepared a QCM sensor for detecting staphylococcal enterotoxin B (SEB) based on molecularly imprinted silica film. They first prepared the silica film by mixing the organosilanes with the target bacteria SEB and then coated the film on the sensor surface. Their results, in terms of sensitivity and selectivity, showed that the combination of MIP and QCM was very effective for the determination of SEB.[179]

Multifunctional nanoparticles for analytical applications

Multifunctional nanoparticles have shown promising applications for detection, catalysis, separation and purification. Most of these applications take advantage of synergistic effects induced by the combination of functional components and the amplification effect associated with the nanoscale dimension.[180] For instance, the high surface-to-volume ratio values of nanoparticles increase the available surface for releasing and binding processes. Combining nanostructured support with molecular imprinting design improves the release of the template as well as the binding of the analyte.[181]

Moreover, multifunctional particles can be designed for one-step detection systems to provide recognition/binding, amplification and transduction without separation in between. The transducer is often directly integrated in the nanoparticles, and features magnetic, optical or electrochemical properties for generating a signal.

Since silica is optically transparent, silica-based imprinted nanoparticles are suitable for selective optical detection based on fluorescence[178,182], phosphorescence[183] and luminescence[184]. For instance, Yang et al. reported the imprinting of a protein, namely, bovine serum albumin (BSA), on the surface of quantum dots through polycondensation of silica in the presence of BSA. When BSA bound in the imprints, the signal of the quantum dots was quenched. The degree of quenching correlated with the number of BSA that had bounded.[185]

Role of silica in novel detection system

The detection of pathogens (viruses, microorganism) and specific proteins as biomarkers of disease or health status using sensors is still an on-going challenge. Especially, when facing viruses, there are hardly any methods available to directly detect the binding event. This is partly due the widespread opinion that imprinting of proteins or viruses poses several challenges (*e.g.*, template stability and availability).

A crucial objective for the development of MIP-based detection systems is to overcome the actual perceived limitations:

a) Absence of a general procedure for MIP preparation;

b) Difficulties in integrating them with a transducer;

c) Difficulties in transforming the binding event into a measurable signal.

Despite its potential in terms of protein imprinting, the number of silica-based MIPs used as receptors is still low compared with other artificial receptors in the field. Only in the recent years has the academic world started to give increased attention to the use of silica-based receptors, but still without considering the broad range of its structures and chemical properties. As form and function of silica can be easily controlled upon reaction conditions and templates, silica-based receptors can overcome the described limitations and to be prepared with internal transduction system for innovative assays as well as purification systems.

2.4 References

1 Lowenstam, H. A. (1981) Minerals formed by oganisms. *Science* **211**, 1126-1136

2 Perry, C. C. and Keeling-Tucker, T. (2000) Biosilicification: the role of the organic matrix in structure control. *J Biol Inorg Chem* **5**, 537-550

3 Ball, P. and Garwin, L. (1992) Science at the atomic scale. *Nature* **355**, 761-766

4 Roach, P., Eglin, D., Rohde, K. and Perry, C. C. (2007) Modern biomaterials: a review - bulk properties and implications of surface modifications. *J Mater Sci Mater Med* **18**, 1263-1277

5 Rai, A. and Perry, C. C. (2010) Facile fabrication of uniform silica films with tunable physical properties using silicatein protein from sponges. *Langmuir* **26**, 4152-4159

6 Colfen, H. and Mann, S. (2003) Higher-order organization by mesoscale self-assembly and transformation of hybrid nanostructures. *Angew Chem Int Ed Engl* **42**, 2350-2365

7 Nudelman, F. and Sommerdijk, N. A. (2012) Biomineralization as an inspiration for materials chemistry. *Angew Chem Int Ed Engl* **51**, 6582-6596

8 Sanchez, C., Arribart, H. and Guille, M. M. G. (2005) Biomimetism and bioinspiration as tools for the design of innovative materials and systems. *Nature Materials* **4**, 277-288

9 Sanchez, C. et al. (2001) Designed Hybrid Organic–Inorganic Nanocomposites from Functional Nanobuilding Blocks. *Chem Mater* **13**, 3061-3083

10 Sanchez, T., Chen, D. T., DeCamp, S. J., Heymann, M. and Dogic, Z. (2012) Spontaneous motion in hierarchically assembled active matter. *Nature* **491**, 431-434

11 Sanchez, C., Soler-Illia, G. J. D. A. A., Ribot, F. and Grosso, D. (2003) Design of functional nano-structured materials through the use of controlled hybrid organic–inorganic interfaces. *Comptes Rendus Chimie* **6**, 1131-1151

12 Nicole, L., Rozes, L. and Sanchez, C. (2010) Integrative approaches to hybrid multifunctional materials: from multidisciplinary research to applied technologies. *Adv Mater* **22**, 3208-3214

13 Sanchez, C. *et al.* (2014) Molecular Engineering of Functional Inorganic and Hybrid Materials. *Chem Mater* **26**, 221-238

14 Sanchez, C., Julián, B., Belleville, P. and Popall, M. (2005) Applications of hybrid organic–inorganic nanocomposites. *J Mater Chem* **15**, 3559-3592

15 Laberty-Robert, C., Valle, K., Pereira, F. and Sanchez, C. (2011) Design and properties of functional hybrid organic-inorganic membranes for fuel cells. Chem Soc Rev 40, 961-1005

16 Sanchez, C., Lebeau, B., Chaput, F. and Boilot, J. P. (2003) Optical Properties of Functional Hybrid Organic–Inorganic Nanocomposites. *Adv Mater* **15**, 1969-1994

17 Clement Sanchez, Philippe Belleville, Popalld, M. and Nicoleab, a. L. (2011) Applications of advanced hybrid organic–inorganic nanomaterials: from laboratory to market. *Chem Soc Rev* **40**, 696-753

18 Sanchez, C. and Lebeau, B. (2011) Design and Properties of Hybrid Organic–Inorganic Nanocomposites for Photonics. *MRS Bull* **26**, 377-387

19 Hench, L. L. and West, J. K. (1990) The Sol-Gel Process. *Chem. Rev.* **90**, 33-72

20 Belton, D. J., Deschaume, O. and Perry, C. C. (2012) An overview of the fundamentals of the chemistry of silica with relevance to biosilicification and technological advances. *FEBS J* **279**, 1710-1720

21 Zachariasen, W. H. (1932) The atomic arrangement in Glass. J. Am. Chem. Soc. 54, 11, 3841-3851

22 Parkinson, J. and Gordon, R. (1999) Beyond micromachining: the potential of diatoms. *Trends Biotechnol* **17**, 190-196

23 Wang, Y., Pan, J., Cai, J. and Zhang, D. (2012) Floating assembly of diatom Coscinodiscus sp. microshells. *Biochemical and Biophysical Research Communications* **420**, 1-5

24 Kröger, N., Deutzmann, R. and Sumper, M. (1999) Polycationic Peptides from Diatom Biosilica That Direct Silica Nanosphere Formation. *Science* **286**, 1129-1132

25 Kröger, N., Lorenz, S., Brunner, E. and Sumper, M. (2002) Self-Assembly of Highly Phosphorylated Silaffins and Their Function in Biosilica Morphogenesis. *Science* **298**, 584-586

26 Sumper, M., Hett, R., Lehmann, G. and Wenzl, S. (2007) A code for lysine modifications of a silica biomineralizing silaffin protein. *Angew Chem Int Ed Engl* **46**, 8405-8408

27 Poulsen, N., Sumper, M. and Kröger, N. (2003) Biosilica formation in diatoms: characterization of native silaffin-2 and its role in silica morphogenesis. *PNAS* **100**, 12075-12080

28 Kröger, N., Deutzmann, R., Bergsdorf, C. and Sumper, M. (2000) Species-specific polyamines from diatoms control silica morphology. *PNAS* **97**, 14133-14138

29 Sumper, M., Brunner, E. and Lehmann, G. (2005) Biomineralization in diatoms: characterization of novel polyamines associated with silica. *FEBS Lett* **579**, 3765-3769

30 Wenzl, S., Hett, R., Richthammer, P. and Sumper, M. (2008) Silacidins: highly acidic phosphopeptides from diatom shells assist in silica precipitation in vitro. *Angew Chem Int Ed Engl* **47**, 1729-1732

31 Betancor, L. and Luckarift, H. R. (2008) Bioinspired enzyme encapsulation for biocatalysis. *Trends Biotechnol* **26**, 566-572

32 Luckarift, H. R., Spain, J. C., Naik, R. R. and Stone, M. O. (2004) Enzyme immobilization in a biomimetic silica support. *Nature biotechnology* **22**, 211-213

33 Jin, R. H. and Yuan, J. J. (2005) Synthesis of poly(ethyleneimine)s-silica hybrid particles with complex shapes and hierarchical structures. *Chem Commun*, 1399-1401

34 Gautier, C., Lopez, P. J., Livage, J. and Coradin, T. (2007) Influence of poly-L-lysine on the biomimetic growth of silica tubes in confined media. *J Colloid Interface Sci* **309**, 44-48

35 Hawkins, K. M., Wang, S. S.-S., Ford, D. M. and Shantz, D. F. (2004) Poly-L-Lysine Templated Silicas: Using Polypeptide Secondary Structure to Control Oxide Pore Architectures. *J AM CHEM SOC* **126**, 9112-9119

36 Patwardhan, S. V., Maheshwari, R., Mukherjee, N., Kiick, K. L. and Clarson, S. J. (2006) Conformation and Assembly of Polypeptide Scaffolds in Templating the Synthesis of Silica: An Example of a Polylysine Macromolecular “Switch”. *Biomacromolecules* **7**, 491-497

37 Roth, K. M., Zhou, Y., Yang, W. and Morse, D. E. (2005) Bifunctional Small Molecules Are Biomimetic Catalysts for Silica Synthesis at Neutral pH. *J AM CHEM SOC* **127**, 325-330

38 Luckarift, H. R., Dickerson, M. B., Sandhage, K. H. and Spain, J. C. (2006) Rapid, room-temperature synthesis of antibacterial bionanocomposites of lysozyme with amorphous silica or titania. *Small* **2**, 640-643

39 Coradin, T., Coupé, A. and Livage, J. (2003) Interactions of bovine serum albumin and lysozyme with sodium silicate solutions. *Colloids and Surfaces B: Biointerfaces* **29**, 189-196

40 Shiomi, T., Tsunoda, T., Kawai, A., Mizukami, F. and Sakaguchi, K. (2007) Biomimetic Synthesis of Lysozyme-Silica Hybrid Hollow Particles Using Sonochemical Treatment: Influence of pH and Lysozyme Concentration on Morphology. *Chem Mater* **19**, 4486-4493

41 Cha, J. N., Stucky G. D., Morse, D. E. and Deming T. J. (2000) Biomimetic synthesis of ordered silica structures mediated by block copolypeptides. *Nature* **403**, 289-292

42 Corriu, R. J. P. and Leclercq, D. (1996) Recent Developments of Molecular Chemistry for Sol - Gel Processes. *Angew. Chem. Int. Ed. Engl.* **35**, 1420-1436

43 Corriu, R. J. P., Guerin, C., Henner, B. J. L. and Wang, Q. (1991) Role of Pentacoordinate Intermediates in the Hydrolysis Reaction of Organic Silicates. *Organometallics* **10**, 3200-3205

44 Hench, L. L. (1998) *Sol-Gel Silica: Properties, Processing and Technology Transfer.* Elsevier

45 Duab, X. and He, J. (2011) Spherical silica micro/nanomaterials with hierarchical structures: Synthesis and applications. *Nanoscale* **3**, 3984-4002

46 Stöber, W. and Fink, A. (1968) Controlles Growth of Monodisperse Silica Spheres in the Micron Size Range. *Journal of Colloid and Interface Science* **26**, 62-69

47 Wang, X. D. *et al.* (2010) Preparation of spherical silica particles by Stober process with high concentration of tetra-ethyl-orthosilicate. *J Colloid Interface Sci* **341**, 23-29

48 Bogush, G. H., Tracy, M. A. and Zukoski, C. F. (1988) Preparation of monodisperse silica particles: Control of size and mass fraction. *Journal of Non-Crystalline Solids* **104**, 95-106

49 Blaaderen, A. V., Geest, J. V. and Vrij, A. (1992) Monodisperse Colloidal Silica Spheres from Tetraalkoxysilanes: Particle Formation and Growth Mechanism. *Journal of Colloid and Interface Science* **154**, 481-501

50 Zhang, J. H., Zhan, P., Wang, Z. L., Zhang, W. Y. and Ming, N. B. (2003) Preparation of monodisperse silica particles with controllable size and shape. *J Mater Res* **18**, 649-653

51 van Bommel, K. J. C., Friggeri, A. and Shinkai, S. (2003) Organic Templates for the Generation of Inorganic Materials. *Angew Chem Int Ed* **42**, 980-999

52 Fujita, N., Asai, M., Yamashita, T. and Shinkai, S. (2004) Sol–gel transcription of silica-based hybrid nanostructures using poly(N-vinylpyrrolidone)-coated [60]fullerene, single-walled carbon nanotube and block copolymer templates. *J Mater Chem* **14**, 2106-2114

53 Hsueh, H. Y., Yao, C. T. and Ho, R. M. (2015) Well-ordered nanohybrids and nanoporous materials from gyroid block copolymer templates. *Chem Soc Rev* **44**, 1974-2018

54 Soler-Illia, G. J. d. A. A., Crepaldi, E. L., Grosso, D. and Sanchez, C. (2003) Block copolymer-templated mesoporous oxides. *Current Opinion in Colloid & Interface Science 8*, 109-126

55 Wan, Y. and Zhao, D. (2006) On the Controllable Soft-Templating Approach to Mesoporous Silicates. *Chem Rev* **107**, 2821-2069

56 Fang, X., Zhao, X., Fang, W., Chen, C. and Zheng, N. (2013) Self-templating synthesis of hollow mesoporous silica and their applications in catalysis and drug delivery. *Nanoscale* **5**, 2205-2218

57 Wang, S., Cai, Q., Du, M., Xue, J. and Xu, H. (2015) Synthesis of 1D Silica Nanostructures with Controllable Sizes Based on Short Anionic Peptide Self-Assembly. *J Phys Chem B* **119**, 12059-12065

58 Chen, C. L. and Rosi, N. L. (2010) Peptide-based methods for the preparation of nanostructured inorganic materials. *Angew Chem Int Ed Engl* **49**, 1924-1942

59 Liu, B., Cao, Y., Huang, Z., Duan, Y. and Che, S. (2015) Silica biomineralization via the self-assembly of helical biomolecules. *Adv Mater* **27**, 479-497

60 Hassan, N., Soltero, A., Pozzo, D., Messina, P. V. and Ruso, J. M. (2012) Bioinspired templates for the synthesis of silica nanostructures. *Soft Matter* **8**, 9553-9562

61 Lagziel-Simis, S., Cohen-Hadar, N., Moscovich-Dagan, H., Wine, Y. and Freeman, A. (2006) Protein-mediated nanoscale biotemplating. *Curr Opin Biotechnol* **17**, 569-573

62 Mao, C., Wang, F. and Cao, B. (2012) Controlling nanostructures of mesoporous silica fibers by supramolecular assembly of genetically modifiable bacteriophages. *Angew Chem Int Ed Engl* **51**, 6411-6415

63 Iskandar, F., Mikrajuddin and Okuyama, K. (2001) In Situ Production of Spherical Silica Particles Containing Self-Organized Mesopores. *Nano Letters* **1**, 231-234

64 Ortac, I. *et al.* (2014) Dual-porosity hollow nanoparticles for the immunoprotection and delivery of nonhuman enzymes. *Nano Lett* **14**, 3023-3032

65 Melde, B. J., Johnson, B. J. and Charles, P. T. (2008) Mesoporous Silicate Materials in Sensing. *Sensors (Basel)* **8**, 5202-5228

66 Coll, C., Bernardos, A., Martinez-Manez, R. and Sancenon, F. (2013) Gated Silica Mesoporous Supports for Controlled Release and Signaling Applications. *Acc Chem Res* **46**, 339–349

67 Tarn, D. et al. (2013) Mesoporous Silica Nanoparticle Nanocarriers: Biofunctionality and Biocompatibility. *Accounts of Chemical Research* **46**, 792-801

68 Burns, A., Ow, H. and Wiesner, U. (2006) Fluorescent core-shell silica nanoparticles: towards „Lab on a Particle“ architectures for nanobiotechnology. *Chem Soc Rev* **35**, 1028-1042

69 Wang, L. et al. (2006) Glow in the biological world. *Anal Chem* **1**, 647-654

70 Yao, G. et al. (2006) FloDots: luminescent nanoparticles. *Analytical and bioanalytical chemistry* **385**, 518-524

71 Lee, J. et al. (2008) Simple synthesis of functionalized superparamagnetic magnetite/silica core/shell nanoparticles and their application as magnetically separable high-performance biocatalysts. *Small* **4**, 143-152

72 Mamaeva, V., Sahlgren, C. and Linden, M. (2013) Mesoporous silica nanoparticles in medicine-recent advances. *Adv Drug Deliv Rev* **65**, 689-702

73 Trewyn, B. G., Slowing, I. I., Giri, S., Chen, H.-T. and Lin, V. S.-Y. (2007) Synthesis and Functionalization of a Mesoporous Silica Nanoparticle Based on the Sol–Gel Process and Applications in Controlled Release. *Acc Chem Res* **40**, 846–853

74 Avnir, D., Coradin, T., Lev, O. and Livage, J. (2006) Recent bio-applications of sol–gel materials. *J Mater Chem* **16**, 1013-1030

75 Shilpa, N., Manna, J. and Rana, R. K. (2015) Bioinspired Nanoparticle-Assembly Route to a Hybrid Scaffold: Designing a Robust Heterogeneous Catalyst for Asymmetric Dihydroxylation of Olefins. *European Journal of Inorganic Chemistry* **2015**, 4965-4970

76 Ciriminna, R. et al. (2015) SiliaCat: A Versatile Catalyst Series for Synthetic Organic Chemistry. *Organic Process Research & Development* **19**, 755-768

77 Margelefsky, E. L., Zeidan, R. K. and Davis, M. E. (2008) Cooperative catalysis by silica-supported organic functional groups. *Chem Soc Rev* **37**, 1118-1126

78 Jin, Y. et al. (2009) Amorphous silica nanohybrids: Synthesis, properties and applications. *Coordination Chemistry Reviews* **253**, 2998-3014,

79 Xu, J. and Perry, C. C. (2007) A novel approach to Au@SiO2 core-shell spheres. *Journal of Non-Crystalline Solids* **353**, 1212-1215

80 Frančič, N., Lyagin, I. V., Efremenko, E. N. and Lobnik, A. (2015) Hybrid sol–gel bio-films: influence of synthetic parameters on behaviour and performance of entrapped His6-tagged organophosphorus hydrolase. *Journal of Sol-Gel Science and Technology* **74**, 387-397

81 Gill, I. and Ballesteros, A. (2000) Bioencapsulation within synthetic polymers (Part 1): sol–gel encapsulated biologicals. *TIBTECH* **18**, 282-296

82 Kim, J., Grate, J. W. and Wang, P. (2008) Nanobiocatalysis and its potential applications. *Trends Biotechnol* **26**, 639-646

83 Ansari, S. A. and Husain, Q. (2012) Potential applications of enzymes immobilized on/in nano materials: A review. *Biotechnol Adv* **30**, 512-523

84 Meunier, C. F., Dandoy, P. and Su, B. L. (2010) Encapsulation of cells within silica matrixes: Towards a new advance in the conception of living hybrid materials. *J Colloid Interface Sci* **342**, 211-224

85 Lakowicz, J. R. (2006) *Principles of Fluorescence Spectroscopy, 3rd edition*. 3 edn, Springer US

86 Aylott, J. W. (2003) Optical nanosensors - an enabling technology for intracellular measurements. *The Analyst* **128**, 309-312

87 Zimmermann, T., Rietdorf, J. and Pepperkok, R. (2003).Spectral imaging and its applications in live cell microscopy. *FEBS Letters* **546**, 87-92

88 Zhang, J., Campbell, R. E., Ting, A. Y. and Tsien, R. Y. (2002) Creating new fluorescent probes for cell biology. *Nat Rev Mol Cell Biol* **3**, 906-918

89 Lippincott-Schwartz, J., Snapp, E. and Kenworthy, A. (2001).Studying protein dynamics in living cells. *Nature Reviews* **2**, 444-456

90 Kerppola, T. K. (2006) Design and Implementation of Bimolecular Fluorescence Complementation (BiFC) Assays for the Visualization of Protein Interactions in Living Cells. *Nat Protoc* **1**, 1278–1286

91 Kerppola, T. K. (2009) Visualization of molecular interactions using bimolecular fluorescence complementation analysis: characteristics of protein fragment complementation. *Chem Soc Rev* **38**, 2876-2886

92 Liu, J., Wen, J., Zhang, Z., Liu, H. and Sun, Y. (2015) Voyage inside the cell: Microsystems and nanoengineering for intracellular measurement and manipulation. *Microsystems & Nanoengineering* **1**, 15020-15034

93 Giepmans, B. N. G., Adams, S. R., Ellisman, M. H. and Tsien, R. Y. (2006) The Fluorescent Toolbox for Assessing Protein Location and Function. *Science* **312**, 217-224

94 Wolfbeis, O. S. (2015) An overview of nanoparticles commonly used in fluorescent bioimaging. *Chem Soc Rev* **44**, 4743-4768

95 Carlsson, N. et al. (2014) Enzymes immobilized in mesoporous silica: a physical-chemical perspective. *Adv Colloid Interface Sci* **205**, 339-360

96 Mateo, C., Palomo, J. M., Fernandez-Lorente, G., Guisan, J. M. and Fernandez-Lafuente, R. (2007) Improvement of enzyme activity, stability and selectivity via immobilization techniques. *Enzyme and Microbial Technology* **40**, 1451-1463

97 Avnir, D. and Frenkel-Mullerad, H. (2005) Sol-Gel Materials as Efficient Enzyme Protectors: Preserving the Activity of Phosphatases under Extreme pH Conditions. *J Am Chem Soc* **127**, 8077-8081

98 Verhaegh, N. A. M. and Blaaderen, A. v. (1994) Dispersions of Rhodamine-Labeled Silica Spheres: Synthesis, Characterization, and Fluorescence Confocal Scanning Laser Microscopy. *Langmuir* **10**, 1427-1438

99 Arriagada, F. J. and Osseo-Asare, K. (1999) Synthesis of Nanosize Silica in a Nonionic Water-in-Oil Microemulsion: Effects of the Water/Surfactant Molar Ratio and Ammonia Concentration. *J Colloid Interface Sci* **211**, 210–220

100 Soenen, S. J., Manshian, B., Doak, S. H., De Smedt, S. C. and Braeckmans, K. (2013) Fluorescent non-porous silica nanoparticles for long-term cell monitoring: cytotoxicity and particle functionality. *Acta Biomater* **9**, 9183-9193

101 Zhao, X., Bagwe, R. P. and Tan, W. (2004) Development of Organic-Dye-Doped Silica Nanoparticles in a Reverse Microemulsion. *Advanced Materials* **16**, 173-176

102 Gustafsson, H., Isaksson, S., Altskar, A. and Holmberg, K. (2016) Mesoporous silica nanoparticles with controllable morphology prepared from oil-in-water emulsions. *J Colloid Interface Sci* **467**, 253-260

103 Venton, D. L. and Gudipati, E. (1995) Entrapment of enzymes using organo-functionalized polysiloxane copolymers. *Biochimica et Biophysica Acta* **1250**, 117-125

104 Glad, M., Norrlow, O., B., S., Siegbahn, N. and Mosbach, K. (1985) Use of silane monombers for molecular imprinting and enzyme entrapment in polysiloxane-coated porous silica. *Journal of Chromatography* **347**, 11-23

105 Cumbo, A., Lorber, B., Corvini, P. F., Meier, W. and Shahgaldian, P. (2013) A synthetic nanomaterial for virus recognition produced by surface imprinting. *Nat Commun* **4**, 1503-1509

106 Correro, M. R., Takacs, M., Sykora, S., Corvini, P. F. and Shahgaldian, P. (2016) Supramolecular enzyme engineering in complex nanometer-thin biomimetic organosilica layers. *RSC Advances* **6**, 89966-89971

107 Correro, M. R. et al. (2016) Enzyme Shielding in an Enzyme-thin and Soft Organosilica Layer. *Angew Chem Int Ed* **55**, 6285-6289

108 Livage, J., Coradin, T. and Roux, C. Encapsulation of biomolecules in silica gels. *J. Phys.: Condens. Matter* **13**, R673–R691 (2001).

109 Husing, N., Reisler, E. and Zink, J. I. (1999) Allosteric Regulation of Enzymatic Reactions in a Transparent Inorganic Sol-Gel Material. *J Sol-gel Sci Technol* **15**, 57-61

110 Gottfried, D. S., Kagan, A., BHoffman, B. M. & M., F. J. Impeded Rotation of a Protein in a Sol-Gel Matrix. *J. Phys. Chem. B* **103**, 2803-2807 (1999).

111 Dave, B. et al. (1995) Synthesis of Protin-Doped Sol-Gel SiO2 Thin Films: Evidence for Rotational Mobility of Encapsulated Cytochrome c. *Chem. Mater.* **7**, 1431-1434

112 Brennan, J. D. Using Intrinsic Fluorescence to Investigate Proteins Entrapped in Sol-Gel Derived Materials. *Appl Spectrosc* **53**, 106A-121A (1999).

113 Shtelzer, S., Rappoport, S., Avnir, D., Ottolenghi, M. and Braun, S. (1992) Properties of trypsin and of acid phosphatase immobilized in sol-gel glass matrices. Biotechnol. *Appl. Biochem.* **15**, 227-235

114 Bhatia, R. B., Brinker, C. J., Gupta, A. K. and Singh, A. K. (2000) Aqueous Sol-Gel Process for Protein Encapsulation. *Chem Mater* **12**, 2434-2441

115 Edmiston, P. L., Wambolt, C. L., Smith, M. and Saavedra, S. S. (1994) Spectroscopic Characterization of Albmin and Myoglobin Entrapped in Bulk Sol-Gel Glasses. *Journal of Colloid and Interface Science* **163**, 395-406

116 Yang, Y. H., Tu, C. F. and Gao, M. Y. (2007) A general approach for encapsulating aqueous colloidal particles into polymeric microbeads. J*ournal of Materials Chemistry* **17**, 2930-2935

117 Liu, S. H. and Han, M. Y. (2005) Synthesis, functionalization, and bioconjugation of monodisperse, silica-coated gold nanoparticles: Robust bioprobes. *Adv Funct Mater* **15**, 961-967

118 Liu, S. and Han, M. Y. (2010) Silica-coated metal nanoparticles. *Chemistry, an Asian journal* **5**, 36-45

119 Huang, L. et al. (2014) A brilliant sandwich type fluorescent nanostructure incorporating a compact quantum dot layer and versatile silica substrates. *Chem Commun* **50**, 2896-2899

120 Yang, P., Ando, M. and Murase, N. (2011) Highly Luminescent CdSe/CdxZn1-xS Quantum Dots Coated with Thickness-Controlled SiO2 Shell through Silanization. *Langmuir* **27**, 9535-9540

121 Ma, Q., Serranoa, I. C. and Palomares, E. (2011) Multiplexed color encoded silica nanospheres prepared by stepwise encapsulating quantum dot/SiO2 multilayers. *Chem Commun* **47**, 7071-7073

122 Haupt, K. (2002) Creating a good impression. *Nat Biotech* **20**, 884-885

123 Whitcombe, M. J., Alexander, C. and Vulfson, E. N. (2000) Imprinted Polymers: Versatile New Tools in Synthesis. *Synlett* **6**, 911–923

124 Sellergren, B. (2000) Imprinted Polymers with Memory for Small Molecules, Proteins, or Crystals. *Angew Chem Int Ed* **39**, 1031-1037

125 Zaidi, S. A. (2017) Molecular imprinting polymers and their composites: a promising material for diverse applications. *Biomater Sci* **5**, 388-402

126 Yang, K., Zhang, L., Liang, Z. and Zhang, Y. (2012) Protein-imprinted materials: rational design, application and challenges. *Analytical and bioanalytical chemistry* **403**, 2173-2183

127 Li, S., Cao, S., Whitcombe, M. J. and Piletsky, S. A. (2014).Size matters: Challenges in imprinting macromolecules. *Progress in Polymer Science* **39**, 145-163

128 Verheyen, E. et al. (2011) Challenges for the effective molecular imprinting of proteins. *Biomaterials* **32**, 3008-3020

129 Liang, C. et al. (2016) A virus-MIPs fluorescent sensor based on FRET for highly sensitive detection of JEV. *Talanta* **160**, 360-366

130 He, K. et al. (2016) Highly selective recognition and fluorescent detection of JEV via virus-imprinted magnetic silicon microspheres. *Sensors and Actuators B: Chemical* **233**, 607-614

131 Jenik, M. et al. (2009) Sensing Picornaviruses Using Molecular Imprinting Techniques on a Quartz Crystal Microbalance. *Anal Chem* **81**, 5320-5326

132 Aherne, A., Alexander, C., Payne, M. J., Perez, N. & Vulfson, E. N. (1996) Bacteria-Mediated Lithography of Polymer Surfaces. *J Am Chem Soc* **118**, 8771-8772

133 Findeisen, A. et al. (2012) Artificial receptor layers for detecting chemical and biological agent mimics. *Sensors and Actuators B: Chemical* **170**, 196-200

134 Chagas-Junior, A. D. *et al.* (2012 Detection and quantification of Leptospira interrogans in hamster and rat kidney samples: immunofluorescent imprints versus real-time PCR. *PLoS One* **7**, e32712

135 Zhang, Z., Li, M., Ren, J. and Qu, X. (2015) Cell-imprinted antimicrobial bionanomaterials with tolerable toxic side effects. *Small* **11**, 1258-1264

136 Seifner, A., Lieberzeit, P., Jungbauer, C. and Dickert, F. L. (2009) Synthetic receptors for selectively detecting erythrocyte ABO subgroups. *Anal Chim Acta* **651**, 215-219

137 Hennion, M.-C. (1999) Solid-phase extraction: method development, sorbents, and coupling with liquid chromatography. *Journal of Chromatography A* **856**, 3-54

138 Kempe, M. and Mosbach, K. (1995) Molecular imprinting used for chiral separations. *Journal of Chromatography A* **694**, 3-13

139 Turiel, E. and Martin-Esteban, A. (2010) Molecularly imprinted polymers for sample preparation: a review. *Anal Chim Acta* **668**, 87-99

140 Nilsson, J., Spegel, P. and Nilsson, S. (2004) Molecularly imprinted polymer formats for capillary electrochromatography. *J Chromatogr B Analyt Technol Biomed Life Sci* **804**, 3-12

141 Martín-Esteban, A. (2013) Molecularly-imprinted polymers as a versatile, highly selective tool in sample preparation. *TrAC Trends in Analytical Chemistry* **45**, 169-181

142 Davis, M. E. and Katz, A. (2000) Molecular imprinting of bulk, microporous silica. *Nature* **403**, 286–289

143 Davis, M. E., Katz, A. and Ahmad, W. R. (1996) Rational Catalyst Design via Imprinted Nanostructured Materials. *Chem Mater* **8**, 1820-1839

144 Adima, A., Moreau, J. J. E. & Wong Chi Man, M. (1997 Chiral organic–inorganic solids as enantioselective catalytic materials. *J Mater Chem B* **7**, 2331-2333

145 Heilmann, J. and Maier, W. F. (1994) Selective Catalysis on Silicon Dioxide with Substrate-Specific Cavities. *Angew Chem Int Ed Engl* **33**, 471-473

146 Wackerlig, J. and Lieberzeit, P. A. (2015) Molecularly imprinted polymer nanoparticles in chemical sensing – Synthesis, characterisation and application. *Sensors and Actuators B: Chemical* **207**, 144-157

147 Menger, M. et al. (2016) MIPs and Aptamers for Recognition of Proteins in Biomimetic Sensing. *Biosensors (Basel)* **6**, 35-53

148 Uzun, L. and Turner, A. P. (2016) Molecularly-imprinted polymer sensors: realising their potential. *Biosens Bioelectron* **76**, 131-144

149 Ashley, J. et al. (2017) Molecularly imprinted polymers for sample preparation and biosensing in food analysis: Progress and perspectives. *Biosens Bioelectron* **91**, 606-615

150 Emir Diltemiz, S., Kecili, R., Ersoz, A. and Say, R. (2017) Molecular Imprinting Technology in Quartz Crystal Microbalance (QCM) Sensors. *Sensors (Basel)* **17**, 454-489

151 Malik, A. A., Nantasenamat, C. and Piacham, T. (2017) Molecularly imprinted polymer for human viral pathogen detection. *Mater Sci Eng C Mater Biol Appl* **77**, 1341-1348

152 Dabrowski, M., Lach, P., Cieplak, M. and Kutner, W. (2017).Nanostructured molecularly imprinted polymers for protein chemosensing. *Biosens Bioelectron* **102**, 17-26

153 Diaz-Garcia, M. E. and Lainio, R. B. (2004) Molecular Imprinting in Sol-Gel Materials: Recent Developments and Applications. *Microchimica Acta* **149**, 19-36

154 Fu, G. et al. (2011) Enhanced lysozyme imprinting over nanoparticles functionalized with carboxyl groups for noncovalent template sorption. *Anal Chem* **83**, 1431-1436

155 Shiomi, T., Matsui, M., Mizukami, F. and Sakaguchi, K. (2005) A method for the molecular imprinting of hemoglobin on silica surfaces using silanes. *Biomaterials* **26**, 5564-5571
156 Li, F., Li, J. and Zhang, S. (2008).Molecularly imprinted polymer grafted on polysaccharide microsphere surface by the sol-gel process for protein recognition. *Talanta* **74**, 1247-1255
157 Kan, X. et al. (2010) Preparation and Recognition Properties of Bovine Hemoglobin Magnetic Molecularly Imprinted Polymers. *J Phys Chem B* **114**, 3999–4004
158 He, C., Long, Y., Pan, J., Li, K. & Liu, F. (2008) Molecularly imprinted silica prepared with immiscible ionic liquid as solvent and porogen for selective recognition of testosterone. *Talanta* **74**, 1126-1131
159 Harvey, D. (2008) The Vocabulary of Analytical Chemistry in *Analytical Chemistry 2.0*, **41**
160 Caceres, C. et al. (2016) Does size matter? Study of performance of pseudo-ELISAs based on molecularly imprinted polymer nanoparticles prepared for analytes of different sizes. *Analyst* **141**, 1405-1412
161 Yonamine, Y., Hoshino, Y. and Shea, K. J. (2012) ELISA-mimic screen for synthetic polymer nanoparticles with high affinity to target proteins. *Biomacromolecules* **13**, 2952-2957
162 Shutov, R. V. et al. (2014) Introducing MINA--The Molecularly Imprinted Nanoparticle Assay. *Small* **10**, 1086-1089
163 Piletsky, S. A. et al. (2000) Chemical grafting of molecularly imprinted homopolymers to the surface of microplates. Application of artificial adrenergic receptor in enzyme-linked assay for beta-agonists determination. *Anal Chem* **72**, 4381-4385
164 Piletsky, S. A. et al. (2001) Substitution of antibodies and receptors with molecularly imprinted polymers in enzyme-linked and fluorescent assays. *Biosensors & Bioelectronics* **16**, 701-708
165 Chianella, I. et al. (2013) Direct replacement of antibodies with molecularly imprinted polymer nanoparticles in ELISA--development of a novel assay for vancomycin. *Anal Chem* **85**, 8462-8468
166 Bedwell, T. S. and Whitcombe, M. J. (2016) Analytical applications of MIPs in diagnostic assays: future perspectives. *Analytical and bioanalytical chemistry* **408**, 1735-1751
167 Pastor, I., Esquembre, R., Micol, V., Mallavia, R. and Mateo, C. R. (2004) A ready-to-use fluorimetric biosensor for superoxide radical using superoxide dismutase and peroxidase immobilized in sol-gel glasses. *Anal Biochem* **334**, 335-343
168 Salinas-Castillo, A., Pastor, I., Mallavia, R. and Mateo, C. R. (2008) Immobilization of a trienzymatic system in a sol-gel matrix: a new fluorescent biosensor for xanthine. *Biosens Bioelectron* **24**, 1059-1062
169 Pastor, I., Salinas-Castillo, A., Esquembre, R., Mallavia, R. and Mateo, C. R. (2010) Multienzymatic system immobilization in sol-gel slides: fluorescent superoxide biosensors development. *Biosens Bioelectron* **25**, 1526-1529
170 Gupta, R. and Chaudhury, N. K. (2007) Entrapment of biomolecules in sol-gel matrix for applications in biosensors: problems and future prospects. *Biosens Bioelectron* **22**, 2387-2399
171 Lebert, J. M., Forsberg, E. M. and Brennan, J. D. (2008) Solid-phase assays for small molecule screening using sol-gel entrapped proteins. *Biochem Cell Biol* **86**, 100-110
172 Forsberg, E. M., Sicard, C. and Brennan, J. D. (2014) Solid-phase biological assays for drug discovery. *Annu Rev Anal Chem (Palo Alto Calif)* **7**, 337-359
173 Besanger, T. R. et al. (2003) Screening of Inhibitors Using Enzymes Entrapped in Sol-Gel-Derived Materials. *Anal. Chem.* **75**, 2382-2391
174 Whitcombe, M. J. et al. (2011) The rational development of molecularly imprinted polymer-based sensors for protein detection. *Chem Soc Rev* **40**, 1547-1571
175 Makote, R. and Collinson, M. M. (1998) Template Recognition in Inorganic-Organic Hybrid Films Prepared by the Sol-Gel Process. *Chem Mater* **10**, 2440-2445
176 Zhang, Z., Long, Y., Nie, L. and Yao, S. (2006) Molecularly imprinted thin film self-assembled on piezoelectric quartz crystal surface by the sol-gel process for protein recognition. *Biosens Bioelectron* **21**, 1244-1251
177 Marx, S., Zaltsman, A., Turyan, I. and Mandler, D. Parathion (2004) Sensor Based on Molecularly Imprinted Sol-Gel Films. *Anal Chem* **76**, 120-126
178 Lulka, M. F., Chambers, J. P., Valdes, E. R., Thompson, R. G. and Valdes, J. J. (1997) Molecular Imprinting of Small Molecules with Organic Silanes: Fluorescence Detection. *Analytical Letters* **30**, 2301-2313
179 Liu, N., Zhao, Z., Chen, Y. and Gao, Z. (2012).Rapid Detection of Staphylococcal Enterotoxin B by Two-Dimensional Molecularly Imprinted Film-Coated Quartz Crystal Microbalance. *Analytical Letters* **45**, 283-295

180 de Dios, A. S. and Diaz-Garcia, M. E. (2010) Multifunctional nanoparticles: analytical prospects. *Anal Chim Acta* **666**, 1-22

181 Mustafa, F., Hassan, R. Y. A. and Andreescu, S. (2017) Multifunctional Nanotechnology-Enabled Sensors for Rapid Capture and Detection of Pathogens. *Sensors (Basel)* **17**, 2121-2165

182 Graham, A. L., Carlson, C. A. and Edmiston, P. L. (2002) Development and Characterization of Molecularly Imprinted Sol-Gel Materials for the Selective Detection of DDT. *Anal. Chem.* **74**, 458-467

183 Fernandez-Gonzalez, A., Badia Laino, R., Diaz-Garcia, M. E., Guardia, L. and Viale, A. (2004) Assessment of molecularly imprinted sol-gel materials for selective room temperature phosphorescence recognition of nafcillin. *J Chromatogr B Analyt Technol Biomed Life Sci* **804**, 247-254

184 Leung, M. K. P., Chow, C.-F. and Lam, M. H. W. (2001) A sol–gel derived molecular imprinted luminescent PET sensing material for 2,4-dichlorophenoxyacetic acid. *Journal of Materials Chemistry* **11**, 2985-2991

185 Yang, Y. Q., He, X. W., Wang, Y. Z., Li, W. Y. and Zhang, Y. K. (2014).Epitope imprinted polymer coating CdTe quantum dots for specific recognition and direct fluorescent quantification of the target protein bovine serum albumin. *Biosens Bioelectron* **54**, 266-272

3 Strategies and Approaches

3.1 Template virus

Besides the high relevance of NorV as a priority pathogen causing water- and food-borne diseases, NorV feature a very simple structure – smooth, icosahedral without envelope. Its structure can be easily constructed in the form of recombinant proteins assembling to virus-like particles (VLP). For a better understanding of what VLPs are, it helps to look at the composition of viruses.

Viruses are vehicles of the size of 15 to 400 nm and consist of two or three parts[1]:

a) The genetic material made from either DNA or RNA, coding the information for replication and structural proteins;

b) A protein coat, called the capsid surrounding the genetic material;

c) In some cases, an envelope of lipids surrounding the capsid outside a cell.

The capsid proteins can be produced via heterologous expression systems separately from the genetic information for replication. The resulting proteins self-assemble into a sophisticated icosahedron, the VLP, which feature an identical or highly related overall structure as their corresponding native virus.[1-3] Since genetic information for the viral replication is not present in them, the VLPs are non-infectious. Because of their structural similarity, VLPs are of particular interest as replacements for the native viruses in cases where only structural or surface properties are required, such as vaccination.[4] Beyond that, VLPs can also replace the native virus for research studies. As cultivation in cell culture has not been possible for human pathogen Noroviruses, they were replaced by VLPs for studies on their structural integrity.[5]

VLPs have been shown to be excellent vaccine antigens because they have an array of antigenic epitopes on their surface, mimicking the surface of native viruses. This property is even more important for the synthesis of artificial antibodies via molecular imprinting. Up to half of the whole virus sphere (in case of icosahedral viruses) is required for generating a recognition site with high specificity and affinity. Because of their high structural similarity and non-pathogenicity, VLPs are tested out as replacement of the native virus for virus imprinting.

In this work, the template virus for the imprinting process was a VLP of norovirus (NorVLP) from predominant genotype II strain 4 (GII.4). The NorVLP consists of an icosahedral capsid that is 30 to 40 nm in diameter and built from 180 copies of protein subunits, with a mass of 59 kDa.

3.2 Silica Nanoparticles as carriers

Monodisperse silica nanoparticles (SNPs) were used as carrier material to design virus-imprinted particles (VIPs) with different transduction systems. They were freshly produced on the basis of the method developed by Stöber; the detailed protocol is described in the experimental section (see 6.2.1).

The surface of the SNPs consists of silanol groups with which organosilanes condensate, forming new silica. The silane condensation at the surface of SNPs improves the control in the direction and rate of silica formation to generate advanced silica structures such as imprints. In the frame of this work, SNPs were modified at the surface with different biomolecules and were subsequently reacted with organosilanes to prepare different functionalized silica particles.

The bare SNPs and functionalized particles were characterized using high-resolution field emission scanning electron microscopy (FESEM). This technique allowed, on the one side, the visualization of the changes on the surface and, on the other side, it helped determine the size of the particles (Fig. 3.1). The statistical analysis of FESEM micrographs using a size analysis software revealed the mean diameter of the particles. At least 100 particles were measured to determine the mean diameter and its standard error (SEM), demonstrating the precision of the size measurements. Using SNPs with high monodispersity allowed accurate monitoring of the formation of silica through the increase in particle size.

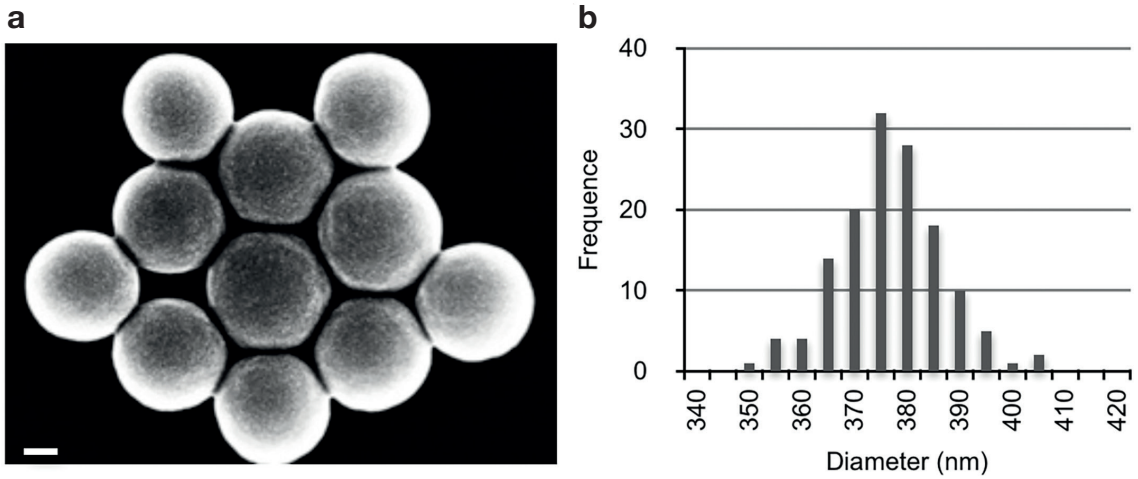

Figure 3.1: Characterization of silica nanoparticles via FESEM –
a) Micrograph, scale bar: 100 nm; b) Distribution of particle diameter.

In the frame of this work, SNPs of different mean diameters were used: 375 nm, 410 nm and 290 nm. The latter were used in particular for the synthesis of multi-layered particles.

3.3 Virus-imprinted particles – Concept

The formation of virus recognition sites on SNPs is illustrated in Fig. 3.2 and consists the following phases:

1. Immobilization of the template virus on the surface of SNP;
2. Surface-initiated growth of a silica layer, named the recognition layer;
3. Removal of the template virus, thus freeing the imprints;

The resulting particles are named “virus-imprinted particles”, in short VIPs.[6,7]

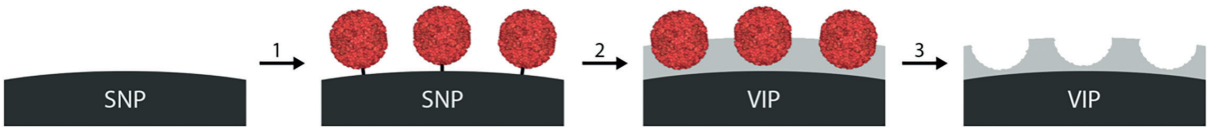

Figure 3.2: Schematic illustration of virus imprinting

I- Immobilization of template virus

The initial step for the VIP synthesis is the immobilization of the template virus on the surface of SNPs through a covalent crosslinking between SNP and template virus. For the crosslinking, SNPs are first modified with aminopropyltriethoxysilane (APTES) and then with glutaraldehyde, which is a homo-bifunctional crosslinker frequently used for immobilization of proteins on amino-activated supports.[3-6] The crosslinking occurs via the two aldehyde groups of glutaraldehyde: one reacts with amino functional groups at the surface of the SNPs that are provided through the modification with APTES; the second aldehyde group reacts with primary amino groups of proteins (such as lysine and N-terminus). Aldehydes and primary amines react by forming an imine bond or Schiff bases, which are interesting for the imprinting because they are unstable under acidic conditions and, thus, reversible. Thus, the virus is first immobilized covalently on silica and removed later by applying acidic conditions.

II- Formation of the recognition layer

After the immobilization of the template virus, the next step consists of the formation of the recognition layer by using the organosilanes TEOS and APTES as building blocks (Fig. 3.3). TEOS with its four hydrolysable ester bonds can form four siloxane (-Si-O-Si-) bonds that provide structural stability to the recognition layer. In APTES, one Si-OH group is substituted with an aminopropyl group that is directly linked with the silicon atom. As this linkage cannot be hydrolysed, one side of APTES cannot participate in the silica network; APTES thus introduces flexibility into the layer as well as other functional groups to interact with the template virus.

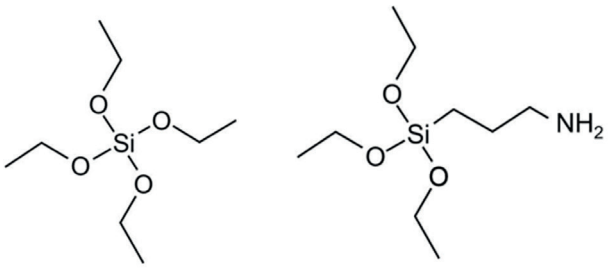

Figure 3.3: Organosilanes in use as building blocks for virus imprinting

Both organosilanes can establish non-covalent bonds with the virus surface before polycondensation of the organosilanes; because of such bonds, the resulting imprints in the recognition layer are chemically adjusted on the template virus for re-binding.[7]

The organosilanes polycondensate through formation of siloxane bonds by following the same mechanism as described previously for the formation of Stöber particles or other silica-based materials (see section 2.2.2). The bond formation depends on the pH as well as on the ionic strength of the reaction solution and requires a catalyst. During imprinting, APTES catalyses the formation of the silica because its amino group reacts basically in water.

The polycondensation starts at the surface of the SNPs due to the presence of silanol groups, continuing the silica network; the recognition layer grows upward. Consequently, the progress of the silica formation during imprinting is later called recognition layer growth (RLG).

III - Virus removal

The virus removal conditions include:

- Ultrasonication to break the silica layer that has formed around each virus.
- Acidic condition (< pH 2) to induce the acid-catalysed hydrolysis of the imine bond anchoring the viruses and, thus, weakening the covalent bond between the virus and SNPs.
- Surfactant (0.1% triton X-100) to favour the disassembly of the virus.

These conditions allow virus removal without altering the recognition layer. When the imprinting is successful, the final, purified particles show the imprints as free cavities on their surfaces via the FESEM.

3.4 Transduction systems for the VIPs

Approach 1: Biocatalytic VIPs

Enzymes are widely used in bioanalytical methods as signal amplification systems owing to their ability to catalyse coloured reactions with fast biocatalytic turnover rates. For instance, in a conventional enzyme-linked immunosorbent assay (ELISA), specific antibodies capture the target molecule, forming a complex that is immobilized on the surface of a microtiter plate. This antibody-target complex is subsequently visualized through an antibody-linked enzyme. The latter generates a signal through the enzymatic conversion of a substrate into a coloured molecule. The conversion rate is proportional to the number of antibody-target complex formed, indicating the concentration of the target molecule.

For the development of a novel transduction system, we considered the following features:

a) The significant size difference between an icosahedral virus (≈ 10000 kDa) and an enzyme molecule (10-100 kDa);

b) The dependency of the enzymatic reaction on substrate uptake;

c) The control of the substrate uptake by the thickness of the silica layer around the enzyme;

The basis of this novel transduction mechanism is the combination of the two different methods to functionalize silica – entrapment and imprinting. The two functionally different silica layers were prepared subsequently – a virus-imprinted layer on top of an enzyme-entrapping layer – forming a biocatalytic VIP. The assumed property of this VIP was that a virus-binding event on the imprints directly modulates the enzymatic activity through steric inhibition of the substrate diffusion to the entrapped enzyme, as illustrated in Fig. 3.4.

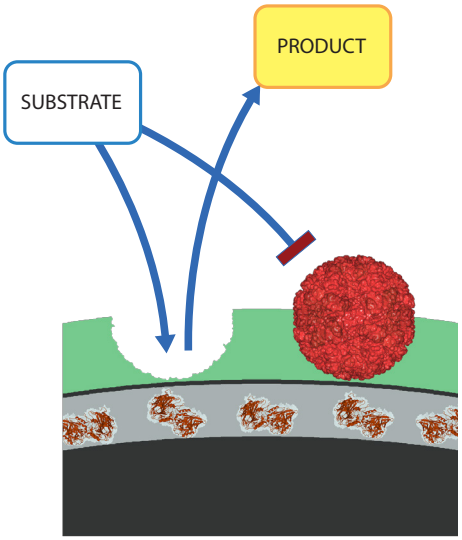

Figure 3.4: Transduction of virus binding to optical signal via biocatalytic VIP

This silica-based transduction system for detection is based on the following assumptions:

i. the selected enzyme preserves its biocatalytic function when entrapped in the silica layer;
ii. The recognition layer hampers substrate uptake by the enzyme, except at open imprints;
iii. Blocking the imprints by binding the target virus decreases the enzymatic activity;

In the frame of this work, all these assumptions were evaluated for proof of concept.

Approach 2: Fluorescent VIPs

Fluorescence dyes/probes, thanks to their high intensity, have been extensively used as optical signals to report specific molecular processes.[8] Indeed, some fundamental processes in living organisms have been investigated using fluorescence microscopy.[9-16] Besides, they have allowed to observe the binding processes taking place in sensor devices as binding modulates the signal of fluorescence dyes.[17-22] Particularly, in combination with small spectrophotometric devices, the modulation of fluorescence signal is a promising transduction system as it does not require further reagents to transduce the binding processes into a visible signal for quantification.[23,24]

However, it is still a challenge to achieve a connection between the fluorescence dye and the specific recognition site of the target molecule that modulates the fluorescence signal.

This connection has been investigated for artificial antibodies/receptors based on molecular imprinting. By forming the receptor artificially, a fluorescence dye can be directly integrated into the recognition site during the imprinting process. Due to the small distance between the target molecule and dye at the recognition site, the subsequent binding of the target molecule affects the properties of the fluorescence dye, for instance, through quenching.[24-26]

One method to integrate a fluorescence dye into the imprints is to modify the dye with the cross-linking part of the monomers and directly integrate it as a monomer into the polymer. This system has already been described in a few publications that demonstrated the quenching-based detection of different template molecules - from small molecules[26-32] up to biomolecules[33-35].

The drawback of this seemingly easy system is the high intensive background signal that reduces the sensitivity of the detection. Since interactions between the template molecule and commonly used fluorescence dyes are quite low, dye molecules are distributed in the whole polymer during imprinting. Consequently, dye molecules are partially integrated in parts of the polymer, where they cannot be affected by the binding of the target molecule. These dyes induce high background fluorescence-inducing, low-quenching intensities.[25]

The background signal becomes more crucial in case of the virus-imprinting in use. The target molecule is far bigger than the molecules that form the recognition site. This size difference between target molecule and monomer indicate that only a small number of the added monomers are really part of the recognition site; most molecules are part of the non-imprinted silica layer that holds the imprints.

To deal with the problem of high background signal, an innovative strategy was developed for doping the recognition site with dye molecules. This strategy involved the integration of a temporary/reversible quenched fluorescence dye, which was activated after the removal of the NorVLP exceptional on the recognition site. By particularly using fluorescence dyes in the imprints, NorVLP-binding was visualized via the quenching of the fluorescence intensity by the presence of the NorVLP, as illustrated in Fig. 3.5.

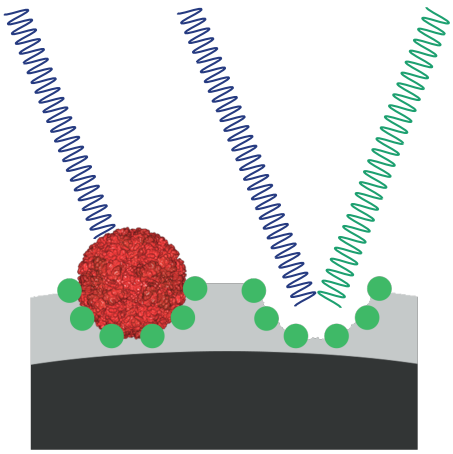

Figure 3.5: Transduction of virus binding to optical signal via fluorescence VIP: fluorophores are excited by radiation (blue waves) and emit light (green waves); in case of NorVLP binding, the emission is quenched by NorVLP.

3.5. References

1 Glasgow, J. and Tullman-Ercek, D. (2014) Production and applications of engineered viral capsids. *Appl Microbiol Biotechnol* **98**, 5847-5858

2 Zeltins, A. (2013) Construction and Characterization of Virus-Like Particles: A Review. *Mol Biotechnol* **53**, 92-107

3 Pattenden, L. K., Middelberg, A. P., Niebert, M. and Lipin, D. I. (2005) Towards the preparative and large-scale precision manufacture of virus-like particles. *Trends Biotechnol* **23**, 523-529

4 Ludwig, C. and Wagner, R. (2007) Virus-like particles-universal molecular toolboxes. *Curr Opin Biotechnol* **18**, 537-545

5 Cuellar, J. L., Meinhoevel, F., Hoehne, M. and Donath, E. (2010) Size and mechanical stability of norovirus capsids depend on pH: a nanoindentation study. *J Gen Virol* **91**, 2449-2456

6 Cumbo, A. (2013) *Virus Imprinted Particles* PhD thesis at University of Basel

7 Cumbo, A., Lorber, B., Corvini, P. F., Meier, W. and Shahgaldian, P. (2013) A synthetic nanomaterial for virus recognition produced by surface imprinting. *Nat Commun* **4**, 1503

8 Lakowicz, J. R. (2006) *Principles of Fluorescence Spectroscopy, 3rd edition*. (Springer US)

9 Aylott, J. W. (2003) Optical nanosensors: an enabling technology for intracellular measurements. *The Analyst* **128**, 309-312

10 Zimmermann, T., Rietdorf, J. and Pepperkok, R. (2003) Spectral imaging and its applications in live cell microscopy. *FEBS Letters* **546**, 87-92

11 Zhang, J., Campbell, R. E., Ting, A. Y. and Tsien, R. Y. (2002) Creating new fluorescent probes for cell biology. *Nat Rev Mol Cell Biol* **3**, 906-918

12 Lippincott-Schwartz, J., Snapp, E. and Kenworthy, A. (2001) Studying protein dynamics in living cells. *Nature Reviews* **2**, 444-456

13 Kerppola, T. K. (2006) Design and Implementation of Bimolecular Fluorescence Complementation (BiFC) Assays for the Visualization of Protein Interactions in Living Cells. *Nat Protoc.* **1**, 1278–1286

14 Kerppola, T. K. (2009) Visualization of molecular interactions using bimolecular fluorescence complementation analysis: characteristics of protein fragment complementation. *Chem Soc Rev* **38**, 2876-2886

15 Liu, J., Wen, J., Zhang, Z., Liu, H. and Sun, Y. (2015) Voyage inside the cell: Microsystems and nanoengineering for intracellular measurement and manipulation. *Microsystems & Nanoengineering* **1**, 15020

16 Giepmans, B. N. G., Adams, S. R., Ellisman, M. H. and Tsien, R. Y. (2006) The Fluorescent Toolbox for Assessing Protein Location and Function. *Science* **312**, 217-224

17 Czarnik, A. W. (1993) Supramolecular Chemistry, Fluorescence, and Sensing. *ACS Symposium Series* **538**, 1-9

18 Prodi, L., Bolletta, F., Montalti, M. and Zaccheroni, N. (2000) Luminescent chemosensors for transition metal ions. *Coordination Chemistry Reviews* **205**, 59–83

19 Epstein, J. R., Biran, I. and Walt, D. R. (2002) Fluorescence-based nucleic acid detection and microarrays. *Analytica Chimica Acta* **469**, 3-36

20 de Lorimier, R. M. et al. (2002) Construction of a fluorescent biosensor family. *Protein Sci* **11**, 2655-2675

21 Hertzberg, R. P. and Pope, A. J. (2000) High-throughput screening: new technology for the 21st century. *Current Opinion in Chemical Biology* **4**, 445–451

22 Hellinga, H. W. and Marvin, J. S. (1998) Protein engineering and the development of generic biosensors. *TIBTECH* **16**, 183-189

23 Sellrie, F., Warsinke, A. and Micheel, B. (2006) Homogeneous indirect fluorescence quenching immunoassay for the determination of low molecular weight substances. *Analytical and bioanalytical chemistry* **386**, 206-210

24 Pope, A. J., Haupts, U. M. and Moore, K. J. (1999) Homogeneous fluorescence readouts for miniaturized high-throughput screening: theory and practice. DDT 4, 350-362

25 Ye, L. and Mosbach, K. (2001) Polymers Recognizing Biomolecules Based on a Combination of Molecular Imprinting and Proximity Scintillation: A New Sensor Concept. *J Am Chem Soc* **123**, 2901-2902

26 Basabe-Desmonts, L., Reinhoudt, D. N. and Crego-Calama, M. (2007) Design of fluorescent materials for chemical sensing. *Chem Soc Rev* **36**, 993-1017

27 Wan, W., Wagner, S. and Rurack, K. (2016) Fluorescent monomers: „bricks“ that make a molecularly imprinted polymer „bright“. *Analytical and bioanalytical chemistry* **408**, 1753-1771

28 Liu, R., Guan, G., Wang, S. and Zhang, Z. (2011) Core-shell nanostructured molecular imprinting fluorescent chemosensor for selective detection of atrazine herbicide. *The Analyst* **136**, 184-190
29 Feng, H. et al. (2014) Surface molecular imprinting on dye–(NH2)–SiO2 NPs for specific recognition and direct fluorescent quantification of perfluorooctane sulfonate. *Sensors and Actuators B: Chemical* **195**, 266-273
30 Wandelt, B., Mielniczak, A. and Cywinski, P. (2004) Monitoring of cAMP-imprinted polymer by fluorescence spectroscopy. *Biosens Bioelectron* **20**, 1031-1039
31 Chen, Z., Álvarez-Pérez, M., Navarro-Villoslada, F., Moreno-Bondi, M. C. and Orellana, G. (2014) Fluorescent sensing of “quat” herbicides with a multifunctional pyrene-labeled monomer and molecular imprinting. *Sensors and Actuators B: Chemical* **191**, 137-142
32 Wu, Y. T. et al. (2015) Monitoring bisphenol A and its biodegradation in water using a fluorescent molecularly imprinted chemosensor. *Chemosphere* **119**, 515-523
33 Liao, Y., Wang, W. and Wang, B. (1999) Building Fluorescent Sensors by Template Polymerization: The Preparation of a Fluorescent Sensor for L-Tryptophan. *Bioorganic Chemistry* **27**, 463–476
34 Nguyen, T. H., Hardwick, S. A., Sun, T. and Grattan, K. T. V. (2012) Intrinsic Fluorescence-Based Optical Fiber Sensor for Cocaine Using a Molecularly Imprinted Polymer as the Recognition Element. *IEEE Sensors Journal* **12**, 255-260
35 Zhang, W. et al. (2014) A fluorescence nanosensor for glycoproteins with activity based on the molecularly imprinted spatial structure of the target and boronate affinity. *Angew Chem Int Ed Engl* **53**, 12489-12493
36 Hongzhi, L. and Shoufang, X. (2017) Functional monomer-template-QDs sandwich structure for mesoporous structured bovine hemoglobin imprinted ratiometric fluorescence sensor. *Talanta* **165**, 482-488
37 Li, D. Y., He, X. W., Chen, Y., Li, W. Y. and Zhang, Y. K. (2013) Novel hybrid structure silica/CdTe/molecularly imprinted polymer: synthesis, specific recognition, and quantitative fluorescence detection of bovine hemoglobin. *ACS Appl Mater Interfaces* **5**, 12609-12616

4 Results and Discussion

4.1 Synthesis of NorVLP imprinted particles

In this section, Norovirus-like particles (NorVLP) were used as safe replacement for human pathogen viruses during the imprinting. The adaptation of the imprinting protocol to the properties of the NorVLP, and the set-up of the binding assay to confirm the ability of the imprinted particles to bind NorVLP will therefore be described in this section.

4.1.1 Imprinting with NorVLP as template virus

Based on the protocol described in section 3.3, the imprinting process was carried out with NorVLP as template virus, using APTES and TEOS as building blocks. Both VLP immobilization and recognition layer growth were performed in freshly filtrated water, which was shortly called “nanopure water”. From the FESEM micrographs, it can be seen that a silica layer covers the resulting particles and some spherical formations on the particles surface, which were assumed to be NorVLP beneath the silica layer (Figure 4.1, left). Removal conditions, including ultrasonication, were applied to partly break this silica layer for removing the NorVLP from the imprints. However, not only the NorVLP, but also the imprinted silica layer on the SNP was removed through ultrasonication. As it can be seen in the FESEM micrographs, in Figure 4.1, the silica layer with the spherical formations was well visible before ultrasonication, while it appeared thinner after ultrasonication for 20 min. This observation indicates that the number of siloxane bonds and, thus, the degree of crosslinking was not sufficiently high in the formed organosilica layer or between the layer and SNP surface.

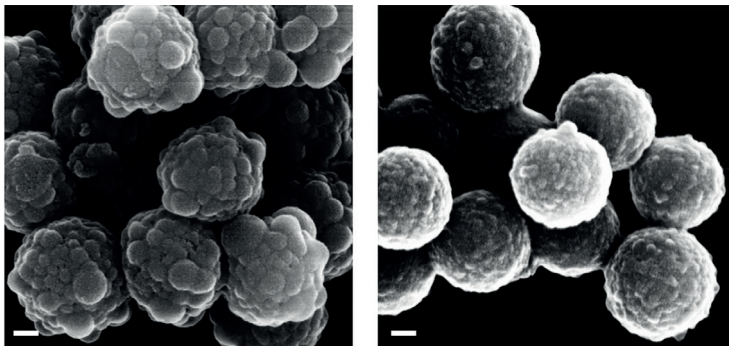

Figure 4.1: Effect of sonication on VIPs - FESEM micrographs of VIPs, after formation of silica layer in nanopure water, before (left) and after (right) sonication for 20 min; scale bar: 100 nm.

In industrial processes for silica-based materials (*e.g.*, rubber) and coatings, higher crosslinking in materials is induced by curing.[1-4] In case of coating, the curing increased the connection with the core material such as steel and thus improved the stability against mechanical forces.[1] Curing also represents the last step in the rubber synthesis, improving the elasticity of the final product.[4] It is often performed at high temperature to evaporate the water in silica and thus induce the hydrolyzation, which leads to the formation of siloxane bonds.

In order to reach a sufficient degree of hydrolyzation - considering that heat-sensitive proteins are integrated in the silica - after the imprinting process, particles were stored at room temperature (RT: 20-25°C) for 18 hours; they were then treated and analysed in the same way as before, including the ultrasonication. The FESEM micrographs showed that particles after being stored at higher temperature did not lose the silica layer at all, indicating improved layer stability. The incubation at RT was performed for all particles after synthesis of the silica layer; this process is named “curing” as well.

The curing was also performed on silica particles with β-Galactosidase entrapped in a silica layer.[5] As the curing had an effect on the activity of β-Galactosidase, the elasticity of the silica layer containing the enzyme was evaluated at different stages of the curing via atomic force microscopy, which showed that the elasticity increased, improving the mobility of the enzyme and, thus, its activity. Interestingly, the change in elasticity was not observed in case control particles that were covered with the same silica layer without the enzyme. This observation indicates that the change was induced by the presence of the enzyme itself. For the virus imprinting, the presence of the template virus during curing might have a similar effect on the stability of the layer, which might induce slight differences between imprinted and non-imprinted particles in terms of layer stability.

After carrying out the imprinting of NorVLP in nanopure water, the surface of the resulting particles showed large spherical structures that represented the immobilized VLP surrounded with a silica layer (see FESEM micrograph in Fig. 4.2). Considering the diameter of the VLP and the SNP, the thickness of the silica layers formed on the surface of VLP and SNP, respectively, was determined. As shown in Figure 4.2, the silica layer grew around the VLP with a rate of ca. 8nm/hour and around the SNP with a rate of around 4nm/hour. This result clearly shows that the silane polycondensation was two times faster at the surface of the immobilized NorVLP than at the surface of the SNP. As a result of the thick silica layer around the VLP, the subsequently performed virus removal did not release the VLP from the SNP surface. Indeed, after stabilizing the formed silica through curing, even a sonication for up to 2 hours did not affect the silica around the VLP.

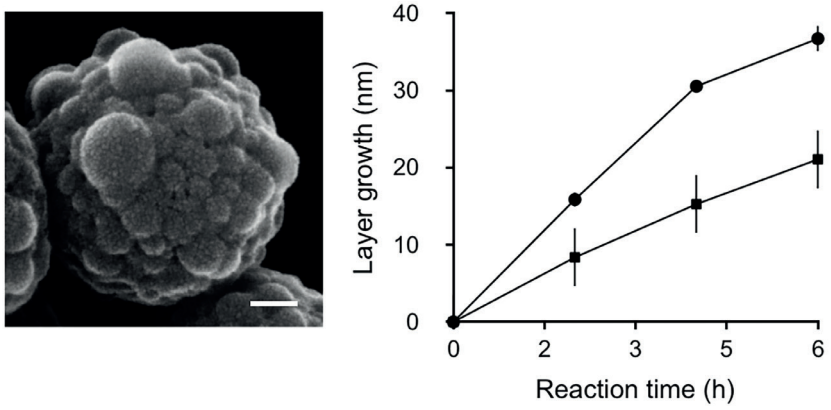

Figure 4.2: Silane polycondensation at the presence of immobilized NorVLP in nanopure water - left: FESEM micrograph of SNP with NorVLP on the surface after 6h polycondensation; right: formation of silica layer on the surface of NorVLP (round) and SNP (square) over time.

In the end, the particles still exhibited VLP-silica formations at their surfaces, but no imprints. Thus, the imprinting process carried out in nanopure water did not result in the generation of imprints because of the high silica formation on the template virus, NorVLP.

VLP had to be reduced without affecting the formation on the surface of the SNPs. However, most of the typical process factors (temperature, ionic strength, pH values, concentration as well as composition of organosilanes) have a general effect on the silica formation and, thus, do not make a distinction between the surface of SNP or NorVLP. Therefore, the interaction between organosilanes and template virus was studied in further detail.

In order to obtain imprinted particles with the NorVLP as template, the silica formation on the In the previous work on VIPs that used plant viruses as template, a thin silica layer was also observed to be surrounding each virus particle.[1] At that time, the silica formation on the plant virus was induced by the use of organosilanes with varying organic groups. Those groups were similar to amino acids and increased the variety of non-covalent bonds between the organosilanes and amino acids of the virus proteins; beside hydrogen bonds and ionic bonds, π-π stacking and van der Waals forces were also possible. With a high number of bonds, there was sufficient amount of organosilanes collected at the surface of the virus to induce silica formation directly on the template. However, the silica layer that had formed on the plant viruses was quite thin and was broken through the previously described treatment for template removal. The thickness of silica layer on the plant viruses was increased when organosilanes that contained additional basic groups were used.[2] Based on these observations, it was assumed that high interactions and catalysing basic groups were responsible for the fast silica layer growth on the NorVLPs.

Interestingly, in case of NorVLP imprinting, only two organosilanes, namely, TEOS and APTES, with both limited interaction and catalytic properties, were sufficient for the layer growth. Therefore, some specific properties of the NorVLP inducing silica formation were assumed.

Comparing the properties of the applied NorVLP with that of the plant viruses, for which the imprinting was successful, a strong difference in the isoelectric point (IEP) could be found. NorVLP has a theoretical pI of 5.6 based on its amino acid coding sequence, which is significantly higher than that of the plant viruses: TYMV (Turnip yellow mosaic virus) with 3.8 and TBSV (Tomato bushy stunt virus) with 4.1. The higher IEP value suggested a higher number of cationic amino acids (AAs) in NorVLP than in the plant viruses.

Cationic AAs are also found in silaffins that are peptides catalysing and templating the formation of biosilica in diatoms. Different studies on silica formation by peptides have shown following common properties of peptides to govern silica formation[7-14]:

1. Positively charged moieties for attracting negatively charged silanes;
2. Basic properties for hydrolysis;
3. Self-assembly prior to silica polycondensation for templating;

To affect the organosilane polycondensation, these cationic AAs needed to be located at the surface. Indeed, looking at the crystal structure of the P2 domain of GII.4 norovirus VA387 strain[6], cationic AAs (such as His292, His297, Arg339, Arg410) can be found on external loops, allowing interaction with the organosilanes present in the reaction mixture (Fig. 4.3).

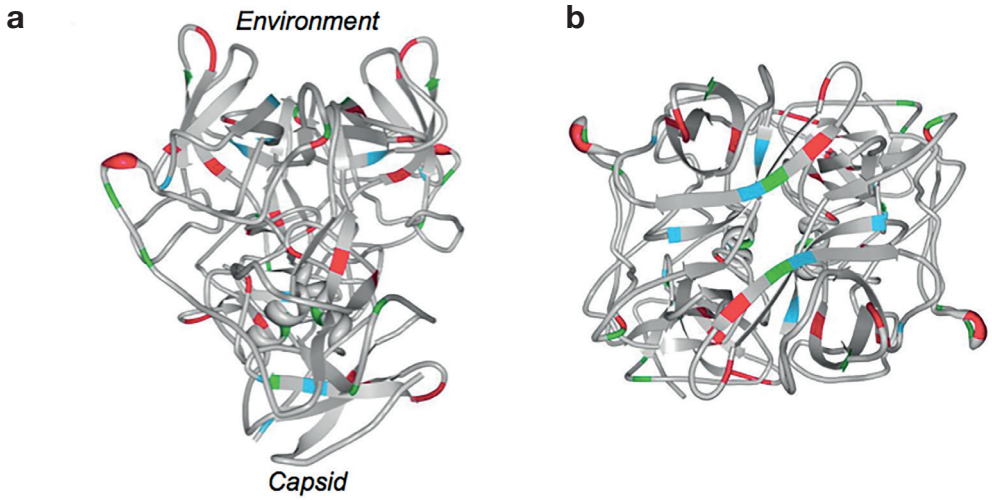

Figure 4.3: Structural analysis using X-ray structure of norovirus VA387 (2OBS) – a: Side view; b: Top view; positively charged amino acids are outlined as follows: lysine in blue, arginine in red and histidine in green. Most of lysine residues are in the inner part of the P2 domain and form together with arginine and histidine the recognition site of the Norovirus capsid. Arginine and histidine residues can also be found on external orientated on flexible loop regions (program in use: Protein Workshop).

In case of NorVLP, there are the cationic and basic properties by external lysine molecules as well as the higher structures for templating, as NorVLP is a protein shell formed from 180 single proteins by self-assembling. This combination of basic groups and highly organized structure is responsible for the high polycondensation rate at the surface of the NorVLP. Since the structure of NorVLP was needed for the imprinting, the effect by the cationic AAs on the silica formation had to be reduced.

The cationic and basic properties of AAs depend naturally also on the applied pH value. Therefore, one can assume, this effect by cationic AAs can be reduced by carrying out the reaction at a different pH value. However, changing the pH was not the best option due to the sensitivity of NorVLP to the applied pH value. Cuellar et al. studied the stability of NorVLP against different pH values, ranging from pH 2 to 10; changes in size and mechanical stability of the VLP were determined. At basic pH, a significant increase in size was observed due to disassembling of the protein units.[15] In order to reduce the effect by cationic AA, the pH value during imprinting should be pH 8 or higher. At high pH, the NorVLP would be negatively charged, as deprotonating is induced, but, at the same time, the VLP would start to disassemble, losing its three dimensional structure.

Alternatively, an additive that overlays the cationic AA present at the surface of the VLPs was tested to inhibit the silica formation at the template surface. The idea was to use a polyanionic

molecule on the basis of the hypothesis that one negatively charged group interacts with the positively charged AA on the VLP, while the other negatively charged groups interact with the surroundings. One known and simple polyanionic molecule is citrate. After carrying out the imprinting using 10mM citrate at pH 6, the recognition layer showed cavities. To confirm that these cavities were induced by the presence of NorVLP, imprinting was performed using different concentrations of NorVLP (25, 10 and 5 µg/ml). The surfaces of the so-produced particles were visualized by means of FESEM; the representative micrographs are given in Fig. 4.4. From these, it can be seen that the number of cavities depends on the applied concentration of NorVLP. Furthermore, the diameter of the observed cavities was compatible with the size of the template virus, at a diameter of 35nm. Therefore, the visual analysis of the produced particles clearly suggested that the cavities represented the virus imprints. Interestingly, the cavities were visible without performing the template removal that would release the template from the imprints. The open cavities were probably the result of physical treatment associated with the sample preparation for the FESEM imaging, which includes drying, vacuum, gold-platinum alloy sputter-coating, and impact with high voltage electrons. Such treatment results in partially damaging the NorVLP, when there is no thick silica layer protecting it. Assuming that the citrate indeed inhibited the formation of the silica layer, protecting the NorVLPs, the structural integrity of the NorVLPs was probably damaged before and/or during FESEM imaging. As a result of the damage, NorVLPs were not visible on the particle surface and, thus, the imprints in the recognition layer seemed empty during imaging.

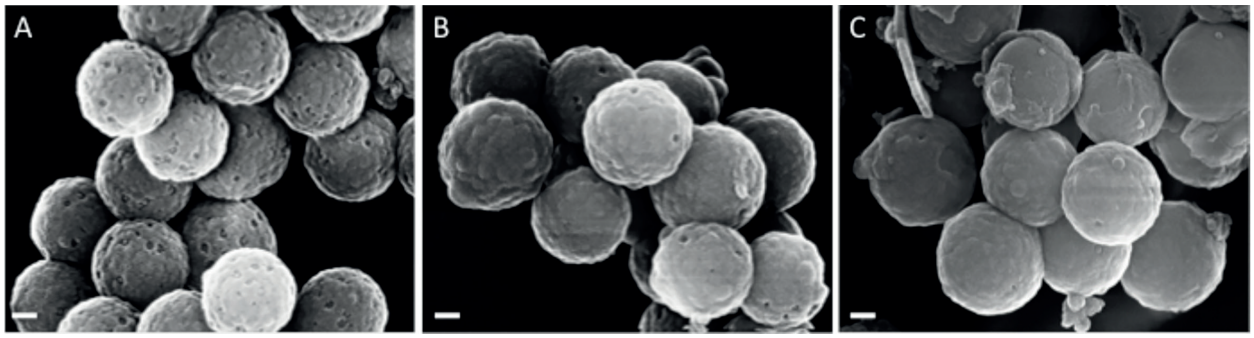

Figure 4.4: Imprinting at different concentration of NorVLP as template - FESEM micrograph of particles after 6h silane polycondensation in 10 mM citrate pH 6 at the presence of 25 (A), 10 (B) and 5 (C) µg/ml NorVLP, respectively; scale bars: 100 nm.

To test the stability of the recognition layer, the imprinted particles were treated with ultrasonication. The FESEM micrographs showed that the recognition layer was removed partially through this treatment. This observation indicates that the presence of citrate weakens the whole silica layer because the ionic strength induced by citrate inhibits the formation of the siloxane groups in the layer. Therefore, when curing was performed, the number of siloxane groups strengthening the silica network was not sufficient to resist the physical stress. In conclusion, the so-prepared imprinted particles could not be further used due to the instability of the recognition layer.

As already mentioned, the silica formation, in particular its shape, can be controlled, among others, with the help of the applied pH, and the presence of salt and catalyser. The presence of

salt, due to its ionic strength, induces the formation of gel-like silica with scattered bonds, while the basic condition or basic catalyser promotes the formation of particular silica with dense crosslinking. For the stability of the recognition layer, the degree of internal crosslinking has to be improved. Therefore, to compensate the effect of the ionic strength by citrate, the idea was to accelerate the silica formation by applying a slightly higher pH.

The recognition layer growth was carried out at different pH values, ranging from pH 6 to 8, and characterized by FESEM. The pH value of the reaction suspension was measured before and after adding TEOS and APTES, respectively. This experiment led to two interesting observations:

1) Basic conditions improved the rate of organosilane polycondensation.
2) The pH value of reaction suspension shifted after adding APTES.

The first observation has already been described in the literature, while the second observation about the pH shift has not been described yet. Therefore, the pH-shift was further investigated by performing the silane polycondensation in different buffer solutions, namely citrate, MES (2-(N-morpholino)ethanesulfonic acid), HEPES (2-(4-(2-Hydroxyethyl)-1-piperazinyl)-ethansulfonacid), and phosphate, all at 10 mM.

As APTES contains an amino group, it reacts like a base when added to water due to the deprotonation of the amino group. The shifting of the pH has not been described because most reactions with APTES have been carried out in organic solvents such as ethanol. For carrying out the imprinting in water without a buffer, 6 µl APTES was added into 6 ml reaction suspension, which increased the pH by one unit (*e.g.*, from 6 to 7). The presence of a buffer can compensate the pH increase induced by APTES, but the buffer capacity had to be considered. Depending on the buffer capacity of the applied buffer, a different buffer concentration was needed to inhibit the effect of APTES. Buffers with low buffer capacity, such as citrate (pK_a 5.4) or MES (pK_a 6.1) at pH 6, did not avoid the pH shift when their concentration was at 10 mM. In contrast, buffers with high buffer capacity, such as phosphate (pK_a 7.2) or HEPES (pK_a 7.5) at pH 7, could avoid the shift at 10 mM, which had consequences on the polycondensation rate. The starting pH needed to be already at 8 to allow the formation of the recognition layer within 6 hours. Considering the ionic strength and buffer capacity, a stable silane layer of 20 nm could be formed in the presence of different salts, namely, NaCl, citrate, MES, HEPES, phosphate and EDTA (Ethylenediaminetetraacetic acid), see representative FESEM micrographs in Fig. 4.5.

Interestingly, the large spherical structures that the NorVLP encapsulated in silica appeared in all conditions, except for when citrate or EDTA were added. This result confirms the initial hypothesis that a polyanion inhibits the silica formation at the surface of the NorVLP. Both citrate and EDTA feature a high number of carboxyl groups – three in case of citrate, four in case of EDTA. These carboxyl groups can interact and cover the positively charged AAs of NorVLP. The imprinting in the presence of citrate was then further optimized.

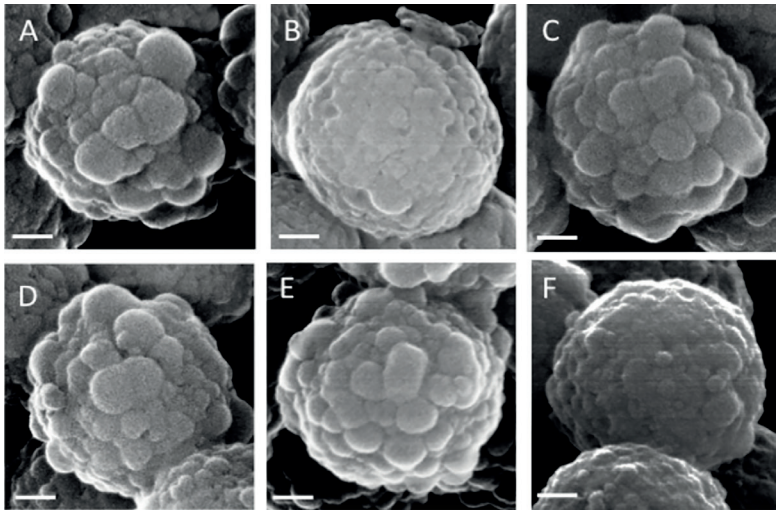

Figure 4.5: Effect of different salts on the recognition layer – FESEM micrographs of particles after 6 h organosilane polycondensation in 10 mM NaCl (A), citrate (B), MES (C), phosphate (D), HEPES (E), EDTA (F); scale bars: 100 nm.

The imprinting was carried out in the presence of increasing concentrations of citrate, namely, 10, 25, 50, 75 and 100 mM, adjusted at pH 7. This pH value improved the polycondensation rate and, thus, the stability of the layer formed. Additionally, at this pH value, citric acid (pK_a at 3.1, 4.8 and 5.4) is expected to be fully un-protonated and does not behave as buffer anymore, even at high concentrations. The so-produced particles were analysed by FESEM to determine the presence of imprints at the surface and the thickness of the recognition layer formed (Fig. 4.6). The FESEM micrographs show that the virus imprints are present as cavities at the surface of imprinted particles for citrate concentrations up to 75 mM. The determination of the thickness shows that the presence of citrate also slows down the silica formation at the surface of the SNPs. For citrate concentrations of 10, 25, 50, 75 and 100 mM, the layer at the surface of the SNPs grew to 32 ± 3 nm, 25 ± 3 nm, 30 ± 2 nm, 17 ± 3 nm, and 8 ± 2 nm, respectively, within 6 hours.

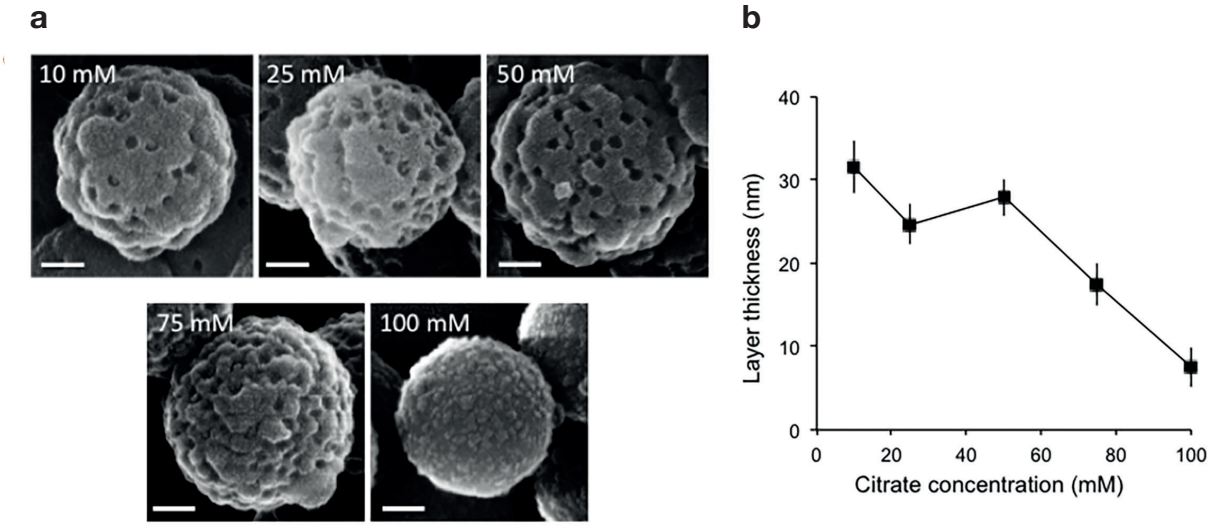

Figure 4.6: NorVLP imprinting at increasing citrate concentrations – a) FESEM micrographs after silica formation; scale bars: 100 nm. b) Thickness of recognition layer after 6 h silane polycondensation.

The low layer thickness for 100 mM citrate explains the absence of imprints in the formed recognition layer. In contrast to the previously imprinted particles that were obtained at lower pH, the treatment with ultrasonication did not affect the recognition layer; neither the silica layer nor the number of imprints changed significantly. This observation confirms that the imprints were not generated through weakening of the formed silica layer, but were rather a result of the locally inhibited growth of the silica layer on the NorVLP surface.

On the basis of these results, the standard protocol to generate NorVLP-imprinted particles included performing the recognition layer growth using 25 mM citrate at pH 7.

4.1.2 Binding assay with NorVLP-imprinted particles

The functionality of the imprints to rebind the template virus was further investigated by performing binding assays. In order to understand whether the binding occurs through the imprints, the binding efficiency of both NorVLP-imprinted particles (VIPs) and non-imprinted particles (NIPs) was determined. The binding efficiency was evaluated by quantifying the amount of unbound virus in the reaction medium. Both conditions for the binding assays and the virus quantification were defined before studying the binding properties of particles.

4.1.3.1 Quantification of NorVLP

The method of choice for the quantification of NorVLP was enzyme-linked-immunoassay (ELISA), which combines natural antibody (Ab) recognition with enzymatically catalysed amplification. Among the different formats for ELISA, indirect and double antibody sandwich ELISA were tested for quantification (Fig. 4.7). Both formats are based on the immobilization of the antigen (Ag) and the subsequent determination of the formed antigen-antibody complex through an enzyme-catalysed colorimetric assay. The main difference between these two formats lies in the way the antigen is immobilized. In indirect ELISA, the antigen, here the NorVLP, was directly immobilized on the surface of a 96-well plate via ionic interactions before the antibodies for detection were added.

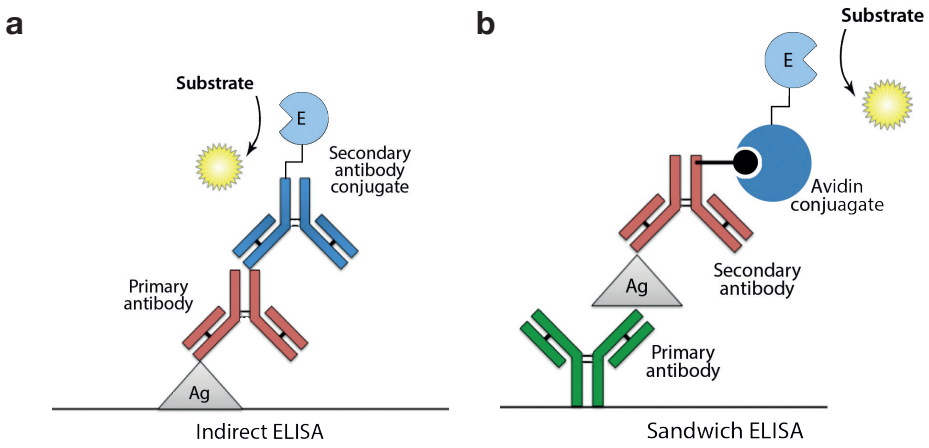

Figure 4.7: Schemata of ELISA formats applied for NorVLP quantification

In case of sandwich ELISA, an antigen-specific antibody was first immobilized on the plate and then the antigen was bound via the antibody. Further details about the two ELISAs are described below.

Indirect ELISA

In brief, the indirect ELISA included the following steps:

1. Adsorption of the sample on the plate = Coating
2. NorV-specific Ab binding on NorVLP = specific recognition
3. Enzyme-conjugated Ab binding the first Ab = formation of transduction system
4. Enzymatic reaction = Visualization of presence of Ag-Ab complex

In indirect ELISA, the number of NorVLP immobilized on the plate was determined via the subsequent binding of two antibodies: a NorV-specific Ab and an enzyme-conjugated Ab; the latter recognized the first Ab through its constant region. After binding the enzyme-conjugated Ab, an enzyme is available for a colorimetric reaction, resulting in a coloury and, thus, detectable product. As the generation of the coloury product depends on the number of formed NorVLP-Ab complexes, the intensity of the colour (or light absorption) is correlated with the concentration of NorVLP immobilized on the plate.

The main advantage of the indirect ELISA is that all reagents – NorV specific Ab and enzyme-conjugated Ab – were commercially available and could be applied directly without further modifications. However, the quantification relied on the efficient coating of NorVLP, which was affected by the composition of the sample, such as protein concentration and composition. Therefore, each modification in the binding assay required its own calibration curve for the virus quantification.

Sandwich ELISA

In a classical sandwich ELISA, the transduction of the formed Ab1-Ag-Ab2 complex to a signal is determined via an enzyme-conjugated Ab. However, this transduction system requires that the two Ag-specific antibodies are from different species, such as mouse, rabbit or sheep. Since the enzyme-conjugated Ab recognizes the species-specific constant part of an Ab, the conjugated Ab binding the on plate immobilized Ab1 independently from antigen can be avoided. As there were no NorV-specific antibodies available from any other species than mouse, the biotin-avidin system was applied as a transduction system.

In brief, the sandwich ELISA using biotin-avidin complex included the following steps:

1. Adsorption of NorV-specific Ab = Coating with 1. Ab
2. Binding of Ag from sample by 1. Ab = 1. Specific recognition
3. Binding of 2. NorV-specific Ab with biotin on bound antigen = 2. Specific recognition

4. Binding of enzyme-conjugated avidin on biotin = Formation of transduction system
5. Enzymatic reaction = Visualization of presence of Ab_1-Ag-Ab_2 complex

Biotin and avidin are known to have the highest natural affinity through non-covalent interactions. Furthermore, biotin is with 244 g/mol a small molecule and, thus, does not disturb the functioning of a protein after conjugation. Biotinylated NorV-specific antibodies were obtained via a commercial biotinylation protocol (see section 6.1).

The main advantage of the sandwich ELISA is that Ag binding is less affected by sample composition and also more specific because the two antibodies bind different sites of the same Ag, reducing cross-reactions.

Calibration curves

After optimization, both ELISAs were obtained in both formats, in terms of signal-to-noise ratio, calibration curves (Fig. 4.8) to determine sensitivity, linearity, precision and limit of detection.

As can be seen from the two calibration curves, the applied concentration of up to 55ng/ml NorVLP was in linear correlation with the measured optical density in both ELISA formats. But the indirect format surpassed the sandwich format in terms of linearity and precision indicated by a coefficient of determination (R^2) and standard deviation of data, respectively. With the indirect format, an R^2 of 0.998 and a very low standard deviation of 0.005 on an average were determined, while with the sandwich ELISA, an R^2 of 0.978 and obvious standard errors of 0.08 at high NorVLP concentrations indicated the upper limit of detection.

Another difference between the two ELISAs can be seen when looking at the OD-values obtained without NorVLP (blank). The blank in sandwich ELISA, with an OD of 0.2, was significantly higher than the blank in indirect ELISA with an OD of 0.06, indicating unspecific binding. In case of the sandwich ELISA, the avidin was found to bind on proteins from the sample when it was not diluted sufficiently. The unspecific binding of avidin reduced the precision as well as the lower limit of detection of the sandwich ELISA.

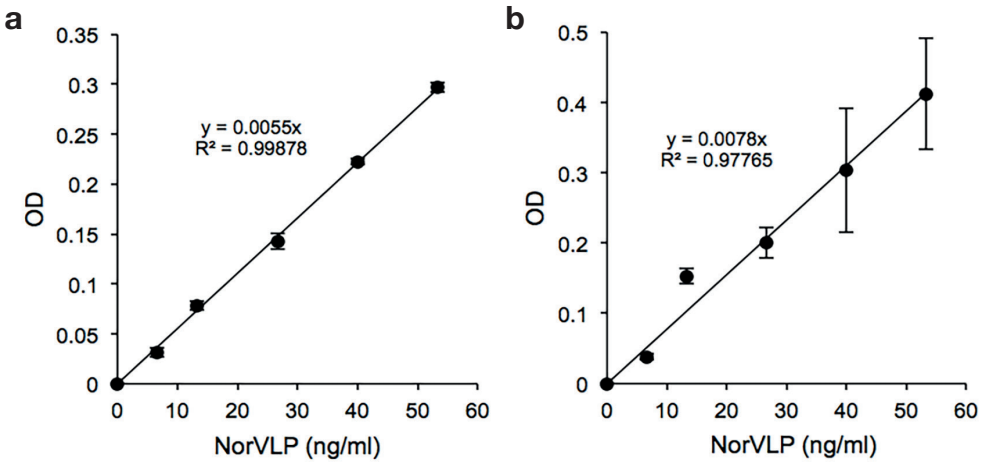

Figure 4.8: Calibration curves obtained through a) indirect ELISA and b) sandwich ELISA;

In conclusion, the indirect ELISA was used as a standard method for the NorVLP detection because of its better reproducibility and sensitivity.

4.1.3.2 Binding Assay

In general, the binding assays were performed as follows:

1. Incubation of VIPs and NIPs, respectively, with NorVLP in well-defined conditions - i.e. contact time, buffer, pH, and ionic strength;
2. Separation of unbound NorVLP from the silica particles through centrifugation;
3. Quantification of the amount of NorVLP in the supernatant via indirect ELISA;
4. Determination of binding efficiency.

The binding efficiency was defined as the relative concentration of the bound NorVLP and it was calculated using the concentration values from the binding assay with particles ($[NorVLP]_R$) and without particles ($[NorVLP]_P$). The latter was used as reference for effects on the NorVLP concentration that were induced by processes other than the binding of the particles, such as adsorption (*e.g.*, on the surface of the reaction vessel), precipitation, and coating efficiency.

The formula used was as follows:

$$Bindings\ efficiency = 1 - ([NorVLP]_P / [NorVLP]_R)$$

The so-defined binding efficiency shows the relative quantity of NorVLP that was removed from the liquid phase through the adsorption on the particles' surface. The adsorption can be due to specific binding via the imprints and unspecific binding via non-imprinted silica surface. To distinguish between these two binding fashions, the binding efficiency of VIPs and NIPs was compared. VIPs, with their improved binding properties, were expected to surpass the NIPs in terms of binding efficiency.

To evaluate the binding properties of the imprints, the first step was finding the binding conditions that shift the mode of binding towards more specific binding. This optimisation included the reduction of unspecific adsorption of NorVLP via the silica surface. For this purpose, the addition of non-template protein and citrate were tested for their influence on the NorVLP binding. Further, the binding assay was studied in terms of contact time and the concentration of particles and template in the assay.

Under standard conditions, the binding suspension (vol: 120 µl) was stirred at 650 rpm at 25 °C for 30 min, and contained the following components:

- Buffer at pH 6 containing 10 mM phosphate, 10 mM citrate and 50 mM NaCl
- Added protein at 75 µg/ml
- NorVLP at 700 ng/ml (= 65 pM)
- Silica particles (VIP or NIP) at 810 µg/ml

Effect of proteins on the binding

In case the target molecule is a protein, like the NorVLP, other proteins such as bovine serum albumin (BSA) are generally added to the binding medium to improve the colloidal stability of the target protein, and thus reduce the degree of precipitation and unspecific adsorption.

When SNP is used to bind NorVLP, the additional proteins not only improve the stability of the NorVLPs, but also function as direct competitors for the binding site on the surface of SNP. Both imprinted and non-imprinted SNP exhibit polar groups on the surface, causing unspecific binding of any protein. It is assumed that the imprints on VIPs enhance the affinity for NorVLP compared to other proteins due to the structurally optimized interactions, making the binding NorVLP-specific. The addition of other proteins should thus affect the unspecific binding of non-imprinted surfaces than the specific binding via the imprints, resulting in different binding efficiencies for VIPs and NIPs. To confirm this hypothesis, binding assays were performed with VIP and NIP using increasing concentrations of BSA and skim milk, respectively.

The binding efficiencies that were determined at increasing concentration of BSA are shown in Figure 4.9. As can be seen in Figure 4.9a, the binding efficiencies for both VIP and NIP were quite similar at any tested BSA concentration. On increasing the BSA concentration from 50 to 120 mg/ml, the binding efficiency decreased from 93 % to 78 % for VIP and from 94 % down to 80 % for NIP, indicating BSA inhibited the NorVLP binding. But considering the standard deviation to the data points, as shown in Fig. 4.9b, this decrease by 20 % is only a bit higher than the obtained standard deviation of the NorVLP detection via ELISA of ±10 % in average. The high standard deviation was attributed to the low concentration of NorVLP that remained in the liquid phase for detection. Furthermore, after increasing the BSA concentration further to 150 mg/ml, the binding efficiency remained unchanged.

Since both VIP and NIP bound NorVLP to the same extent, it was to be expected that NorVLP was mainly bound unspecifically to the silica surface. The addition of BSA, thus, did not inhibit the binding of NorVLP on the non-imprinted silica surface.

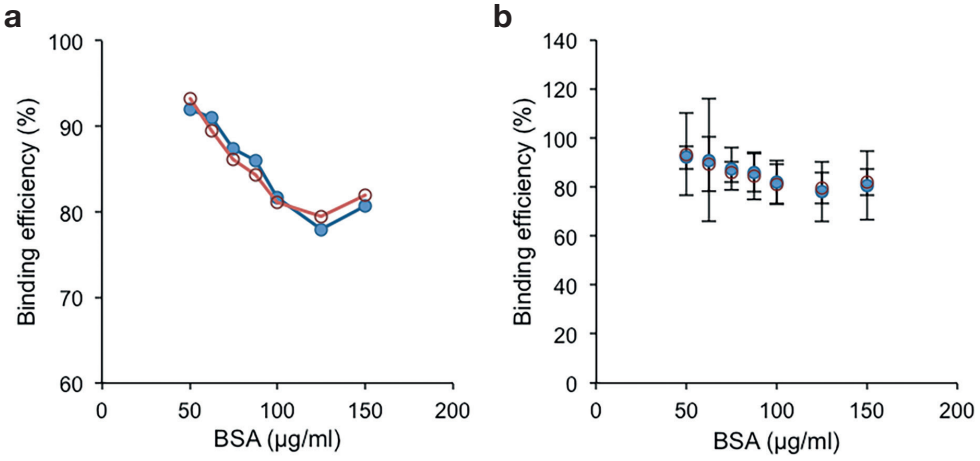

Figure 4.9: Binding efficiency at varying concentration of BSA – Data points of VIP in blue and of NIP in red are depicted a) without standard deviation for better understanding of the trend and the comparison of collected data; b) with standard deviation to understand their precision.

The fact that BSA did not affect the binding of NorVLP might be explained with the IEPs of the two proteins. At the applied pH of 6 for the binding, BSA, with an IEP of 4.7, was negatively charged, while NorVLP, with an IEP of 6, had a neutral overall charge. The BSA molecules were mostly repulsed from the negatively charged surface of the silica and remained in solution, while NorVLP could come very close to the silica surface for binding. With this significant difference in charge, BSA could not compete with the NorVLP for the binding regions on the silica particles. Hence, to reduce the unspecific binding of NorVLP on silica, the added proteins needed to bind on the non-imprinted silica surface at a similar rate or faster than NoVLP.

Alternative to BSA, skim milk was tested as a competitor for the silica surface in the binding assay; skim milk contains a mixture of different proteins with varying IEPs, ranging from 6 to 9. Part of the protein mixture is expected to be strongly positively charged and to be quickly adsorbed by the silica surface, occupying mainly the non-imprinted sites.

Indeed, the binding efficiency of NorVLP by VIP and NIP determined at increasing concentration of skim milk (Figure 4.10) showed an inhibition of the NorVLP binding. Starting from 94 % at 10 mg/ml skim milk, the binding efficiency decreased at 150 mg/ml skim milk down to 15 % and 9 % for VIP and NIP, respectively. Of note, at 75 mg/ml skim milk, the binding efficiencies were 70 % for VIPs and 40 % for NIPs, indicating higher specific binding by VIPs than by NIPs. This difference between the data points of VIP and NIP is also significantly higher than the standard deviations. This skim milk concentration inhibited mainly the unspecific binding, while specific binding via imprints still occurred significantly. These results not only show that skim milk can compete with NorVLP for the binding sites, but also distinguished between VIP and NIP. This was thus the first proof that the prepared VIP owned specific binding properties for NorVLP due to the imprints.

Skim milk at 75 µg/ml was then used in the following assays to provide the condition for specific binding.

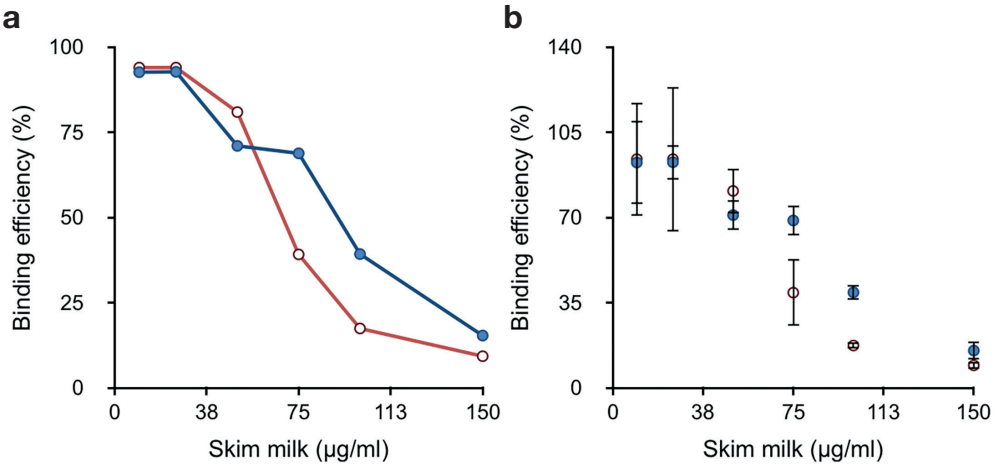

Figure 4.10: Binding efficiency at varying concentration of skim milk – Data points of VIP in blue and of NIP in red are depicted a) without standard deviation for better understanding of the trend and the comparison of collected data; b) with standard deviation to understand their precision.

Effect of citrate

Citrate, which was part of the binding medium to stabilize NorVLP in solution, was tested for its effect on the interaction between NorVLP and silica particles. The collected binding efficiencies of VIP and NIP were plotted against the citrate concentration, as shown in Figure 4.11. It can be seen that the binding efficiency of NorVLP decreased from 80 % to 10 % in case of VIP and from 40 % to 10 % in case of NIP, when the citrate concentration was increased from 10 to 100 mM. These results demonstrate that citrate efficiently prevents the NorVLP binding.

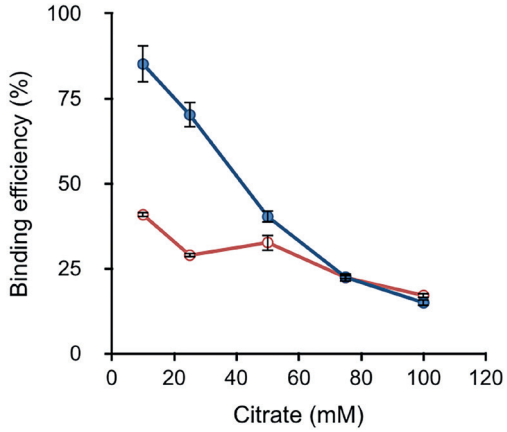

Figure 4.11: Binding efficiency at varying concentration of citrate – Data points of VIP in blue and of NIP in red are depicted with standard deviations.

Based on these results, citrate was further tested to remove the bound NorVLP from the surface of VIPs. For this purpose, VIPs were first incubated with NorVLP at standard binding conditions and then separated from the unbound NorVLP via centrifugation. The pelleted particles with bound NorVLP were washed with citrate solution at different concentrations. The NorVLP that were released from the particles through this process were obtained via centrifugation and determined via indirect ELISA. These values were correlated to the amount of previously bound NorVLP and plotted against the citrate concentration used for washing (Fig. 4.12). It can be seen that citrate at 200 mM released all of the prior bound NorVLP from the particles.

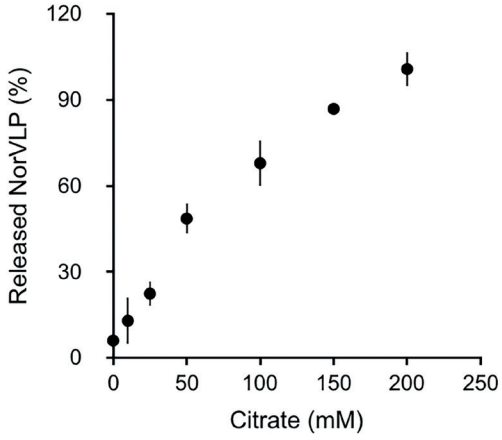

Figure 4.12: Release of NorVLP from VIPs through washing with different concentrated citrate solution Detected NorVLP concentration was correlated with the concentration of prior bound NorVLP.

This finding is particularly interesting as it offers the possibility of washing the particles after use or using the particles to concentrate viruses by releasing the viruses into a smaller volume.

Effect of particle concentration

The effect of particle concentration on the binding was assessed through two experimental modes. In Mode 1, particle concentration was changed while the concentration of all other components was kept constant. In Mode 2, beside the particle concentration, the concentration of skim milk was also changed to keep the relative ratio of particles to skim milk constant. The binding efficiencies for both modes were plotted against time, as shown in Figure 4.14. After reducing only the particle concentration from 810 to 90 µg/ml (Mode 1, 4.13 a), the binding efficiency decreased from 80 % to 0 %. In contrast, on varying both the particle and skim milk concentration (Mode 2, 4.13b), the binding efficiency did not change significantly. This result indicates that the binding efficiency depends on the particles-to-skim milk ratio. In mode 1, as the particle concentration was decreased, the skim milk concentration per particle increased. Consequently, proteins from skim milk occupied more sites on the particle surface and thus prevented NorVLP binding. When the skim milk-to-particles ratio was kept constant, like in mode 2, the percentage of the particles' surface occupied by skim milk and or NorVLP did not change. This result also proves that the protein from skim milk are indeed binding on the silica surface, inhibiting unspecific NorVLP binding as competitive inhibitor.

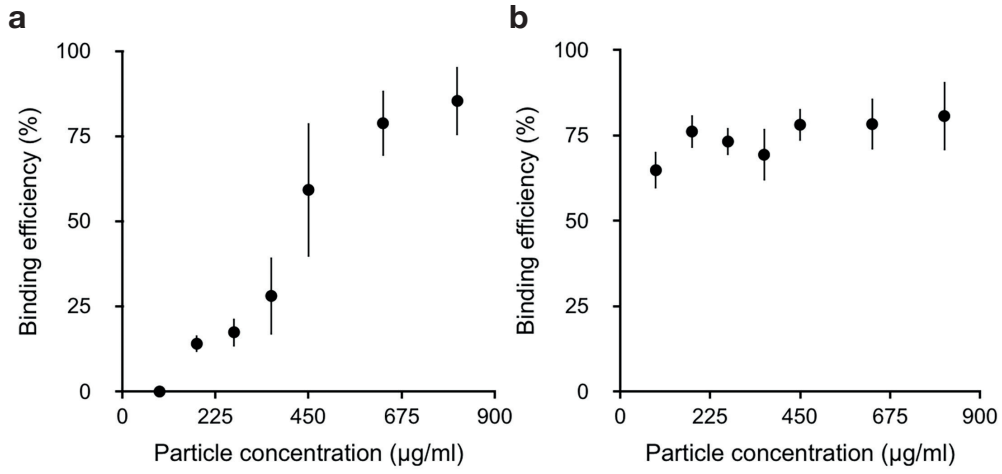

Figure 4.13: Particle concentration effect – a) Binding efficiency at varying concentration of VIP, while concentration of skim milk was kept constant; b) Binding efficiency at varying concentration of VIP and skim milk, while ratio was kept constant;

Effect of template concentration

The effect of template concentration on the binding was assessed by varying the NorVLP concentration from 30 to 1400 ng/ml. The determined binding efficiencies were plotted against the initial amount of NoVLP (Fig. 4.14). It can be seen that there was no change in the binding efficiency at the chosen template concentrations.

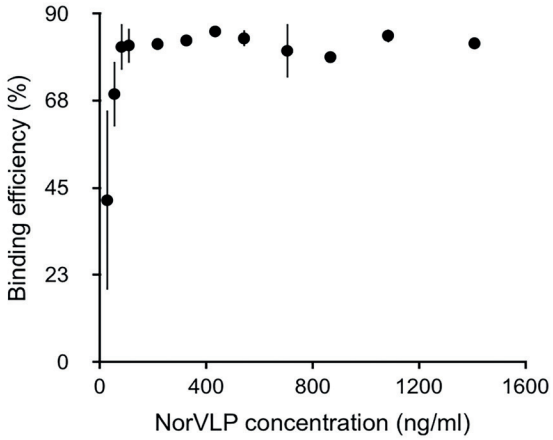

Figure 4.14: Binding efficiency of VIP at varying concentration of NorVLP

The low values at 30ng/ml were rather a result of the detection limit of the ELISA. The fact that the VIP efficiently bound even at higher concentrations of NorVLP indicates that the imprints were not saturated with NorVLP yet.

Contact time

After optimizing the binding conditions, a time course of the binding process was obtained by determining the binding efficiency at different time points – 0, 2.5, 5, 10, 20 and 30min. The determined binding efficiencies of VIP and NIP were plotted against the time, as shown in Fig. 4.15. It can be seen that most of the NorVLP was bound after 5min, and the VIP bound up to 80% and NIP up to 30% of the added NorVLP. The improved binding property by the imprints was thus proven to be reproducible as well.

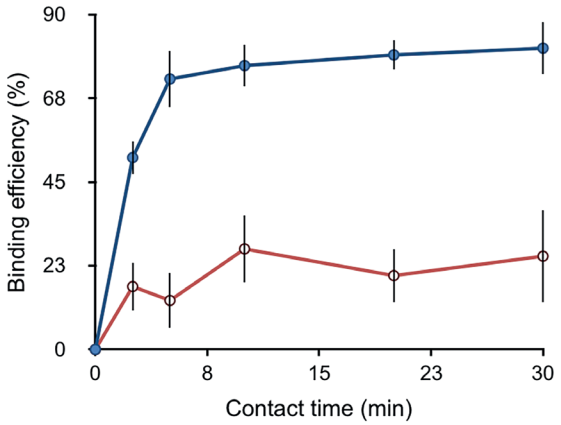

Figure 4.15: Binding efficiency observed over time – Data points of VIP in blue and of NIP in red are depicted with standard deviations.

4.1.3 Outlook for general virus imprinting protocol

One criterion for imprinting techniques is the possibility to imprint more than one template. To date, most of the imprinting protocols published have failed because they depend on specific properties of the template. The first templates for the virus imprinting protocol applied here were the two plant viruses, TYMV and TBSV, with similar properties in terms of size and amino acid composition. In this work, NorVLP, as safe analogue for human pathogen virus, was tested as template using the same protocol expanded with several modifications.

The findings reported in this chapter of the thesis clearly demonstrate that:

1) NorVLP can be used as template for virus imprinting by applying citrate as additive.

2) The produced, imprinted particles specifically bind and thus recognize the template NorVLP.

The virus imprinting protocol can thus be applied on different icosahedral viruses, considering the presence of cationic amino acids in the outer protein shell, which can induce the complete encapsulation of the template with silica. The encapsulation can be avoided by the addition of sufficient concentration of citrate overlaying the cationic charge.

Properties found for NorVLP are probably also true for other human pathogen viruses. Considering that each potential host cell features a negatively charged glycocalyx at its surface, a positively charged virus shell supports the binding between virus and its host cell. With the addition of citrate, we are thus one step closer to a generally applicable protocol for virus imprinting. The protocol might be further adapted on icosahedral virus particles with more sophisticated surface structure. Besides the icosahedral protein shell, many viruses express specific structured proteins at their surface to recognize the host cells, such as Rotavirus, Adenovirus and Coxsackievirus. Another challenge for the imprinting would be the binding of those viruses with a protective envelope around their capsid, such as Influenza virus. However, further adaptation and application of the virus imprinting protocol depends on the availability of these viruses in a non-infectious state at gram quantities.

The best option for the virus imprinting protocols is the availability of virus-like particles that are structural homologs of the wild viruses. However, since there have been limited applications for structural homologs of VLPs, their number is still low. An increase in the motivation to synthesize structural homologs of VLPs might occur after proving the possibilities of the VIPs as recognition units in detection systems. Therefore, the work in the next chapters focuses on combing the recognition layer with different transducing systems to create innovative detection systems.

4.2 Biocatalytic imprinted particles

In this section, the first of the two transduction systems to convert the NorVLP binding into an optical signal is presented; it is based on an enzymatic reaction that depends on the number of NorVLPs that are bound by the VIP through its imprints. The necessary enzyme is entrapped within a first silica layer on the silica nanoparticle surface, which is subsequently covered by the recognition layer containing the imprints.

The development of the detection system was carried out in the following steps:

1. Feasibility test of successive formation of the enzyme and recognition layers
2. Enzyme-catalysed colorimetric assay
3. Entrapment of the enzyme in silica
4. Virus-imprinting of biocatalytic particles
5. Finalization of the detection assay

4.2.1 Feasibility test

Such a transduction system, which is based on the subsequent formation of two functionally different silica layers, has not been reported before in literature. Both silica-based imprinting and enzyme encapsulations have been applied separately, but never in combination; in fact, it was not even known whether this was feasible. Therefore, the first experiments in this context were to prove the chemical feasibility of forming the recognition layer on a silica layer containing enzymes. The crucial point for a successful combination of both processes was the right compromise between the conditions for silica formation on one side and the preservation of the delicate enzymatic functionality on the other. Therefore, several phases of the imprinting process needed to be adapted.

In the frame of a project with the aim to stabilize enzymes for their application in biotechnology, biocatalytic active silica particles were generated to provide lactose-free milk by entrapping β-galactosidase (βgal) from *Kluyveromyces lactis* (EC: 3.2.1.23), in an organic silica layer.[5] These silica particles were used for the feasibility test and are referred as βgal-SNP in this work. The surface of these particles was imprinted using the previously developed NorVLP-imprinting protocol. The resulting imprinted βgal-SNPs were also tested for their use as detection assay.

4.2.1.1 Formation of imprinted layer on enzyme-containing silica layer

In the first approach, the imprinting protocol was applied without modifications when performing the immobilization of NorVLP in nanopure water and then the imprinting in 25 mM citrate buffer at pH 7, as illustrated in Fig. 4.16.

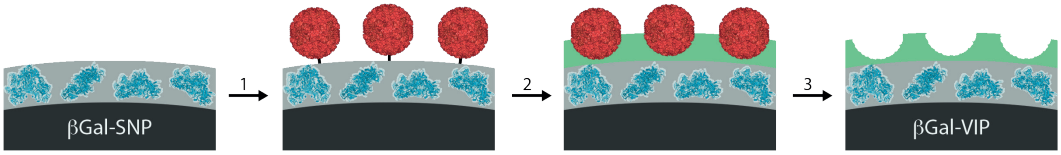

Figure 4.16: Schematic illustration of virus-imprinting directly on βgal-SNPs including Step 1: NorVLP immobilization; Step 2: Recognition layer growth; Step 3: NorVLP Removal

The surface and size of the so-modified βgal-SNPs were characterized by means of FESEM: the formation of the imprinted layer was confirmed by the presence of the characteristic imprints and the increase in diameter by 24 nm on average (Fig. 4.17a). However, after sonication for 20 min, particles with partially or totally removed imprinted layer were found (see Fig. 4.17b); the particles without imprinted layer were identified as βgal-SNPs due to their size of ca. 411 nm, which corresponds to the size of SNP (375 nm) with 18 nm protection layer. It was assumed that the formed silica layer was removed from the βgal-SNPs through sonication.

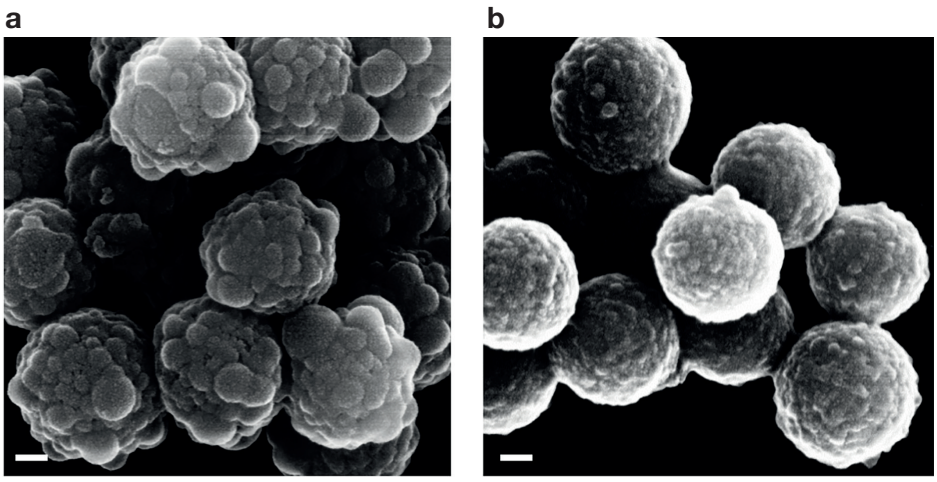

Figure 4.17: NorVLP imprinting directly on βgal-SNPs - FESEM micrographs a) before and b) after sonication) sonication for 20 min; scale bar: 100 nm.

In the previous section, layer removal was attributed to a lack of crosslinking siloxane bonds that stabilize the silica network. In case of βgal-SNPs, it was assumed that there was not sufficient crosslinking between the already present organosilica layer and the newly formed imprinted layer. The previously reported synthesis of NorVLP-imprinted particles was carried out on a smooth silica surface with limited number of amino functions from the immobilization. In contrast to the surface of bare silica, the surface of βgal-SNPs exhibits an organosilica layer with a greater amount of organic functional groups gained from the enzyme entrapment, with high quantities of TEOS and APTES. The organic side of APTES cannot participate in the siloxane formation; consequently, it reduces the number of possible linkages and, thus, represents a dead end for the silica formation.

To circumvent this difference in surface composition, βgal-SNPs were incubated for one hour with TEOS alone to form an ultra-thin silica layer on their surface before proceeding with the

imprinting. The FESEM analysis of the so-prepared particles showed that the majority of them conserved the imprinted layer even after sonication. This result proves the possibility to form two functional silica layers subsequently on the same particle surface. The initial treatment with TEOS was performed for all further imprinting experiments on biocatalytic particles.

4.2.1.2 Stabilization of enzymatic activity during imprinting

One requirement for the detection system was that the enzyme should preserve its biocatalytic function after being embedded in the organosilica layer and after virus imprinting; therefore, the next step was to ensure the enzymatic activity of the imprinted biocatalytic particles. In this context, the imprinting protocol was modified to avoid inactivation of the enzyme as follows:

1. All chemical modifications on the particle surface were carried out in a buffer solution, stabilizing the biocatalytic function.
2. Imprinting process was carried out at pH 6 instead of 7 to avoid inactivation of the enzyme at basic conditions.

The so-modified βgal-SNPs were tested for their enzymatic activity via two different spectrophotometric activity assays (Fig. 4.18).

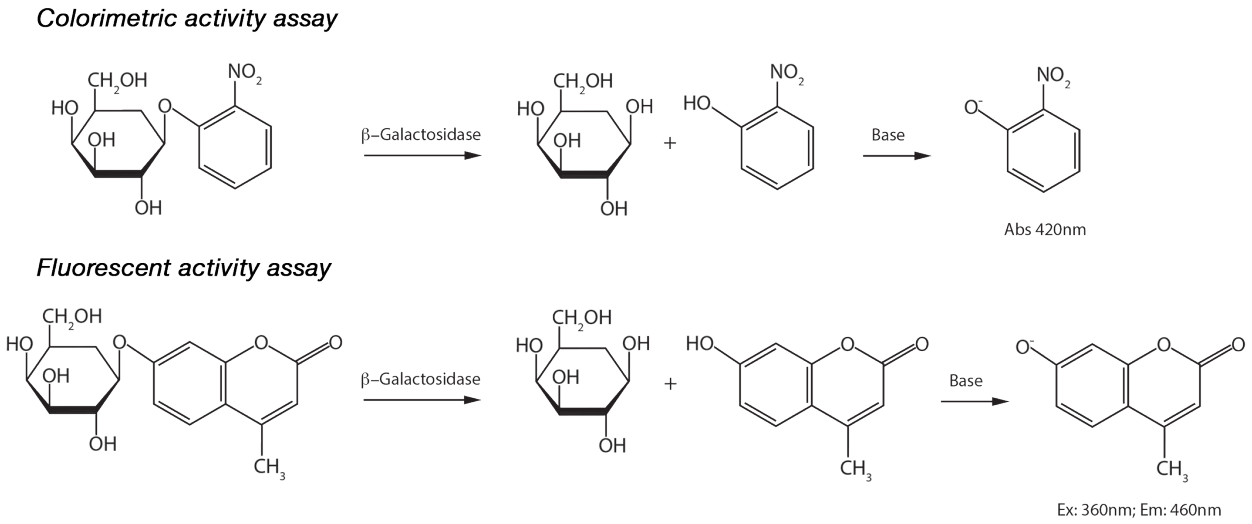

Figure 4.18: β-Galactosidase assays – Colorimetric activity assay with o-nitrophenyl-β-D-galactopyranoside (ONPG) as substrate and fluorescent activity assay with 4-methyl-umbelliferone β-D-galactopyranoside (MUG) as substrate.

As a first test, a colorimetric activity assay was performed, which is based on the conversion of the artificial substrate *o*-nitrophenyl-β-D-galactopyranoside (ONPG) to galactose and 2-nitrophenol. After a defined reaction time, basic conditions were realized by adding sodium carbonate to let the 2-nitrophenolat absorb light at 420 nm; the basic conditions also stopped the enzymatic reaction by inactivating the enzyme. In case of the biocatalytic particles, the reaction was first stopped and then centrifuged to obtain a particle-free supernatant for the measurement of the absorbance.

It was assumed that the activity decreases after virus imprinting, since the recognition layer prevents the substrate uptake by the enzyme, except at the imprints. Indeed, the imprinted βgal-SNPs showed low activity close to the detection limit of the colorimetric activity assay. For this reason, a fluorescence-based assay utilizing substrates that fluoresce upon hydrolysis was employed to provide increased sensitivity. In this assay, 4-methylumbelliferone β-D-galactopyranoside (MUG) was hydrolysed to galactose and to the fluorescent molecule 4-methylumbelliferone (MUB), which can be determined by excitation with a light of 360 nm wavelength and filtration of the emitted light at 460 nm. This conversion can be observed as end-point measurement under basic conditions as well as continuous measurement, giving more details about the enzymatic reaction.

Stabilizing of enzymatic activity during chemical modifications

The β-galactosidase and βgal-SNPs were stored in phosphate buffer at pH 6.5, containing 100 mM potassium phosphate and 5 mM $MgCl_2$. Mg^{+2} is the cofactor for the β-galactosidase and it is bonded tightly inside the enzyme. The leakage of the Mg^{+2} from the β-galactosidase was avoided by adding it in excess during reactions and storage. Because of the high ionic strength of the phosphate ions, the phosphate buffer reduces the reactivity of organosilanes. Therefore, the immobilization and silica entrapment of β-galactosidase were performed in 10 mM MES buffer at pH 6.2 with 5 mM $MgCl_2$, (MES buffer), in order to preserve the biocatalytic functions of βgal-SNPs. The same buffer was applied for the chemical modification steps prior to the imprinting. To understand the reason for the decrease in the enzymatic activity, βgal-SNPs were differently treated. The activities of βgal-SNPs were determined via colorimetric activity assay after each treatment. A portion of the particles was treated with all chemical modifications and washing steps of the imprinting protocol: the enzymatic activity dropped to 7 % and to 0.7 % of starting activity after the first two chemical modifications and washing steps. Another portion of particles was only washed, which included repeated centrifugation and re-suspending: the enzymatic activity dropped to 31 % and to 1.8 % of starting activity after the first and the second washing, respectively.

Thus, the washing alone reduced the enzymatic activity significantly, while the chemical modification contributed additionally to the activity loss. Washing includes centrifugation of the suspended particles, which compressed the particles so that they formed aggregates. The particles probably also remained aggregated during the reaction process in the activity assay. Due to the steric hindrance induced by the aggregates, the substrate cannot pass through to all particles in the inner portion of an aggregate. The limited access to substrate results in a reduced conversion rate even with intact enzyme molecules.

Particle aggregation induced by centrifugation did not occur in the case of bare SNPs that feature a negatively charged surface in water. Therefore, the idea was to add citrate to particle suspension to overlay the particles with a negative charge and thus improve their colloidal stability. As was already used for VLP stability and to reduce silane polycondensation on the VLP

surface during imprinting, the multianionic property of citrate was expected to reduce the formation of aggregates.

A first proof of the effect of citrate could be observed when small aliquots of βgal-SNPs (250 µl, at 3.2 mg/ml) were incubated in different solutions: MES buffer, nanopure water, 25 mM citrate at pH 6, and 25 mM citrate at pH 7 to estimate also the effect of the imprinting conditions on the enzymatic activity. After stirring for one hour at 10 °C and 600 rpm, the activity of the particles was determined via colorimetric activity assay, and is shown in relation to the activity of untreated βgal-SNPs in Fig. 4.19. It can be seen that the enzymatic activity decreased significantly in water (down to 44%) and in MES buffer (down to 43%), while the activity remained high in the solutions containing citrate - 97 % at pH 6 and 94 % at pH 7. These results indicate the assumed effect of citrate, but also that the availability of magnesium ions is less important for the stability of the enzymatic activity than the prevention of particle aggregation. The citrate solution at pH 7 was also tested to estimate the effect of the imprinting conditions on the enzymatic activity.

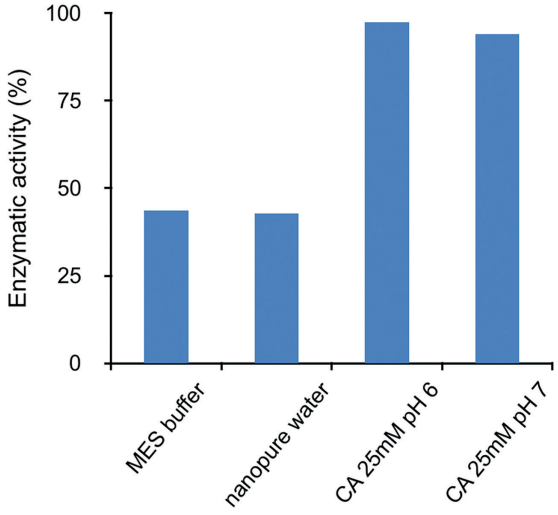

Figure 4.19: Enzymatic activity of βgal-SNPs after incubation for 1 h at different solution.

Based on these results, 10 mM citrate was added to each chemical modification step prior to the imprinting. The enzymatic activity of the so-modified particles was measured via fluorescent activity assay after different modification steps. Their values are shown in direct comparison with the activity of particles that were modified in nanopure water in Figure 4.20 with both data sets in relation to the activity of untreated βgal-SNPs. In the solution containing citrate, activity decreased to 74 % and 55 % after modification with TEOS and APTES, respectively, while in nanopure water, the activity decreased to 41 % and 10 % after the same steps. After performing the modification with glutaraldehyde and template binding, particles showed significantly low activity, close to the detection limit, in both conditions. The reduction of the activity at this step can be attributed to the modification with glutaraldehyde, inducing particle clumping. Nevertheless, at this step, the activity of particles incubated in citrate was higher than that in nanopure water— 5 % against 2 %. These data demonstrate that the addition of citrate improved the activity of modified particles.

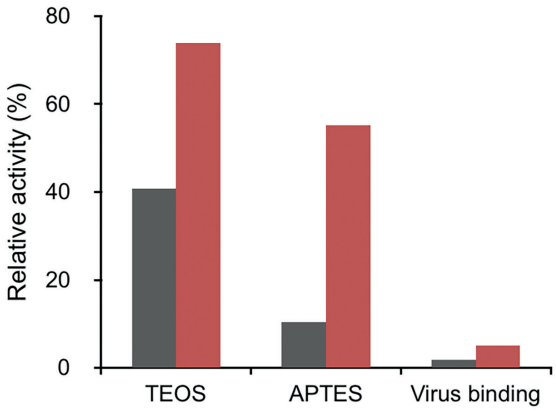

Figure 4.20: Enzymatic activity of βgal-SNPs after modification nanopure water (black) and 10 mM citrate pH 6 (red).

After modifying the βgal-SNPs in 10 mM citrate at pH 6, the immobilization of NorVLP and the subsequent silica formation were performed in 25 mM citrate at pH 7. The so-prepared particles showed a thick layer of 20 nm, with a high number of imprints when they were analysed using FESEM. This observation proves that the addition of citrate did not affect the efficiency of the chemical modification and, thus, the quality of the imprinting.

Stabilizing of enzymatic activity during imprinting

Incubating biocatalytic particles in strong acidic or basic solutions might inactivate the entrapped enzyme. Therefore, conditions with neutral pH values were tested for the imprinting on βgal-SNPs. With regard to the increase of the pH by APTES, the citrate solution, which was at pH 6 for the immobilization of NorVLP, had the final pH value of 7 during the imprinting process. However, performing the imprinting at pH 7 instead of pH 8 reduced the reaction rate of the organosilane polycondensation. Consequently, a significantly longer reaction time of up to 80 h was required to form a sufficiently thick recognition layer.

While performing the imprinting at pH 7, the layer growth on the particles was observed overtime by means of FESEM analysis (Fig. 4.21), and the biocatalytic function of the particles was determined by means of activity assay (Fig. 4.22).

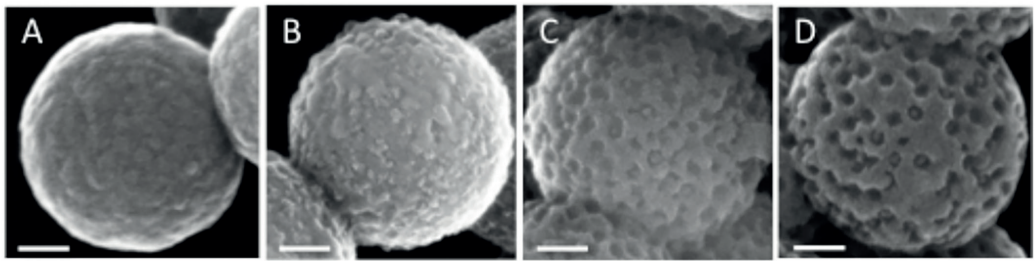

Figure 4.21: Imprinting on βgal-SNP at pH 7 - a) FESEM images after 20 h (A), 40 h (B), 62 h (C) and 88 h (D) of polycondensation reaction; scale bar: 100 nm.

As can be seen from Figure 4.22a, the silica layer increased with an average rate of approximately 7nm per day. Thus, for the first two days, there was a thin layer of 10nm that was partially removed during the sample preparation for the FESEM, affecting the size measurement. As can be seen from Figure 4.22b, the enzymatic activity decreased with an average rate of 23% per day in correlation with the thickness of the silica layer. This correlation gave the first indication that the silica layer affects the enzymatic activity due to the reduced substrate diffusions.

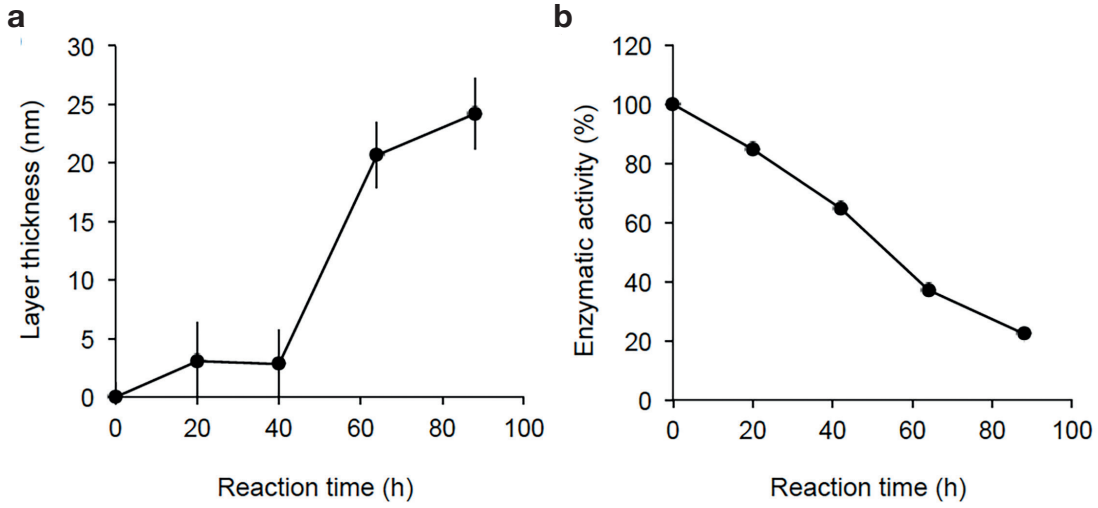

Figure 4.22: Imprinting on βgal-SNP at pH 7 monitored overtime via a) Thickness of silica layer and b) Enzymatic activity in relation to starting activity.

4.2.1.3 Detection of NorVLP by imprinted βgal-SNPs

Finally, particles were synthesized using the two asked functionalities: β-galactosidase activity and NorVLP binding. The first one was demonstrated by the fluorescence activity assay, in which 1mg imprinted βgal-SNPs showed 15% of original enzymatic activity. The second function was carried out in the presence of a 24nm recognition layer visualized by FESEM.

These imprinted βgal-SNP were tested for their use in a detection system, in which the NorVLP binding was transduced into a spectroscopic detectable signal. In this context, the enzymatic activity of these particles was determined in the presence of NorVLP via fluorescence assay (Fig. 4.23).

As shown in Figure 4.23a, there was indeed a decrease in fluorescence signal after the addition of NorVLP. However, as shown in Figure 4.23b, the blank (reaction solution without particles) showed a similarly strong decrease in the signal, too. It can be assumed that the added NorVLP quenched the fluorescence signal of the product. Therefore, the imprinted βgal-SNPs were not used further for the detection system due to incompatibility of the available activity assays with the binding process.

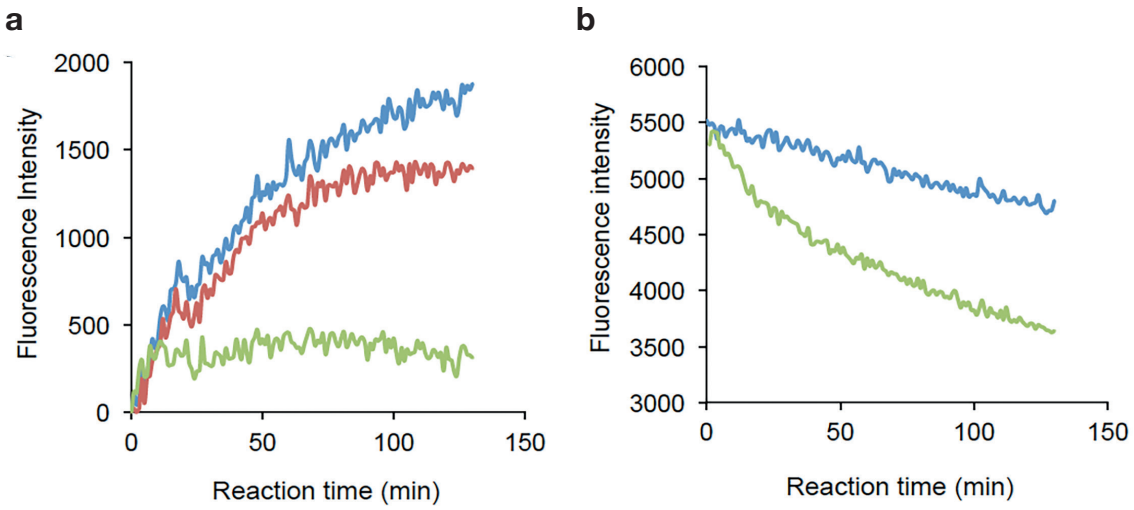

Figure 4.23: NorVLP detection by imprinted βgal-SNP via continuous fluorescence assay – a) Normalized signal by biocatalytic VIPs that were incubated with different concentration of NorVLP: 0 µg/ml (blue), 2.6 µg/ml (red) and 14.6 µg/ml (green); b) Original signal by samples without VIPs (blank) that were incubated with 0 µg/ml (blue) and with 14.6 µg/ml (green) NorVLP.

4.2.2 Enzyme-catalysed colorimetric assay for the detection system

The enzyme acid phosphatase (AP, EC 3.1.3.2) from potato (*Solanum tuberosum*) was chosen for the detection system due to the following reasons:

- High stability
- No cofactor required
- Colorimetric activity assay with high sensitivity
- Enzymatic activity at binding conditions (pH 6)

To measure the activity of AP, a colorimetric activity assay was used, which is based on the conversion of the artificial substrate p-nitrophenyl phosphate (pNPP) to phosphate and 4-nitrophenol (Fig. 4.24). After a defined reaction time, basic conditions were realized by adding sodium carbonate to let the 2-nitrophenolate absorb light at 405 nm; the basic conditions also stopped the enzymatic reaction by inactivating the enzyme. In case of the biocatalytic particles, the reaction was first stopped and then centrifuged to obtain a particle-free supernatant for the measurement of the absorbance.

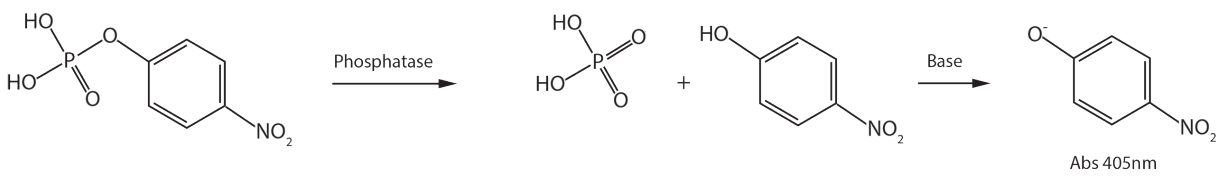

Figure 4.24: Acid phosphatase assay with p-nitrophenyl phosphate as substrate.

Before synthesizing biocatalytic particles with AP, conditions for the activity assay were established to quantify the enzymatic activity via end-point measurements. At first the reaction time in which the production rate correlates with the enzymatic activity was determined. For this purpose, activity assays were performed with different amounts of enzyme and stopped after different time intervals. The absorbance of the product 4-nitrophenolate was measured and transformed to concentration values through a calibration curve of 4-nitrophenolate (ε: 17.8 $mM^{-1}cm^{-1}$, d: 0.6 cm, R^2: 0.999). The unit of the enzymatic activity (U) is defined as the amount of enzyme that hydrolyzes 1 µmol of pNPP per minute at standard conditions.

The measurement results are shown in Fig. 4.25:

a) The higher the enzyme concentration, the faster is the increase in the product concentration, i.e. (in other words) the higher the production rate.

b) The production rate is constant up to 20 min for all enzyme concentration.

c) The production rate of second highest enzyme concentration decreased after 20 min, indicating that the concentration of the substrate is too low (to sustain the reaction); the concentration level was still below the maximum detection limit.

d) The product concentration with the highest enzyme concentration reached the maximum detection limit in 20 min; consequently, no production rate decrease (reaction plateau) could be detected.

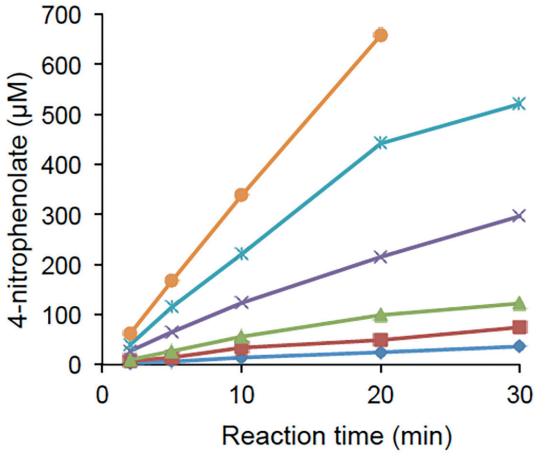

Figure 4.25: Acid phosphatase assay with varying enzyme concentrations - a) Increase of product concentration over time; Enzyme concentration in use: 0.45, 0.9, 1.8, 3.6, 7.3 and 11 µg/ml.

Fig. 4.26 shows that the production rate obtained from a reaction time of 20 min correlates with the enzyme concentration linearly, allowing an enzyme concentration ranging from 0.009 to 0.22 U/ml to be quantified. Additionally, it can be seen that the specific activity of the used enzyme solution was 3 U/mg.One requirement for the quantification of enzymatic activity is that it does not depend on concentration of applied substrate; therefore, substrate was applied in excess to the activity assay.

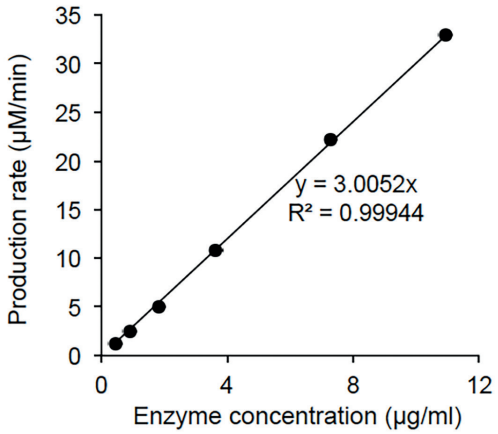

Figure 4.26: Acid phosphatase assay with varying enzyme concentrations - Production concentration at 20 min plotted against the enzyme concentration; Enzyme concentration in use: 0.45, 0.9, 1.8, 3.6, 7.3 and 11 µg/ml.

The substrate independency was controlled through determination of the kinetic constants of the reaction. For the Michaelis constant (K_M) of the substrate pNPP and the maximal velocity at substrate saturation (v_{max}), activity assays were carried out with 0.023 U/ml AP for 10 min at varying concentrations of substrate, ranging from 2 to 18 mM. At high concentrations of pNPP, 4-nitrophenolate was also formed without an enzymatic reaction due to auto-hydrolysis of pNPP. This additional signal was determined by measuring the reaction solution without enzyme (blank) and was subtracted from the signal of the reaction with enzyme. After plotting the product concentration against the substrate concentration (Fig. 4.27), an apparent K_M of 0.25 mM pNPP and v_{max} of 19 µM/min or mU/ml were calculated; the latter correlates with the enzyme concentration of 0.023 U/ml that was used in the assays. All successive assays were carried out with 6mM substrate, which saturated the enzymatic reaction with substrate. After estimating the optimal conditions to measure the enzymatic activity, the next step was the immobilization and entrapment of AP on silica particles.

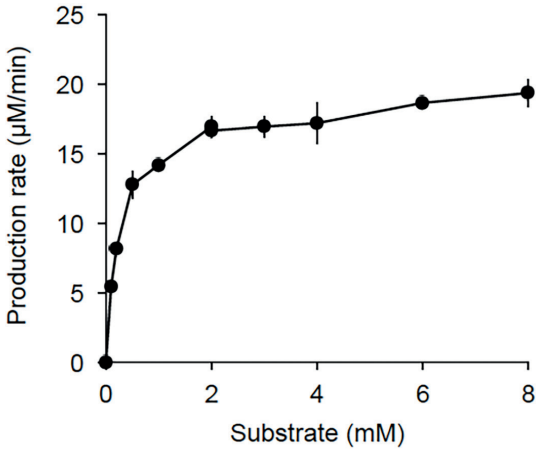

Figure 4.27: Acid phosphatase assay with varying substrate concentrations - Production concentration at 10 min is plotted against the substrate concentration; Enzyme concentration in use: 0.023 U/ml.

4.2.3 Entrapment of AP in silica

To prepare biocatalytic particles for the detection system, AP was first immobilized on SNPs and then entrapped in organosilica formed by the polycondensation of APTES and TEOS, as illustrated in Fig 4.28.

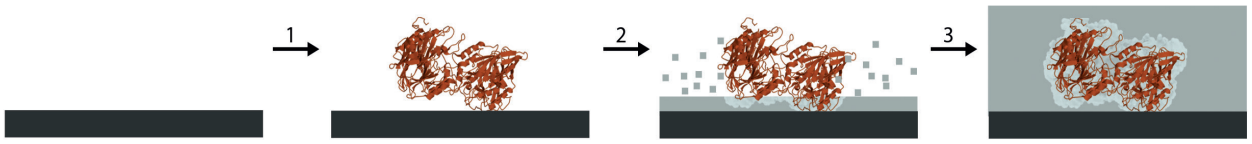

Figure 4.28: Schematic illustration of acid phosphatase (AP) encapsulation including the following steps - Step 1: AP immobilization on SNP; Step 2: Organosilane polycondensation; Step 3: Curing of the final layer completely covering AP

Similar to NorVLP, AP was covalently immobilized through the crosslinker, glutaraldehyde, that connects the amino groups of the protein with the amino-functional groups on the APTES-modified SNPs. The efficiency of the immobilization was evaluated using two values – immobilization yield and activity recovery[16], which are defined as follows:

- Immobilization yield (%) = 100 x [(starting activity - activity in supernatant)/starting activity]
- Activity recovery (%) = 100 x (activity in particle suspension/starting activity)

Both values were determined after separation of particles and unbound enzyme, and were calculated in relation to the starting activity. After AP was immobilized on the silica particles, these were incubated with organosilanes to form the silica layer on the particles surface.

Immobilization and entrapment of AP on silica

As first step for the immobilization of AP, the pH value that allowed the highest immobilization yield on the silica particles was determined. For this purpose, AP (at 32 µg/ml) was incubated with unmodified SNPs (at 3.2 µg/ml) in the following 50 mM buffer solutions: acetate buffer at pH 5 and 5.5, MES buffer at pH 6 and 6.5, and HEPES at pH 7. After 1 h incubation, the unbound AP molecules in solution were separated from the particles through centrifugation and determined via activity assay. The resulting concentrations of AP in solution were used to calculate the AP immobilization yields as described before (Fig. 4.29).

The highest value of 54 % was found at pH 6, while the other pH between 5 and 6.5 had a yield of ca. 40 %; the lowest yield was at pH 7. Generally, the immobilization of proteins is most efficient at the pH values close to IEP of the protein, as the colloidal stability is reduced and less repulsion occurs between the protein molecules. AP is found in the form of varying isoenzymes with slightly different IEP, which might explain the immobilization behaviour of AP.

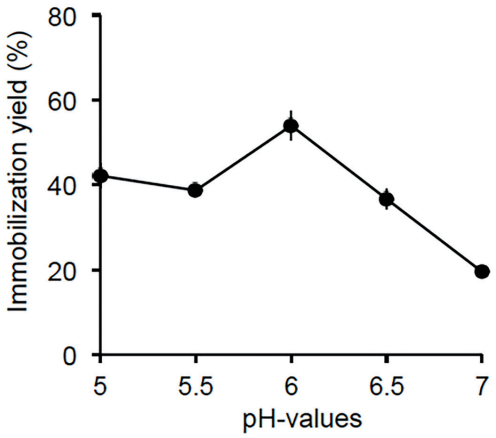

Figure 4.29: Immobilization yield of AP on unmodified SNPs at different pH values.

On the basis of these results, covalent immobilization of AP was tested in nanopure water and in MES buffer, both at pH 6. After 1 h incubation of AP (at 40 µg/ml) and SNPs (at 3.2 µg/ml), supernatant and particles were separated and their enzymatic activity was tested (AC alternative: measured) to obtain immobilization yield and activity recovery, respectively. In nanopure water, the covalent immobilization was very efficient, with an immobilization yield of 96 ± 2 % and an activity recovery of 95 ± 5 %. In MES buffer, the immobilization yield had a value of 99 ± 1 % and an activity recovery of 88 ± 4 %, which was similarly efficient. The values for activity recovery showed high standard deviations because particles could not be completely solubilized in every sample after centrifugation. The particles with immobilized AP on their surface (SNP_{AP}) were incubated with organosilanes for 2 h at 20 °C; FESEM characterization showed particles with different sizes due to variation in the thickness of the formed silica layer from 5nm up to 40nm (Fig. 4.30).

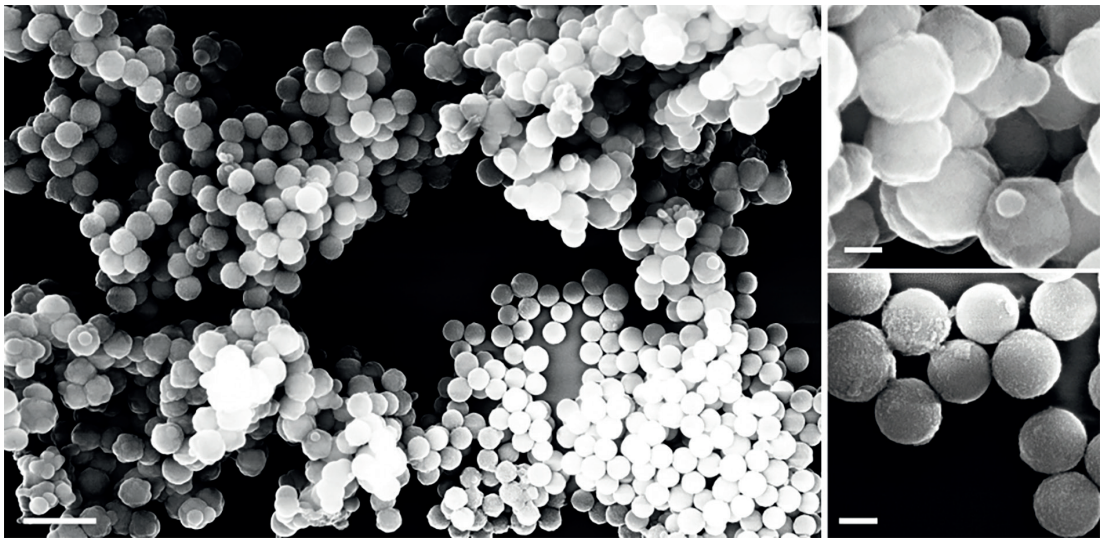

Figure 4.30: Polydispersity of biocatalytic particles - FESEM micrographs of SNP_{AP} after 4 h organosilane polycondensation. Particles with silica layer from 5 nm (right bottom) to 40 nm (right top) can be observed. Scale bars: 1 µm (left) and 200 nm (right), respectively.

The reason for the different thick silica layers was assumed to be a result of particle aggregation, which induced a delayed silica layer growth on some particles. As illustrated in Fig. 4.31, when particles were present in aggregates during organosilanes polycondensation, the added organosilanes in the solution reacted primarily with external particles of the aggregates, leading to a fast silica formation (ca. 20 nm/h). After a thick layer (approximately 30 nm) was formed on the external particles, their solubility was improved, resulting in their separation form the aggregate. Later, the particles in the core of the aggregate could be reached by the organosilanes, also inducing a silica layer growth on them.

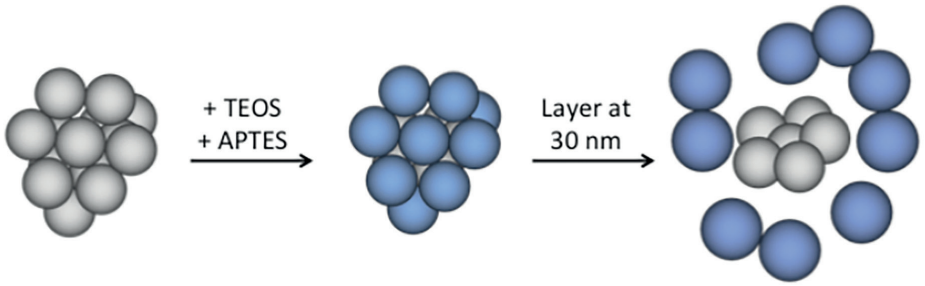

Figure 4.31: Schematic illustration of silica layer formation on aggregated particles: At the begin of the organosilane polycondensation reaction the silica formation occured mainly on particles that were positioned at the outer side of particle aggregates. When the formed silica was around 30 nm thick, they disassembled from the aggregate; unmodified SNP_{AP}, in grey and SNP_{AP} with silica layer in blue.

To have such a significant effect on the silica formation, the particle aggregation took place most probably before adding the organosilanes and, thus, directly after immobilization of the AP. Since no centrifugation was applied between the immobilization and the silica formation reaction, particle aggregation was probably induced by decrease of colloidal stability of the particles. This assumption was strengthened through the measurement of the ζ-potential of the particles before (SNP) and after immobilization of AP (SNP_{AP}).

In nanopure water, SNP_{AP} showed a ζ-potential of 6.90 ± 0.16 mV, a significantly lower ζ-potential than the unmodified SNP with a potential of - 85.2 ± 1.7 mV. In contrast to SNP, SNP_{AP} did not feature a significant high charge to induce repulsion between the particles, avoiding aggregation. To circumvent the formation of aggregates due to low ζ-potential, the idea was to co-immobilize BSA beside AP on the surface of particles. BSA has a similar size as AP, but has an IEP of 4.7.

As with AP, the pH value for immobilization was determined by incubating BSA at 32 µg/ml with unmodified silica particles (at 3.2 mg/ml) in different buffer solutions. The immobilization yield of BSA at different pH values was determined via commercial Bio-Rad® Protein assay based on Bradford, and is shown in Fig. 4.30. The highest immobilization yield value of 74 % for BSA was found at pH 5, which is close to its IEP of 4.7, while the yields were below 30 % at pH values above 5. The reason for the low yields is that BSA has a strong negative charge at pH values above its IEP, thus reducing the contact with the SNP. Therefore, it can be assumed that the co-immobilization of BSA would allow charging the particles negatively at pH 6.

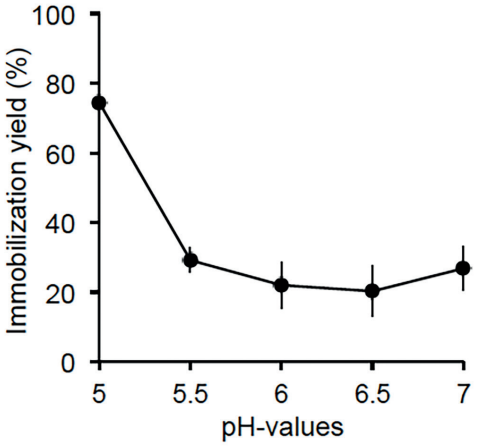

Figure 4.32: Immobilization yield of BSA on unmodified SNPs at different pH values.

Immobilization of AP and BSA on silica

As both AP and BSA could be sufficiently immobilized at pH 5 (AP: 40 %, BSA: 74 %), covalent immobilization of both proteins at 40 µg/ml on SNPs (at 3.2 mg/ml) was carried out in an acetate buffer solution of 50 mM and pH 5 with following variants:

a) AP immobilization and BSA addition after 10 min.

b) BSA immobilization and AP addition after 10 min.

c) AP immobilization without any further protein addition.

All variants were incubated for 30 min in total, after which the enzymatic activity was determined in the supernatant and on the particles. The obtained activity values of all variants are shown in Figure 4.31. As can be seen from Fig. 4.33a, immobilization of BSA before AP reduced the yield by 15 %, as the BSA partially occupied the surface of SNPs. In contrast, the activity recovery through the immobilization of BSA before AP increased significantly - see Fig. 4.33b. It can be thus understood that the activity of the particles depends on the number of immobilized AP and on the degree of aggregation.

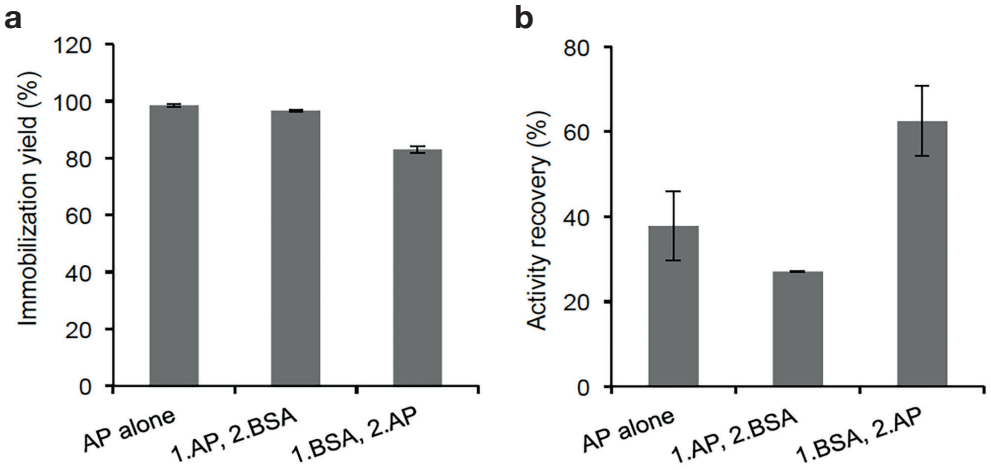

Figure 4.33: Effect of BSA on the immobilization of AP on SNP – a) Immobilization yield: AP activity in supernatant; b) Activity recovery: AP activity on particles.

The aggregate formation was also visualized via FESEM analysis (Fig. 4.34). In the absence of BSA, the particles formed complex aggregates with ca. 20 µm x 4 µm, shortly after AP immobilization. Through co-immobilization of BSA and AP on the particles' surface, the size of aggregates was found to be significantly smaller with dimensions ca. 2 µm x 2 µm. These results demonstrate that particle aggregation can be reduced by the immobilization of BSA on the silica particles before AP. As the measurement of ζ-potential indicated, the effect of the immobilized BSA can be attributed to the increase in the ζ-potential from 6.90 ± 0.16 mV to -24.05 ± 0.92 mV, improving the colloidal stability of the particles.

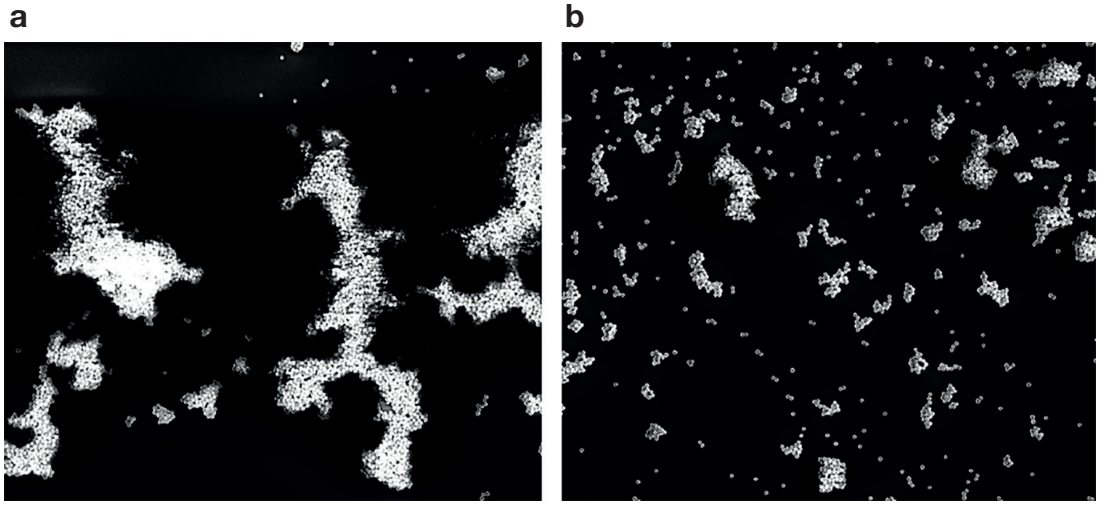

Figure 4.34: Particles aggregation after immobilization - FESEM images of particles after immobilization of AP (a) and particles after co-immobilization of BSA and AP (b). Scale bar: 2 µm.

To increase the immobilization yield of AP, immobilization of BSA and AP was carried out in MES buffer at pH 6 without a delay between the addition of BSA and AP. Also, at this condition, particles with high colloidal stability were obtained because immobilization yield of both proteins was similar as before. Since the aim was to have highly biocatalytic particles, slightly more AP than BSA was added.

At standard conditions - AP at 44 µg/ml (corresponding to 290 U/L), BSA at 27 µg/ml and SNP at 3.2 mg/ml - the supernatant showed an activity of 0.8 ± 0.09 U/L that corresponded to 0.3 % of applied AP, indicating that over 99 % of AP was immobilized on the particles. Additionally, the total protein concentration determined via Biorad protein assay showed that both AP and BSA were immobilized with a yield above 90 %.

Entrapment of AP and BSA in silica

After immobilization of AP and BSA on the surface of SNPs, they were further reacted with TEOS and APTES to entrap the proteins in silica. On the one side, the function of this silica layer is to protect the enzyme against external factors and, on the other side, to offer a smooth layer for the imprinting.

Considering the estimated dimensions of 4 x 6 x 7.5 nm for an AP dimer,[17] and 8 x 8 x 8 nm for a BSA dimer[18], a silica layer should have a thickness of at least 10 nm to fully cover both proteins with silica.

The surface and size of the so-prepared biocatalytic SNPs were characterized by means of FESEM. As can be seen from Fig. 4.35a, the surface of the unmodified SNPs changed from smooth to rough after few hours of reaction. The roughness indicates that the silica formation occurred not only at the surface of the SNP but also at the surface of the immobilized proteins. After continuing the reaction for 4 h, the outer surface of SNP became smooth again because the silica completely covered all proteins without interspaces. As can be seen from Fig. 4.35b, the thickness of the silica layers increased linearly at a rate of 3 nm/h to a maximum thickness of 12 ± 0.9 nm, which was reached after 4 h. At the applied conditions, the thickness did not increase further afterwards due to a reduced polycondensation rate, which is likely induced by the consumption of the APTES and TEOS. Another explanation might be that the proteins have a catalytic effect on the silica formation, which is significantly reduced when the proteins are already covered with silica.

The AP activity during the silica formation was monitored overtime via phosphatase activity assay (Fig. 4.35c). The AP activity dropped from 90 ± 1.2 U/g (U per g SNP) to 11 ± 0.2 U/g concomitantly with the silica formation. This loss in enzymatic activity was also observed when βgal was entrapped in silica and it can be attributed to the high interaction between the silica network and the enzyme, blocking the enzyme in a catalytically inactive state.

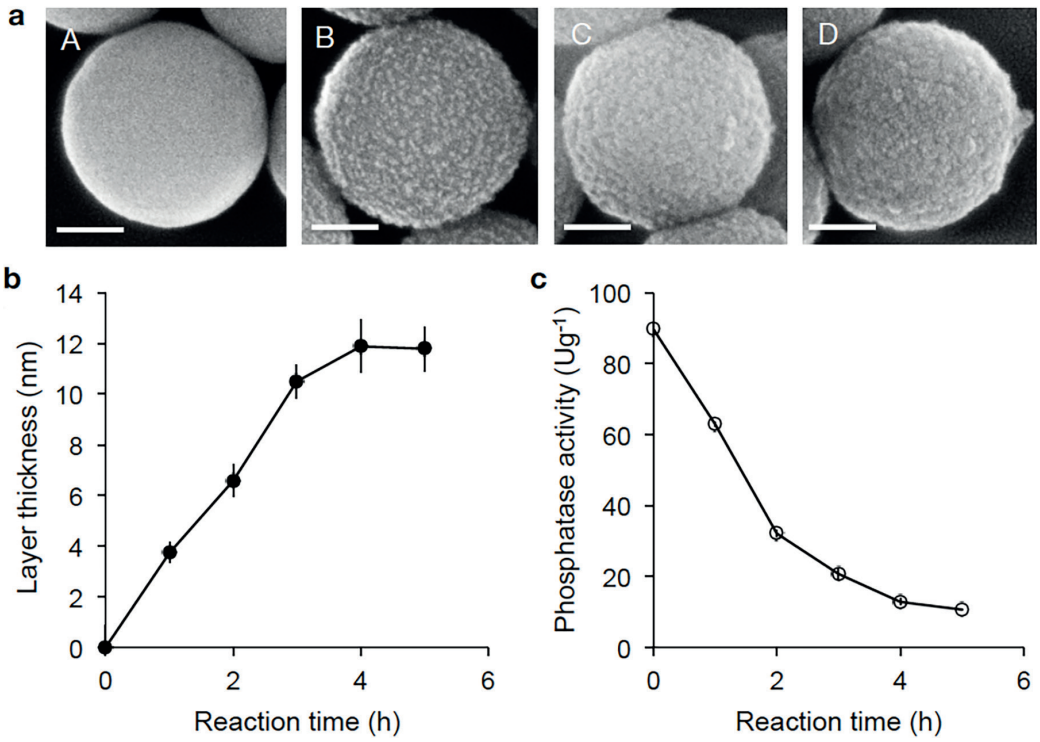

Figure 4.35: Entrapment of BSA and AP in silica – a) FESEM image after 0 h (A), 2 h (B), 3 h (C) and 4 h (D) organosilane polycondensation; Scale bar: 100 nm. b) Silica formation and c) phosphatase activity overtime.

As demonstrated with βgal-particles, applying a curing recovers enzymatic activity through the reorganization of the protective silica layer to a „soft" layer with improved flexibility.[24] Accordingly, the prepared particles after silica formation were incubated at 25 °C for 24 h to induce the curing. Later, the particles with a 12 nm-thick and smooth enzyme-protecting silica layer showed a recovered activity of 32.4 ± 0.4 U/g, which corresponded with 36 % of the phosphatase activity that was immobilized on the particles before the silica formation. These biocatalytic particles were named SNP*cat* and used for the virus imprinting.

4.2.4 Virus-imprinting on biocatalytic particles

Based on the observations described in the feasibility test (section 4.2.1), the imprinting on the SNPcat was performed. As illustrated in Fig. 4.36, the imprinting process included:

1. Modification of the particle surface with TEOS to stabilize the layer connection;
2. Modification with APTES and glutaraldehyde to covalently immobilize NorVLP;
3. Polycondensation of organosilanes to generate the recognition layer;

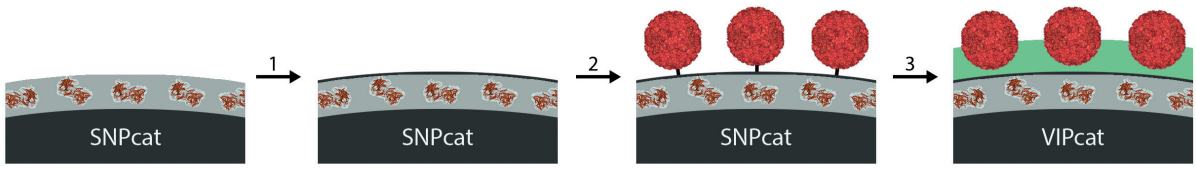

Figure 4.36: Schematic illustration of virus-imprinting on biocatalytic SNPs including Step 1: Modification with TEOS; Step 2: NorVLP immobilization; Step 3: Recognition layer growth.

For a successful imprinting, it was crucial that the biocatalytic particles did not aggregate during the imprinting process to have the surface of all particles exposed to the reacting organosilanes. However, the surface of SNP*cat* presented a mixture of silanol and amino groups, which originated from integrated TEOS and APTES, respectively, and which reduced the colloidal stability of SNPcat significantly.

After the formation of the biocatalytic layer, all proteins, including the BSA that improved the colloidal stability, were covered with silica, which caused the SNP*cat* to clump in clusters after pelleting. Since pelleting also occurred during storage due to gravitation, the storage media had a significant effect on the formation of aggregates during the imprinting process. For instance, a high polydispersity could be observed after imprinting when the SNP*cat* were stored in nanopure water. The polydispersity was significantly reduced when SNP*cat* were stored instead in a citrate solution (50 mM at pH 6).

Considering the findings from section 4.2.1 that showed the improvement in colloidal stability by citrate, all modification steps were performed in 10 mM citrate at pH 6 to avoid aggregation during the imprinting process.

Ad step 1: Modification with TEOS

At this stage of the work, a deeper study was carried out to clarify the effect of the treatment of biocatalytic particles with TEOS before the imprinting process. Therefore, the imprinting on biocatalytic particles was performed with and without the treatment with TEOS to reproduce the previously observed improvement by TEOS in the connection between the biocatalytic layer and the imprinted layer.

The so-prepared imprinted SNP*cat* were treated with ultrasonication to test the stability of the formed imprinted silica layer. The FESEM analysis showed no significant differences between the imprinting with and without the prior treatment with TEOS. The imprinted layer was in both cases stably connected and, therefore, not affected by the treatment with ultrasonication. This observation contradicts the one made during the feasibility test, where the imprinted layer seemed to be removed by ultrasonication. At the time, it was assumed that the modification with TEOS is required to achieve covalent attachment between the enzyme-protecting silica layer and the imprinted layer.

This assumption could not be confirmed with the phosphatase-containing particles, providing another reason for the previously observed loss of the imprinted silica layer.

The presence of biocatalytic particles without imprinted layer after ultrasonication might be explained with the occurrence of particle aggregation during the silica formation as follows:

1. Particles formed aggregates as a result of the washing process.
2. During imprinting, particles in the core of an aggregate remained unmodified because the organosilanes did not react with their surfaces.
3. The treatment with ultra-sonication separated the aggregated particles from each other, releasing the unmodified particles from the core of the aggregate.

Therefore, it appeared from the FESEM analysis that the ultra-sonication induced the removal of the imprinted layer, but actually there was no imprinted layer at all at the beginning of the treatment. The observation in the preliminary tests needs to be interpreted rather as the result of aggregation because the particles were incubated in nanopure water before the imprinting.

The fact that a stable recognition layer was also formed on SNP*cat* without the treatment with TEOS disconfirms the previous assumption that TEOS is required to connect the recognition and the biocatalytic layers.

Nonetheless, the treatment of βgal-SNPs with TEOS reduced the number of non-imprinted particles, which might be explained by an increase in the colloidal stability. The TEOS formed silanol-enriched silica layer on the surface of SNP*cat*, which was negatively charged, thus enhancing the repulsive electrostatic forces among the particles. Indeed, the ζ-potential of SNP*cat* increased slightly from -3.76 ± 0.12 mV to -6.83 ± 0.23 mV through the modification with TEOS. As a result of the modification with TEOS, the degree of aggregation was reduced as well as the number of particles without layer growth at the end of the imprinting.

In combination with the incubation in citrate solution, the degree of aggregation was sufficiently low to obtain a homogenous recognition layer growth.

Ad step 2: Modification with APTES and glutaraldehyde

To covalently immobilize NorVLP for the imprinting, particles were modified with APTES and then with glutaraldehyde, as described in the previous sections – 4.1.1 and 4.2.1.

Ad step 3: Formation of recognition layer

After the modification steps, the immobilization of NorVLP and the imprinting were performed subsequently. It was crucial to choose an adequate pH value for the imprinting to prevent the inactivation of AP by the basic conditions during silica formation. The effect of different pH values on the functionality of AP was determined by stirring SNP*cat* overnight (17 h) in citrate solutions with different pH values at 10 °C, simulating the conditions of imprinting. The enzymatic activity was determined after this incubation and is shown in relation to the starting activity in Fig. 4.37. It can be seen that the SNP*cat* lost their activity partially only after the incubation at pH 8.

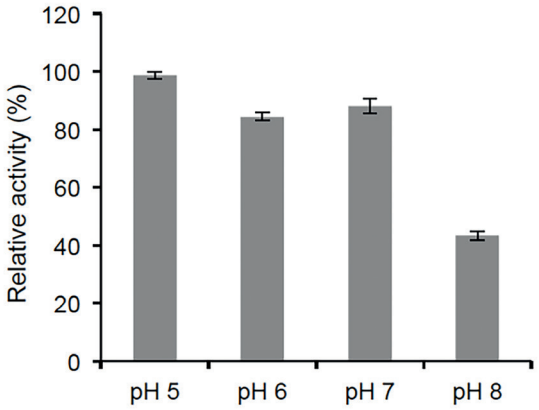

Figure 4.37: Effect of pH value on the activity of SNPcat imprinting conditions

Considering the pH increase induced by the addition of APTES, it was assumed that a starting pH value of 6 preserves the activity of the entrapped AP during the silica formation. Therefore the immobilization and the silica formation were carried out in 25 mM citrate at pH 6. The surface and size of the VIPcat were characterized by means of FESEM: the thicker the layer, the more visible the virus imprints (Fig. 4.38).

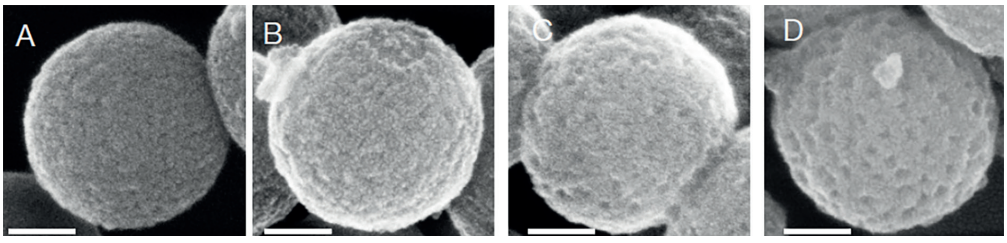

Figure 4.38: NorVLP imprinting on biocatalytic particles observed via FESEM image after 0 h (A), 24 h (B), 48 h (C) and 72 h (D) organosilane polycondensation; Scale bar: 100 nm.

The thickness of the silica layers increased linearly at a rate of 0.25 nm/h to a maximum thickness of 16 ± 0.8 nm after 72 h (Fig.4.39a). The AP activity during the silica formation was monitored via phosphatase activity assay; the activity dropped from 32.4 ± 0.4 U/g to 4.5 ± 0.1 U/g concomitantly with the silica formation (Fig.4.39b). This decrease in activity can be attributed to the thickening silica layer that limited substrate diffusion from the bulk to the catalytic site of the entrapped AP.

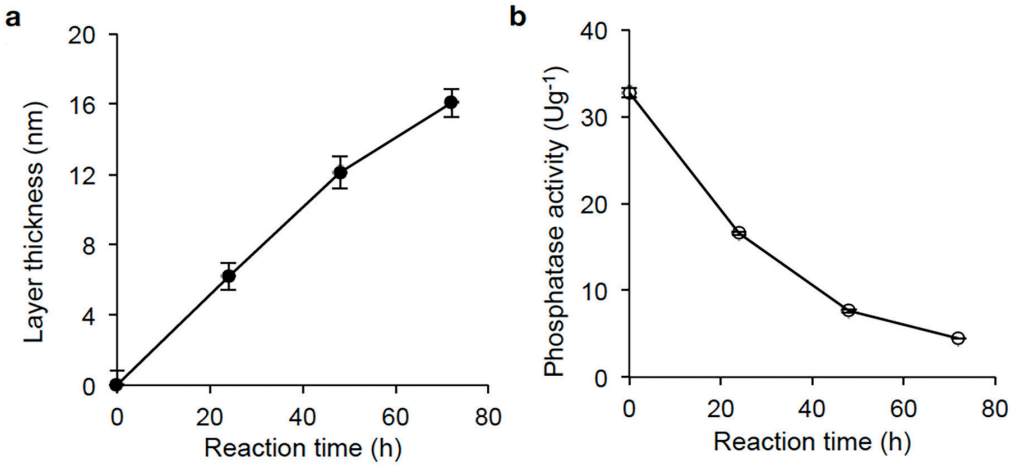

Figure 4.39: NorVLP imprinting on biocatalytic particles via a) Silica formation and b) Phosphatase activity overtime.

The final step to obtain biocatalyitic VIPs (VIP*cat*) was the removal of NorVLP from the particles surface to open the imprints. For this purpose, after curing the particles were treated with ultra-sonication in 0.1 N HCl and 0.1 % Triton X-100 for 30 min.

However, these conditions inactivated the entrapped AP completely, which could be attributed to the very acidic pH of 1.2 induced by HCl. As an alternative for efficient removal of NorVLP, VIP*cat* were treated with ultra-sonication in 50 mM acetate buffer at different pH values.

To evaluate the removal efficiency, the treated particles were incubated at 37 °C for 30 min in a buffer solution that stabilized NorVLP in the solution. The NorVLPs that were not removed during the sonication were partially released from the VIP*cat* during the incubation. The later released NorVLPs were quantified via indirect ELISA (the obtained values are shown in Fig. 4.40a). It can be seen that only the most acidic conditions, 0.1 N HCl and acetate buffer at pH 3, showed no release of remaining NorVLP. In contrast to HCl, the acetate buffer did not inactivate the entrapped AP in VIP*cat*, as can be seen from the activity values of VIPcat after removal in Fig. 4.40b.

After the removal of NorVLP in acetate buffer pH 3, the AP activity of VIP*cat* increased to 12.8 ± 0.2 U/g. This increase is probably a result of emptying the imprints that allowed better diffusion of the substrate to the entrapped AP. This observation correlates with the assumption of the detection system, in which the non-imprinted silica layer prevents substrate uptake, while open imprints give access to the biocatalytic site. Consequently, occupation of the imprints by NorVLP should reduce the substrate uptake and thus the conversion rate of VIP*cat*.

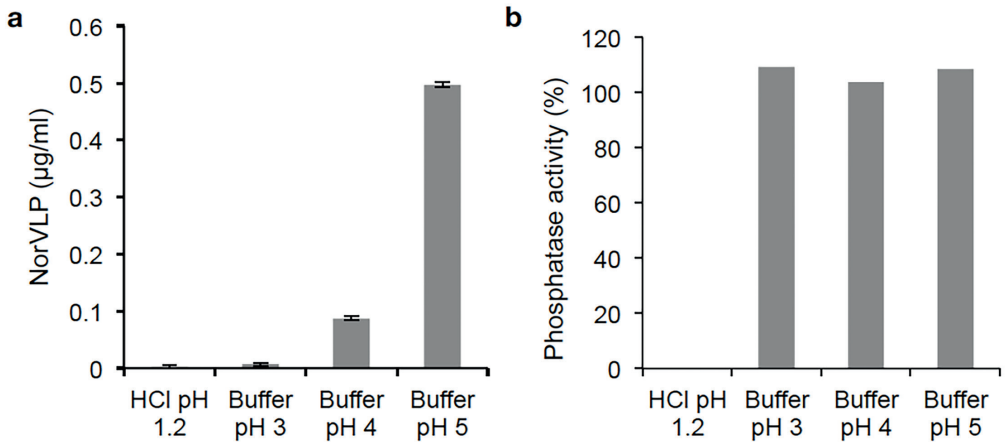

Figure 4.40: Removal of NorVLP at different pH values – a) Concentration of remaining NorVLP on VIP*cat* and b) AP activity of VIP*cat* after performing the removal in acetate buffer at different pH values in relation to untreated particles;

To confirm that the binding of NorVLP on the imprints was the main cause of the decrease in the reaction rate, non-imprinted biocatalytic particles (NIP*cat*) were prepared by following the same synthetic procedure without the addition of NorVLP. The surface and size of the NIP*cat* were characterized by means of FESEM. As the imprinting was performed without a template virus, imprints were not formed on the particles' surface (Fig. 4.41a). The thickness of the silica layers increased linearly at a rate of 0.4 nm/h to a maximum thickness of 18 ± 1 nm, which was reached after 48 h (Fig.4.41b). The AP activity during the silica formation was monitored via phosphatase activity assay; already in the first 20 h of the reaction, the AP activity dropped from 35.1 ± 0.6 U/g to 6.5 ± 0.1 U/g and then further to 1.5 ± 0.1 U/g (Fig.4.41c).

Both the silica formation on the particles and the decrease in activity occurred significantly faster in case of the NIP*cat* than in case of VIP*cat*. One explanation for these results might be the occurrence of particle aggregation during the organosilane polycondensation. As the organosilanes did not react with the particles in the aggregate core, the higher concentration of organosilanes per particle resulted in a faster reaction rate. The reason for the particle aggregation might be that, without the NorVLP as physical obstruction, the distance of modified SNP*cat* could get small enough to allow strong interactions between the particles via glutaraldehyde and APTES. Due to the aggregation, there might also be SNP*cat* without any second silica layer on their surface. The resulting NIP*cat* showed a non-imprinted silica layer of 17.5 ± 0.9 nm and a phosphatase activity of 11.1 ± 0.3 U/g, which is lower than the activity of VIP*cat* with 12.8 ± 0.2 U/g. This result confirmed, on one side, the improved substrate accessibility to the entrapped enzyme through the open imprints, and on the other side, it showed that the additional silica layer over the biocatalytic layer did not completely hamper the substrate diffusion to the entrapped enzyme. However, for the interpretation of the activity values, it has to be considered that the determined activity is the sum of the enzymatic activities of all particles that were present in the reaction mixture. This mixture consisted particles with a partially broken silica layer as well as SNP*cat* without second silica layer, which increased the total phosphatase activity because they did not feature a complete second silica layer, inhibiting their substrate uptake.

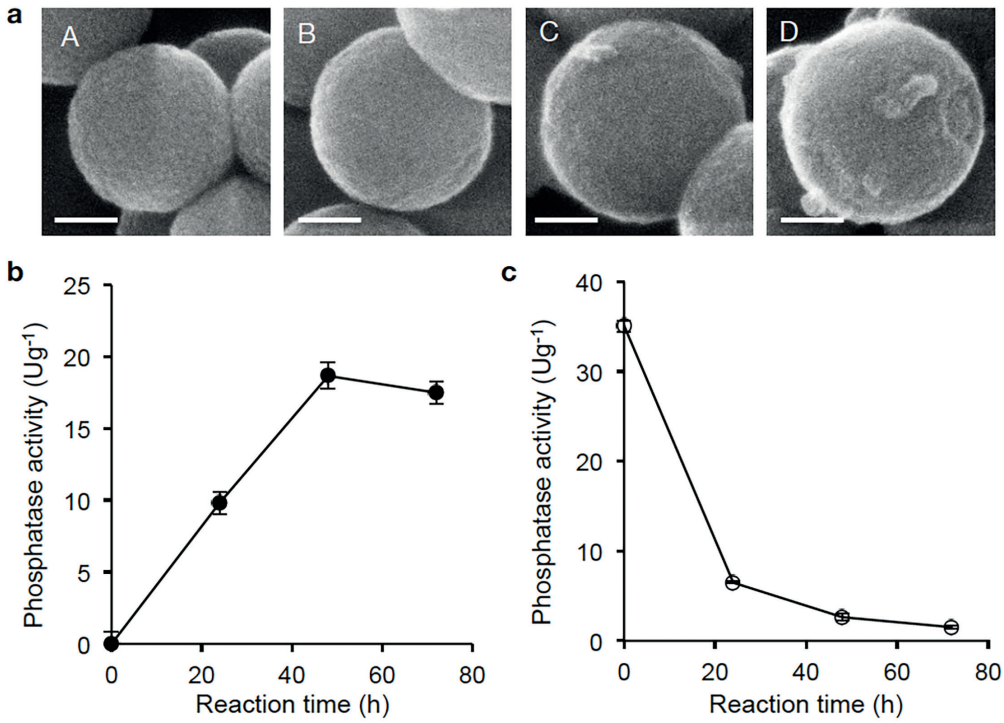

Figure 4.41: Silica layer formation in case of non-imprinted particles – a) FESEM image after 0 h (A), 24 h (B), 48 h (C) and 72 h (D) organosilane polycondensation (Scale bar: 100 nm), b) Silica formation and c) Phosphatase activity overtime.

4.2.5 Detection of NorVLP

VIPcat containing the two requested functionalities – acid phosphatase activity and NorVLP binding – were tested for their use in a detection system. For the proof of concept, it was important to demonstrate the ability of VIP*cat* to transduce the NorVLP binding into a spectroscopic detectable signal. In this context, the effect by NorVLP on the enzymatic activity was estimated by performing the activity assay in the presence of NorVLP.

Assuming that the phosphatase activity decreases when the template virus is bound on the imprints, the application of VIPcat as a detection system was assayed in two different modes, both consisting of NorVLP binding by VIPcat followed by an enzymatic activity assay:

a) Separate: binding and activity assay performed in respectively different conditions

b) Continuous: binding and activity assay performed in the same conditions

Separate mode

The advantage of the separate mode was that the NorVLP binding and the enzymatic reaction were performed in their respective optimal conditions. First, the binding assay was performed as described in section 4.1.3. Then VIP*cat* were separated from the unbound NorVLP through centrifugation and then re-suspended in the conditions for the activity assay that was performed directly afterwards.

The requirement for the detection of NorVLP was that the NorVLP remained bound at the imprints during the activity assay. In this context, the amount of unbound NorVLP was quantified via indirect ELISA after performing the binding assay and when performing the activity assay to monitor a possible release of NorVLP. It was found that VIP*cat* at 0.8 mg/ml bound 75 % of the added NorVLP at 3.6 mg/ml; this binding efficiency correlates with the one found for VIPs in section 4.1.2. After re-suspending the VIP*cat*, 50 % of the previously bound NorVLP were released. But during the activity assay, the NorVLP remained bound on the VIP*cat*. The release of NorVLP through the re-suspending seems quite reproducible, thereby mainly affecting the sensitivity of the detection system. In conclusion, approximately 40 % of the NorVLP that was present during the binding assay was bound on the VIP*cat* during the activity assay, blocking the substrate uptake.

After performing the detection assay with the separation step, a slight decrease of 11 % could be observed in the activity, as shown in Fig. 4.42.

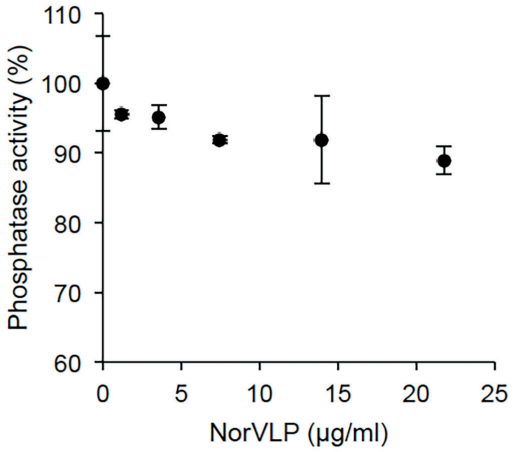

Figure 4.42: Effect of NorVLP on the phosphatase activity of VIP*cat* in the separate mode

However, the determined standard errors indicate a low reproducibility of this assay. The main reason for the low reproducibility could be the separation step, which consists of centrifugation and re-suspending. Centrifugation induces the aggregation of particle, while re-suspending the partly released previously bound NorVLP, but might also break the recognition layer. These factors also affect the activity of the non-imprinted.

Continuous mode

Based on the assumption that only bound NorVLP inhibits the enzymatic reaction, a detection assay was tested without separating the binding process and enzymatic reaction. As illustrated in Figure 4.43, VIP*cat* were first mixed with varying concentrations of NorVLP and then aliquoted in a transparent and flat microtiter plate. The AP substrate was added to the aliquots and was converted by the biocatalytic layer when the pNPP reached the biocatalytic site via the imprints. This conversion was determined by continuously measuring the absorbance of the formed 4-nitrophenolate at 405 nm overtime.

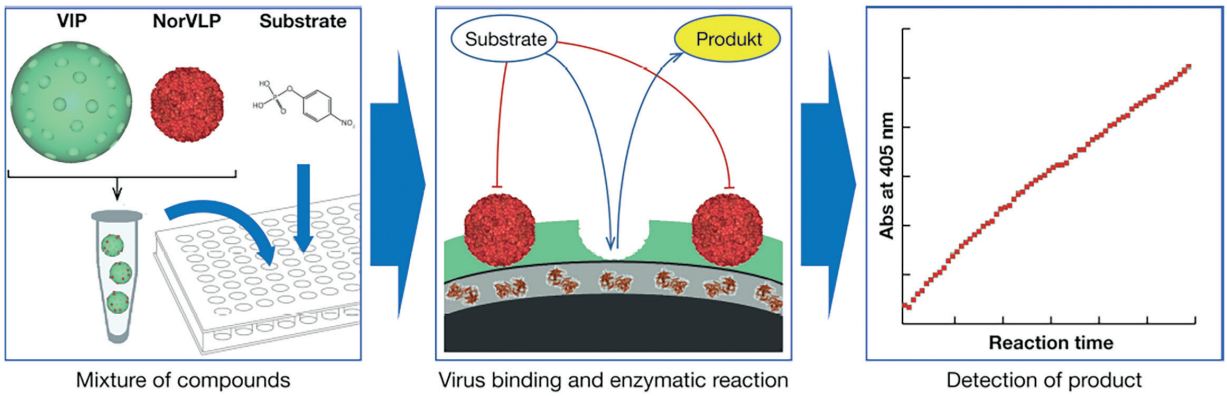

Figure 4.43: Schematic illustration of the detection assay in continuous mode.

As there was no separation, the measurement of the activity differed radically from the former performed activity assays for the following reasons.

a) The reaction was continuously observed, giving details about the reaction process;

b) Silica particles remained in solution during the measurement of the absorbance;

c) Basic pH value were not applied to maximize the light absorbance of 4-nitrophenolate;

d) Reaction solution was not stirred;

One consequence was that the measured absorbance was significantly lower than in the original activity assay protocol, in which the particles were removed after stopping the reaction with a strong base. Since stirring/mixing was not possible during the continuous measurement, diffusion of the substrate was reduced and, thus, its conversion. Besides this, the silica particles pelleted to the ground of the well. To avoid the effect of pelleting on the light transmission for the absorbance measurement, low concentration of particles were used. Additionally, the reaction was performed in MES-buffer at pH 6, instead of acetate buffer at pH 5 to allow binding of NorVLP. In sum, low conversion rates were expected and, thus, long incubation times were required to determine a NorVLP effect on the activity. After performing the detection of NorVLP with this continuous assay, the collected absorbance curves showed three distinguishable phases for the reaction process (Fig. 4.44).

Phase 1: Equilibration of the reaction conditions (Equilibration phase)

In the first hour of the reaction process, strong variations in the curves were observed. In most cases, the signal decreased shortly and then increased steadily. As the signal is determined directly after mixing the substrate with the particle suspension, it was assumed that the signal is affected from the movement of the particles that scatter the transmitted light. Since the reaction mixture was not stirred during the measurement, the particles would stop moving after a while, remaining either in suspension as „sol" or pelleted on the bottom of the well. The scattering by the particles then remained constant over the whole measurement and could be subtracted from the signal as background noise.

Phase 2: Rebinding of NorVLP and substrate diffusion (Diffusion phase)

Although the particles were incubated with NorVLP before starting the enzymatic reaction, not all of the present NorVLP can be bound in the imprints at this state. It is also possible that weakly bound NorVLP were removed from the surface of the particles through the mixing with the substrate. With still unbound NorVLP in the reaction mixture, both NorVLP binding and enzymatic reaction might occur at the same time. Therefore, the observed signal increase seemed to be not affected by the presented NorVLP. At a certain point, NorVLP binding was completely bound and affected the enzymatic reaction significantly, indicating the start of the third phase.

Phase 3: Inhibition of substrate diffusion (Inhibition phase)

Depending on the number of occupied imprints, the reaction rate decreased because the amount of substrate that reached the enzyme was reduced though the occupation. At this phase, which started after ca. 400 min, the difference in reaction rate was observed to be the highest and depended more significantly on the present NorVLP concentration than in the previous phases.

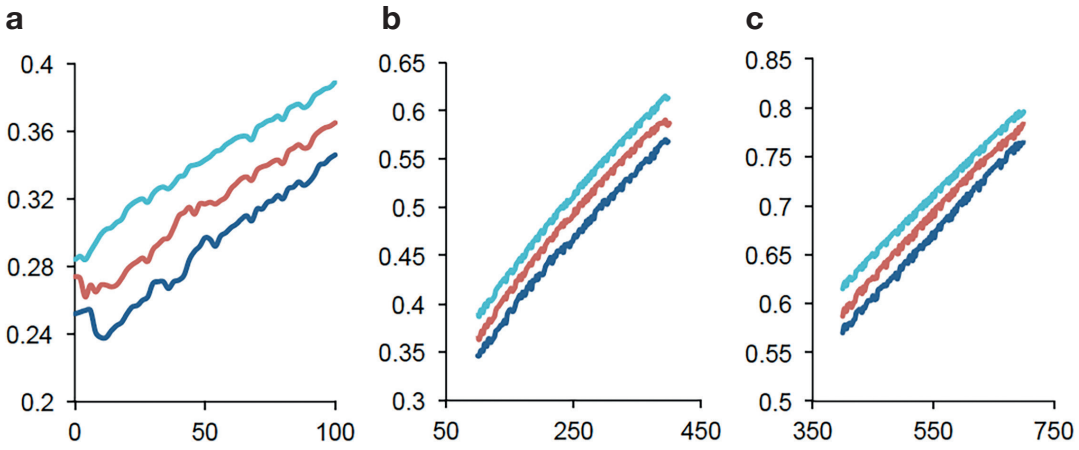

Figure 4.44: Representative production curves of VIP*cat* with 0 (blue), 6 (red) and 12 µg/ml (cyan) NorVLP separated into three distinguishable phases: a) Equilibration phase, b) Diffusion phase and c) Inhibition phase; x-axis: Reaction time in min, y-axis: Absorbance at 406 nm.

The normalization of the production curves, so that all curves start at 400 min with zero absorbance, allowed better visualization of the decrease in the reaction rate by the present NorVLP (Fig.4.45a). The phosphatase activity from the third phase of the reaction process (400 to 700 min) plotted against the NorVLP concentration (Fig. 4.45b) showed a linear correlation (R^2: 0.9934) up to 1 nM. This observation indicates that the NorVLP occupied the imprints, reducing the substrate uptake and, thus, the reaction rate. After increasing the NorVLP further up to 2.6 nM, the activity values remained constant, indicating that all imprints were occupied with NorVLP.

These data prove that reaction rate depend on the number of open imprints that were not occupied with NorVLP, because the substrate reached the biocatalyitc site better at the open imprints. However, the activity of NIP*cat* already indicated that substrate uptake does not occur only via the imprints.

After occupying all imprints, still 88 % of the total activity was found, indicating that substrate uptake was not completely blocked by the bound NorVLP. This remaining activity can be interpreted as background activity that was found to vary slightly from batch to batch. Since this activity was a result of the substrate diffusion through partially broken silica layer, its intensity depended on the degree of layer rupture that occurred during the removal of NorVLP.

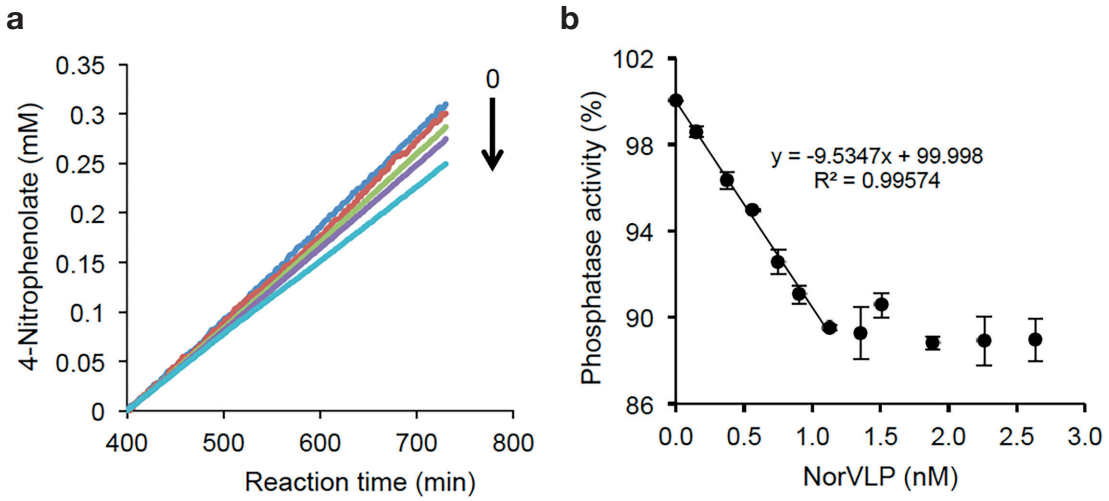

Figure 4.45: Effect of NorVLP on the phosphatase activity of VIP*cat* - a) Representative curves of the product concentration obtained at different NorVLP concentrations; b) Phosphatase activity at different NorVLP concentrations in relation to activity obtained without NorVLP with standard deviation from four measurements.

The function of the imprinted layer as a linker between the enzymatic reaction and the binding process was determined by evaluation of the NorVLP effects on the activity of SNP*cat* and NIP*cat*. The phosphatase activities of SNP*cat* and NIP*cat* were determined under the same reaction conditions as VIP*cat* and are shown in direct comparison in Fig. 4.46. In contrast to the VIP*cat*, the presence of NorVLP did not affect the activities of both SNP*cat* and NIP*cat*. These results indicate that the correlation between reaction rate and NorVLP concentration was achieved through the presence of the imprinted layer.

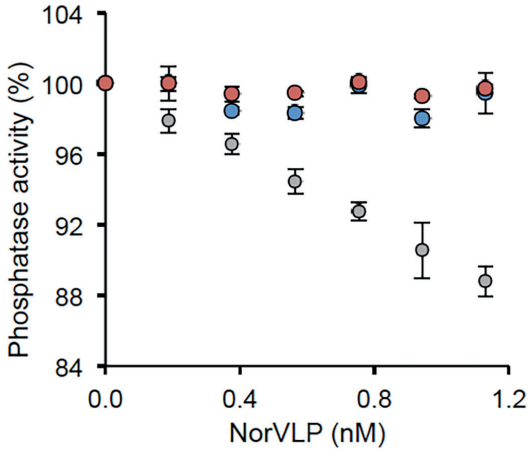

Figure 4.46: Effect of NorVLP on the activity of NIP*cat* (blue) and SNP*cat* (red) - Phosphatase activities at different NorVLP concentrations in relation to activity obtained without NorVLP with standard deviation from four measurements in comparison with the data obtained from VIP*cat* (grey).

The specificity of the developed detection system was tested by applying a non-template virus that is similar to NorVLP in shape (icosahedral) and size (30 to 40 nm). In this context, the effect of the plant virus, turnip yellow mosaic virus (TYMV), on the phosphatase activity of VIP*cat* was assayed. The activity values in the presence of increasing concentration of TYMV and NorVLP, respectively, are shown in Fig. 4.47. In comparison with the template virus NorVLP, the same concentrations of TYMV did not affect the activity of the VIP*cat* at all. This result indicates the specific binding of the template virus through the imprints, allowing the detection assay to respond specifically to the template virus.

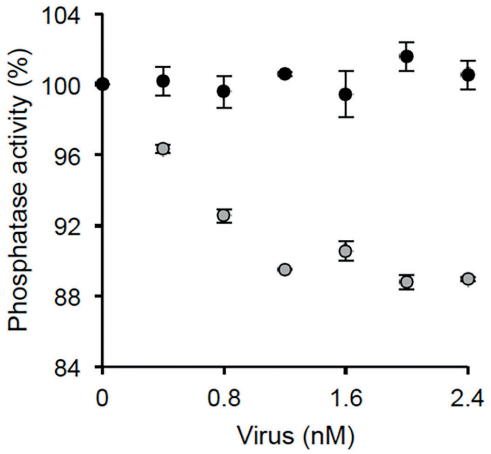

Figure 4.47: Effect of plant virus on the activity of VIP*cat* - Phosphatase activity of VIP*cat* at different concentration of TYMV (black) and NorVLP (grey), resp. in relation to activity obtained without virus with standard deviation from four measurements.

4.2.6 Proof of concept for colorimetric transduction system

Two different methods to functionalize silica – entrapment and imprinting – were combined to form a novel transduction system for detection. In this transduction system, the presence of a target molecule was visualized with a colorimetric enzymatic reaction, which is commonly also used in other detection systems such as ELISA. What is innovative in the presented transduction system is how the correlation between enzymatic activity and target molecule was generated. The key word to describe the principle of transduction is „steric inhibition": the target molecule sterically inhibits the enzymatic reaction. Steric inhibition by the binding of an icosahedral virus is possible through the size of the virus molecule as this is sufficiently high to induce a significant reduction in the substrate uptake by the enzyme, which can be detected.

This silica-based transduction system for detection was based on the following assumptions, which were all confirmed in the frame of this work:

1. The selected enzyme preserves its biocatalytic function when entrapped in the silica layer.
2. The recognition layer hampers substrate uptake by the enzyme, except at the open imprints.
3. Blocking the imprints by the binding of the target virus decreases the enzymatic activity.

First of all, the silica, which was generated by the condensation of TEOS and APTES, allows the enzyme to preserve its activity. The hydrophilic and „soft" surrounding provided by the silica enables sufficient enzyme flexibility for the catalytic reaction or the regeneration of the catalytic site. In case of acid phosphatase (AP), 36 % of the original activity remained active in a silica layer of 12 nm thickness. The full activity could not be preserved because the catalytic site of the enzyme might be partly blocked in a non-active state or be covered with excessive silica, reducing the substrate diffusion; the latter condition seems logical, considering the dimensions of 4 x 6 x 7.5 nm for an AP dimer.

With the increase in the silica layer above the enzyme with the formation of the recognition layer, the substrate needed to pass through the silica layer for a longer distance. As a result of the reduced substrate diffusion, the reaction rate of the AP was reduced. This effect of the growing silica layer was observed during the imprinting; the activity decreased to 5 % of the original activity. Opening the imprints through the removal of the template virus increased the accessibility of the substrate to the enzyme: the activity increased to 14 % of the original activity. These observations confirmed the second assumption because the recognition layer hampered the substrate uptake by the enzyme, except at the open imprints.

At last, conditions were found that allow observing the decrease of the enzymatic activity in linear correlation to the added NorVLP. As this effect by NorVLP was only observed in case of imprinted particles, it was demonstrate that the imprints were the linker between the NorVLP concentration and enzymatic activity. Blocking the imprints by NorVLP reduced the substrate uptake by the enzyme, confirming steric inhibition of the enzymatic reaction. A non-template virus, such as TYMV, did not cause a decrease in the activity of VIPcat, indicating that only specific binding on the imprints induced steric inhibition of the enzymatic reaction. These results demonstrated that the developed VIP*cat* worked properly as transduction system for the specific quantification of viruses.

An outstanding feature of the detection system using VIP*cat* is that the quantification can be performed without preliminary separation of the bound and unbound virus. As the detection assay consists simply of mixing VIP*cat* firstly with the sample and then with the substrate, the time required for detection depends mainly on the enzymatic reaction. In the actual state of the assay, the enzymatic reaction with 12 h of incubation for a sufficiently high signal gives room for improvement. Nevertheless, the possibility to perform the detection without any laborious washing or separation steps presents the tremendous advantage of the usage of VIP*cat* compared to established binding-based methods such as ELISA. By reducing the number of steps, the number of required devices decreases, resulting in an easily usable detection device that is highly relevant for point-of-care diagnostics.

In conclusion, the combination of two functionally different silica layers provides a new type of transduction system for the detection of viruses in form of a colorimetric one-step assay.

4.3 Fluorescent imprinted particles

In this section, the second transduction system that applies fluorescence to visualize the binding of NorVLP is presented: it is based on quenching that is induced by the NorVLP when it is bound by the imprints and thus gets close to a fluorescence dye. The degree of quenching correlates with the amount of bound NorVLP, thus allowing the quantification of NorVLP.

4.3.1 Synthesis concept for fluorescent VIPs

To locate fluorescence dyes on the imprints for quenching, a new synthesis protocol was developed. As illustrated in Fig. 4.48, the protocol consists of the following steps:

1. Immobilization of NorVLP on silica nanoparticles (SNP);
2. Integration of a fluorescence dye in an inactive state into the recognition layer;
3. Covering the fluorescent recognition layer with another silica layer;
4. Removal of template virus;
5. Activation of the surface exposed fluorescence dye at the imprints.

The detailed procedure, spanning from the integration of the fluorescence dye to the locally activation, has been described in the following sections.

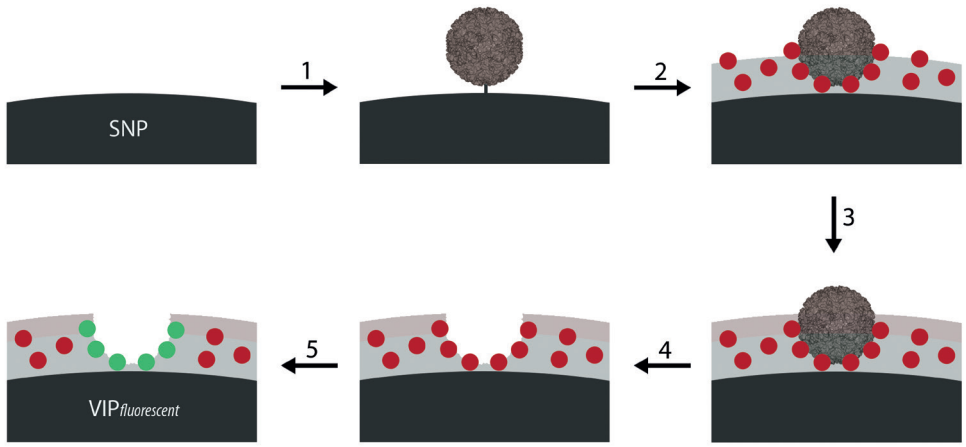

Figure 4.48: Schematic illustration of synthesis concept.

4.3.2 Integration of fluorescence dye into recognition layer

For the synthesis of fluorescent VIP, the green fluorescence dye, fluorescein, was used because it can be reversibly „inactivated". For instance, conjugation of acetyl groups as esters on the xanthene group renders the dye non-fluorescent.[19] Removing these esters through hydrolysis results in the recovery of the fluorescence properties of fluorescein.[20]

4.3.2.1 Preparation of fluorescence dyes for integration

Fluorescence dye can be integrated into silica by conjugation with APTES at its amino-functionalized site, while its silane-functionalized site remains unchanged for later crosslinking.[21-24] To yield active and inactive fluorescein, respectively, fluorescein was first conjugated with APTES and then acetylated, as illustrated in Fig. 4.49.

As described by Feng et al.[21], fluorescein isothiocyanate (FITC) was conjugated with APTES by an addition reaction of the amine group of APTES with isothiocyanate of FITC. For this work, 600 mg of FITC dye was reacted in anhydrous ethanol with an excess of APTES for 6 h under a dry nitrogen atmosphere and protected from light. From the reaction mixture, FITC-APTES conjugate was purified with a yield of 26 %.

The synthesis of the APTES-conjugated fluorescein diacetate (FDA-APTES) was carried out through adjusting common protocols for esterification on the properties of the silane-functionalized fluorescein. For this work, 120 mg of FITC-APTES dye was reacted with 56 µl acetyl chloride in DMF overnight at room temperature using 4-Dimethylaminopyridine (DMAP) as nucleophilic catalyst for the esterification. During the reaction, the fluorescence and colour decreased significantly, indicating quenching by the acetylation. From the reaction mixture, FDA-APTES conjugate was purified with a yield of 3 %.

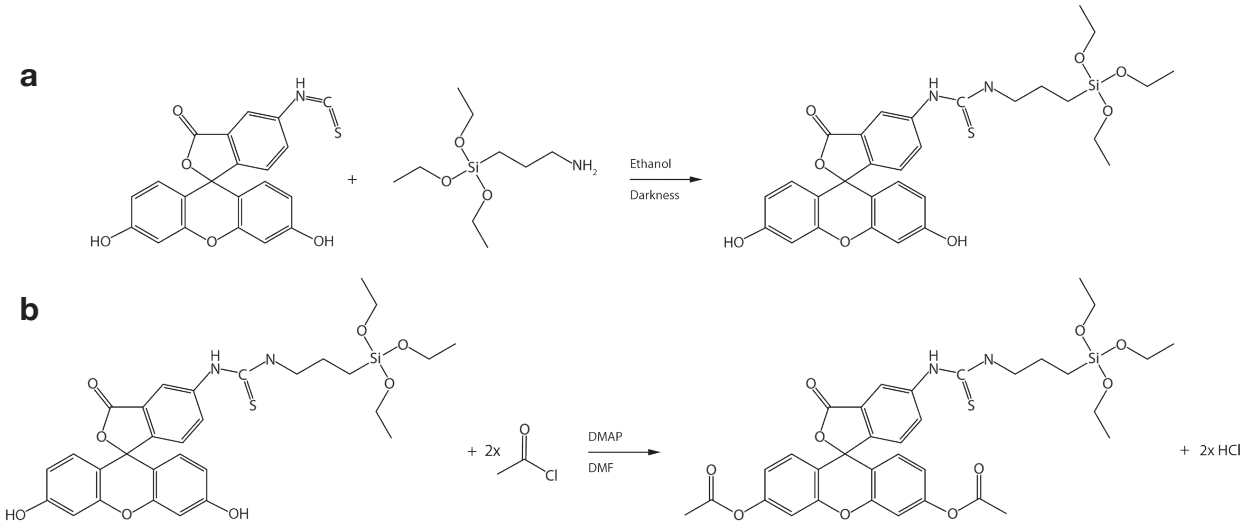

Figure 4.49: Schema for synthesis of the conjugates: FITC-APTES (a) and FDA-ITC-APTES (b).

The yielded fluorescein-conjugates - fluorescein-APTES and FDA-APTES - were characterized via their fluorescence properties in water. Thereby, absorbance spectra, emission spectra and excitation spectra were collected (Fig. 4.50). As shown in absorbance spectrum (Fig. 4.50a), both fluorescein-conjugates feature an absorbance at 490 nm. Measuring the emission spectra with the excitation wavelength (λ_{EX}) at 485 nm demonstrates the fluorescence signal with maximal intensity at the emission wavelength (λ_{EM}) at 520 nm (Fig. 4.50b). Measuring the excitation spectrum with the λ_{EM} at 515 nm confirms the absorption/excitation maximum at 490 nm (Fig. 4.50c).

The absorption maximum at 490 nm and emission maximum at 520 nm fits with the values found in literature - 494 nm and 512 nm, respectively. In case of fluorescein-APTES, the intensities of both absorbed and emitted light was significantly high, while in case of FDA-APTES, very small peaks were observed, indicating the quenching by the ester groups. The direct comparison of the fluorescein-conjugates at the same molar concentration shows that the fluorescence signal by fluorescein-APTES was 10-fold higher than the signal by FDA-APTES (Fig. 4.50d).

In the following experiments, fluorescence measurement were carried out with the excitation wavelength (λ_{EX}) at 490 nm and the emission wavelength (λ_{EM}) at 520 nm.

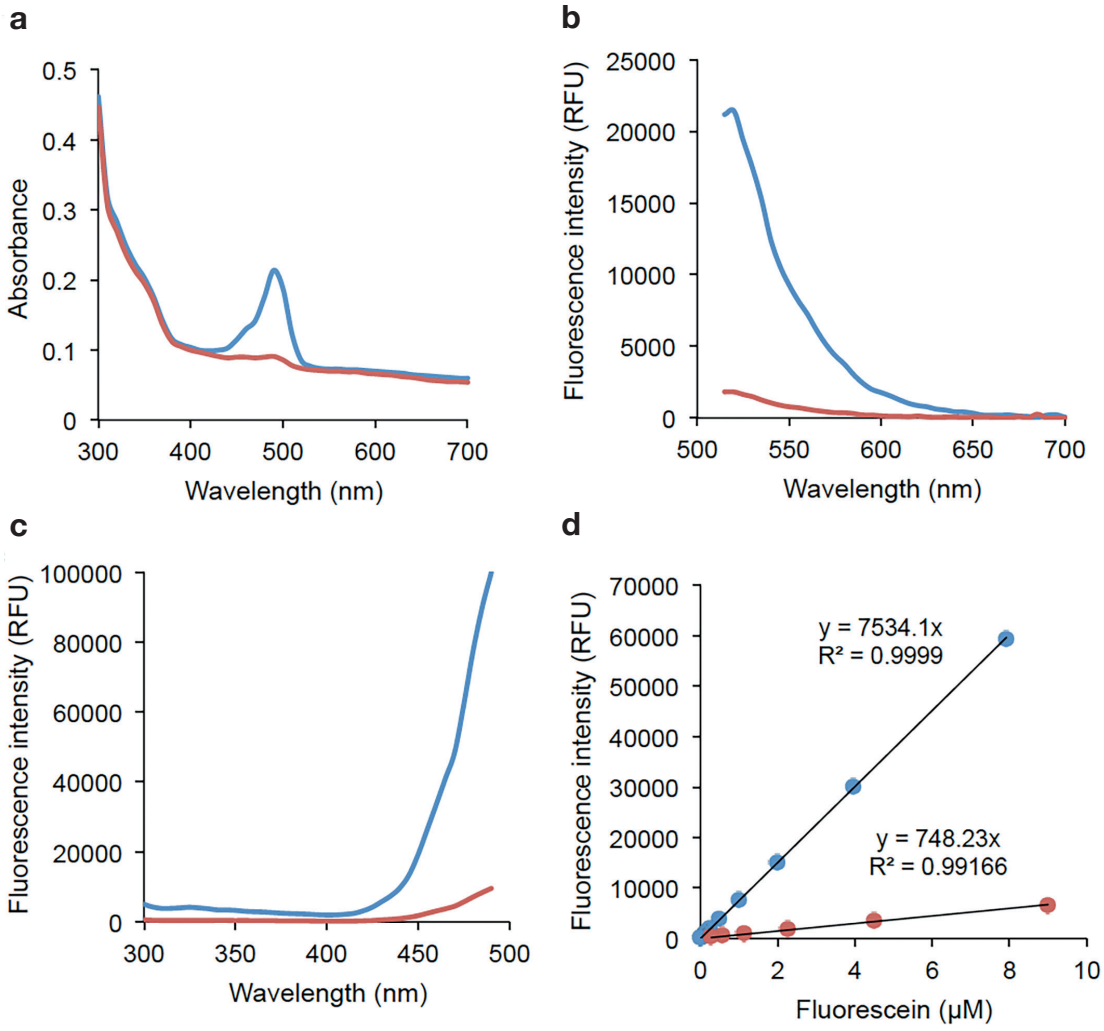

Figure 4.50: Fluorescence properties of fluorescein-conjugates – a) Absorbance spectra b) Emission spectra and c) Excitation spectra of fluorescein-conjugates showing maximal absorbance/excitation at 490 nm and emission at 520 nm; d) Fluorescence intensity per µM of fluorescein-conjugate (blue) and FDA-conjugate (red).

4.3.2.2 Preparation of recognition layer with fluorescent dyes

Fluorescent VIPs were prepared by performing the NorVLP-imprinting, as described in section 4.1, with the addition of the respective fluorescein-conjugates – fluorescein-APTES and

FDA-APTES. After immobilization of NorVLP, particles were subsequently reacted with TEOS, fluorescein-conjugate and then with APTES to form the recognition layer.

The surface and size of the imprinted particles were characterized by means of FESEM: the thickness of the silica layers increased linearly at a rate of 2.3 nm/h to a maximum thickness of 14 ± 0.9 nm after 6 h in case of both fluorescein-conjugate (Fig 4.51a). When the active fluorescein-APTES was applied, the integration of fluorescein was observed by fluorescence measurements of the particle suspension; the fluorescence signal of the particles increased during the recognition layer growth as fluorescein-APTES was incorporated into the silica layer by the organosilane polycondensation (Fig. 4.51b).

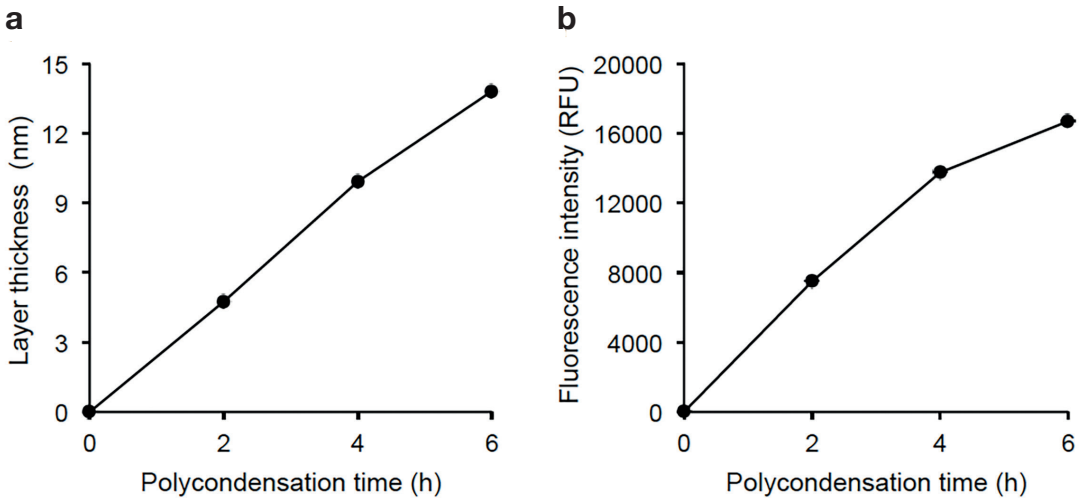

Figure 4.51: Integration of fluorescein-conjugate into the growing silica layer– a) Formation of silica layer overtime; b) Fluorescence of particles by the integrated FITC-conjugate.

Performing the VIP synthesis with FDA-APTES, the organosilane polycondensation was performed for 8h to obtain a slightly higher layer with fluorescein-containing imprints before building up the second silica layer on it.

After formation of the fluorescent recognition layer, the remaining not integrated fluorescein-conjugates were removed from the reaction mixture through washing the particles carefully to avoid the removal of NorVLP. The second layer was formed with the same concentration of TEOS and APTES at the same conditions as before, but without the fluorescein-conjugate. The organosilane condensation continued on the particles with a velocity of 2 nm/h to a thickness of 25 ± 1 nm after 4 h (Fig. 4.52). Since there was no fluorescein-conjugate added to the reaction mixture, the fluorescence signal did not change during the formation of the second silica layer. The so-prepared VIPs owned a recognition layer that consisted of a 17nm-thick internal silica layer with fluorescein-conjugate and an 8nm-thick external silica layer without fluorescence dye.

After curing of the final silica layer, acidic conditions were applied to remove NorVLP through ultrasonication. The surface of resulting particles characterized by means of FESEM showed the characteristic imprints of VIPs. This result proves that NorVLP remained bound at the particles surface during both separately performed silica layer formations.

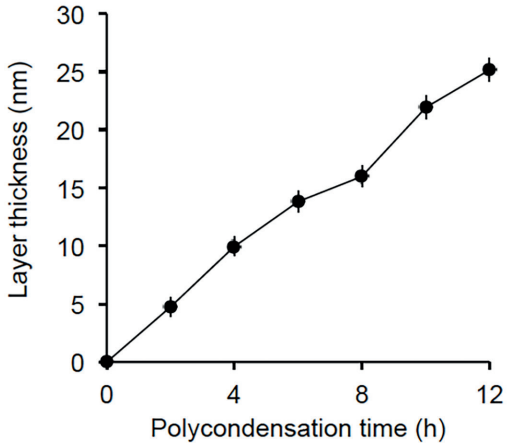

Figure 4.52: Silica layer growth on VIP with two separately performed silica formation – 1. silica layer with FDA integration (0-8h) and 2. layer with only organosilanes (8-12h);

The fluorescence intensity of particles was determined by measuring the signal at different particles concentration as a dilution series. The fluorescence intensities (in relative fluorescence units, RFU) were plotted against the particle concentrations to determine the intensity per mg/ml particles as shown in Figure 4.53 and it can be seen that:

a) The linear increase in the fluorescence intensity with the particles concentration confirms that the signal arrives from the particles.

b) Imprinted fluorescein-containing particles (VIP_F*) showed a strong fluorescence signal of 44611 RFU per mg/ml particles (corresponding to 297 RFU/µg particles)

c) Imprinted FDA-containing particles (VIP_FDA) had a signal of 1912 RFU per mg/ml particles (corresponding to 12.7 RFU/µg), which is more than 20 times lower than the fluorescence intensity of VIP_F*.

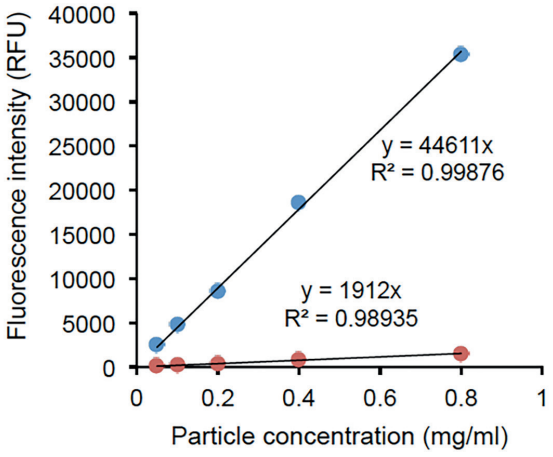

Figure 4.53: Fluorescence intensity of imprinted particles containing fluorescein (blue) or FDA (red) in the silica layer.

Beside fluorescent VIPs, non-imprinted fluorescent particles (NIPs) were also prepared with similar silica compositions as their imprinted versions. All prepared particles and their fluorescence intensities are summarized in Table 4.1.

Table 4.1: *Prepared and tested fluorescent particles*

Name	Imprints	Flourescence dye	Second layer	Flourescence intensities	Illustration
VIP_F*	yes	Flourescein-APTES	yes	44611 RFU/mg/ml 297 RFU/µg	
VIP_FDA	yes	FDA-APTES	yes	1912 RFU/mg/ml 12.7 RFU/µg	
NIP_F*	no	Flourescein-APTES	no	35774 RFU/mg/ml 209 RFU/µg	
NIP_{EX}	no	FDA-APTES	no	1554 RFU/mg/ml 10.4 RFU/µg	
NIP_{IN}	no	FDA-APTES	no	1658 RFU/mg/ml 10.5 RFU/µg	

4.3.3 Activation of fluorescence dye

The integrated fluorescein diacetate (FDA) was „activated" by basic hydrolysis of the acetate groups, which render the fluorescence signal. The hydrolysis was performed by:

a) Hydroxide ions ($[OH]^-$)

b) Potassium tert-butoxide (*t*-butoxid)

c) Esterase

The mechanism by which esters are cleaved involves:

1. Attack of the carbonyl group of the ester by a nucleophile;
2. Formation of tetrahedral immediate;
3. Release of the alkoxid group that takes the proton of carboxylic acid forming alcohol;

4.3.3.1 Hydrolysis by basic conditions

Fluorescein diacetate is known to be sensitive to high basic pH values that induce auto-hydrolysis.[24] In case of FDA-containing silica particles, exposing these particles to basic conditions might particularly affect the FDA at the surface, while the internal FDA might be less affected due to the coverage with silica, providing an own buffered microenvironment.

To verify that hydrolysis occurred preferentially at the exposed FDA, two kinds of fluorescent NIPs were prepared:

1) NIP with only the FDA-containing silica layer and, thus, with partly exposed FDA (NIP_{EX});
2) NIP with a silica layer on top of the FDA-containing silica layer covering all FDA molecules, which were thus completely integrated in silica (NIP_{IN});

A fluorescence dye that is completely surrounded by silica is isolated from the environment and is thus stabilized against external factors such as the pH value. Any factor that affects preferentially the surface-exposed FDA should only induce an increase in the fluorescence intensity in case of NIP_{EX}. Therefore, using these two NIPs - NIP_{EX} and NIP_{IN} – it can be concluded which FDA molecules were hydrolysed.

At first, the effect of the applied pH value on the fluorescence intensity of FDA-containing particles was intensively studied on the two NIPs - NIP_{EX} and NIP_{IN}. Both particles at 0.4 mg/ml were put in a Trizma buffer solutions at pH 7, 8 and 9, respectively. The fluorescence intensity was determined after 2 min and after 14 h incubation (Fig. 4.54).

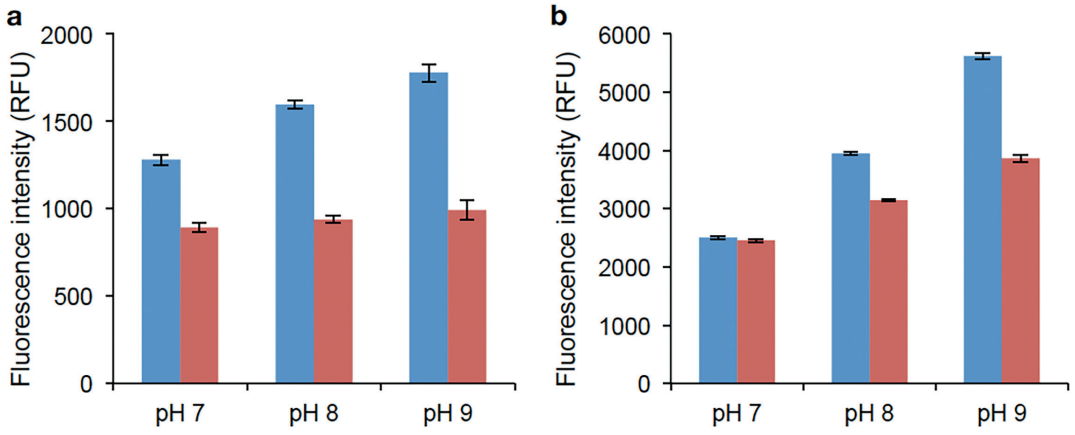

Figure 4.54: Effect of environmental pH on non-imprinted particles with partially exposed FDA (NIP_{EX}, blue) or completely integrated FDA (NIP_{IN}, red) in the silica layer – Fluorescence intensities after incubation in Trizma solutions at different pH values for a) 2 min and b) 14 h.

A feature of fluorescein is that its fluorescence intensity in water depends on the applied pH values, making fluorescein a useful pH indicator. This feature was also observed in case of NIP_{EX} and NIP_{IN}, but with different sensitivity against the applied pH values. As it can be seen in Fig.4.54a, the fluorescence signal of NIP_{EX} rose with increasing pH values, while the signal of NIP_{IN} did not change.

NIP_{EX} were thus strongly affected by the applied pH values than NIP_{IN}, indicating the isolating effect by silica that covered the fluorescein.

As can be seen from Fig.4.54b, longer incubation in these buffer solutions increased the fluorescence intensity, indicating the occurrence of the ester hydrolysis. The increase occurred in both NIP_{EX} and NIP_{IN} with similar high intensities; integrated FDA was thus also hydrolysed. In relation to the starting fluorescence intensity, the highest increases (295 % for NIP_{EX} and 289 % for NIP_{IN}) were observed in Trizma buffer solutions at pH 9.

It was assumed that there is a different kinetic for the hydrolysis depending on whether the FDA is exposed or inside the silica. Therefore, the previous experiment was repeated by incubating the particles in Trizma buffer at pH 9 with repeated fluorescence measurements during 4 h of incubation.

As can be seen from Figure 4.55, during the 4 h of incubation, both types of NIPs showed an increase in the fluorescence intensity in relation to the starting fluorescence. In case of NIP_{EX}, the fluorescence signal increased in 1 h from 1874 to 3294 RFU, corresponding to a rise of 1420 RFU. Afterwards, the signal increase slowed down, resulting in a total rise of 2013 RFU after 4 h. At the same time, NIP_{IN} showed a steady signal increase, reaching a total rise of 1801 RFU.

The results of the last experiments indicate that ester hydrolysis also occurred inside the silica immediately after exposing the particles to basic conditions. Therefore, the activation of FDA cannot be achieved without partly activating the integrated FDA. The hydrolysis of internal FDA was caused either by the diffusion of $[OH]^-$ present in the water to the FDA in the silica or by the high environmental pH value changing the pH in the silica, inducing the deprotonation of water molecules in between the silica network.

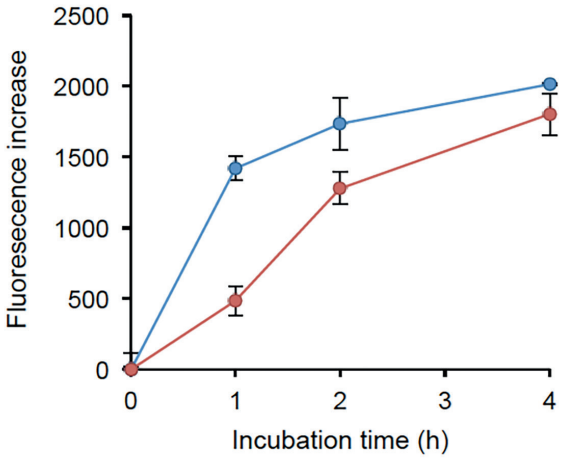

Figure 4.55: Effect of Trizma buffer at pH9 on non-imprinted particles with partially exposed FDA (NIP_{EX}, blue) or completely integrated FDA (NIP_{IN}, red) in the silica layer.

In conclusion, when FDA-containing NIPs were exposed to basic conditions, NIPs with partially exposed FDA reacted faster to the environmental pH than NIPs with completely integrated FDA.

Under basic conditions, hydroxide ions induced ester hydrolysis independently from the position of the FDA in the silica layer. To specifically hydrolyse the exposed FDA, the nucleophile requires a certain size to limit the diffusion through the silica. At the same time the pH value should be set below pH 7 because the internal FDA might be hydrolysed by the present hydroxide ions.

4.3.3.2 Hydrolysis by *t*-butoxid

Potassium tert-butoxide (*t*-butoxid) is the chemical compound with the formula $K^+[(CH_3)^3CO]^-$. It is a strong base depending on the solvent, which is useful in organic synthesis.[25] The hydrolysis by *t*-butoxid as base occurs via a similar mechanism as before via $[OH]^-$ - the nucleophile interacts with the carboxyl group of the ester, inducing hydrolysis. However, the outstanding property of *t*-butoxid is that it forms a tetrameric cubic-type cluster, making it a steric base. As result of the cluster formation, *t*-butoxid diffusion through the silica layer should be significantly reduced; therefore hydrolysis by *t*-butoxid is limited to FDA exposed on the surface.

Furthermore, the reaction of *t*-butoxid can take place in solvent without water. Therefore, the risk for the hydrolysis of internal FDA by hydroxide ions can be reduced. However, the choice of the solvent was limited due the solubility of the silica particles. The balance between the solubility of particles and *t*-butoxid was found with 1-butanol.

Free FDA and Butoxid

The effect of *t*-butoxid on the FDA was first studied on the free FDA-conjugate through incubating FDA at 3 µM with different concentrated *t*-butoxid in 1-butanol. The *t*-butoxid concentration in use were: 0 (control), 3 µM (equimolar to FDA), 6 µM (twofold more than FDA) and 30 µM (tenfold more than FDA). The fluorescence signal was measured after 20 min incubation and is shown in Fig 4.56; the more *t*-butoxid was added, the more the fluorescence signal increased, indicating the ester hydrolysis by *t*-butoxid.

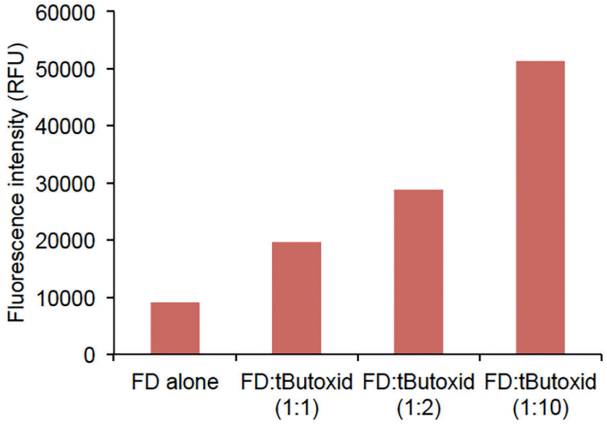

Figure 4.56: Effect of *t*-butoxid on free FDA-conjugate – measured fluorescence signal after 20 min of incubation in 1-butanol; *t*-butoxid concentration in use: 0 (=control), 3 µM (equimolar to FDA), 6 µM (two times more than FDA) and 30 µM (ten times more than FDA).

Fluorescence particles and t-butoxid

For the hydrolysis by *t*-butoxid, particles were suspended in solvent for the reaction and then washed with alcohol and water subsequently for the fluorescence measurement. This solvent exchange induced particle aggregation that was sufficient to reduce the fluorescence intensity, covering the intensity increase by hydrolysis. For instance, fluorescein-containing NIPs (NIP_F*) lost 77 % of their original fluorescence signal by performing the solvent exchange.

To reduce the degree of aggregation after solvent exchange, particles were treated to an intensive re-suspending process involving sonication and stirring in high concentrated citrate solutions; the fluorescence intensity could be recovered up to 90 %. The hydrolysis of FDA on particles was performed using this re-suspending protocol.

FDA-particles and t-butoxid

The different FDA-containing particles (NIP_{EX} and NIP_{IN} and VIP, at 1 mg/ml) were incubated with *t*-butoxid (at 50 mM) in the same conditions (1-butanol, room temperature, stirring at 400 rpm) to observe the effect on the fluorescence intensity by it. Aliquots were taken after 0 and 24 h and tested for fluorescence after washing and re-suspending. Afterwards, the final particle concentration of each sample was determined as further control.

In case of the two NIPs, the measured fluorescence intensities at 0 and 24 h were as follows: for NIP_{EX}, the respective intensities were 1500 RFU per mg/ml and 2150 RFU per mg/ml, while for NIP_{IN}, they were 1585 RFU per mg/ml and 1570 RFU per mg/ml. These values confirm cleavage of mainly surface-exposed FDA because only the NIP_{EX} with partially-exposed FDA showed an increase in the fluorescence intensity by a factor of 1.4, while NIP_{IN} remained unchanged.

In case of VIPs incubated with t-butoxid, the measured fluorescence intensities were 1900 RFU per mg/ml at 0 h and 3700 RFU per mg/ml at 24 h. With that the fluorescence intensity of VIPs increased by a factor of 2 by the incubation with *t*-butoxid.

To control whether the increase of the fluorescence intensity was caused through the ester cleavage by *t*-butoxid, the NIP_{EX} were also incubated without *t*-butoxid in the same conditions. Without the presence of *t*-butoxid, the measured fluorescence intensities were 1520 RFU per mg/ml at 0 h and 1435 RFU per mg/ml at 24 h. The fact that there is no fluorescence increase without *t*-butoxid confirms the function of *t*-butoxid.

These results indicate the partial cleavage of the quenching acetyl-groups from surface-exposed FDA by *t*-butoxid during the incubation for 24h. Longer incubations of 48h were also tested for their effect on the fluorescence intensity. However, the long exposure time in solvent led to loss of particles because they adhered to the reaction vial. The reduced particle concentration affected the fluorescence measurement and, in addition, made the process unattractive to yield particles for the NoVLP detection.

In conclusion, exposing FDA-containing particles to *t*-butoxid in 1-butanol, only VIPs and NIPs

with partially-exposed showed any fluorescence increase because the steric base could not reach the silica-integrated FDA. However, the intensive re-suspending process and the loss of particles during the reaction and re-suspending process represent drawbacks for this method for yielding high quantities of fluorescent particles.

4.3.3.3 Hydrolysis by esterase

Esterase (Carboxylester hydrolases, EC 3.1.1.1) catalyses the hydrolysis of carboxylic acid esters. In contrast to the previously described basic hydrolyses in buffer or solvent, the enzymatic hydrolysis of esters occurs in an internal part of the enzyme, the active site. The active site consists of a catalytic triad, namely serine, histidine, aspartate, that generates a charge-relay network to polarise and activate the nucleophile; the latter attacks the carbonyl on the ester, forming a tetrahedral intermediate. The subsequent rearrangement and collapse of this intermediate releases the substrate without acyl moiety, while an acyl-enzyme intermediate remains. In an additional hydrolysis reaction, water attacks this acyl-enzyme to release the acid.[26] The chemical reaction mechanism is the same as before, but the reaction takes plays in its own microenvironment, independently from the external pH and there is an additional step, the regeneration of the active side, to consider.

An interesting point of esterase is that most of them show broad substrate recognition, allowing ester hydrolysation on very different substrate, including the fluorescein diacetate. The hydrolysis of fluorescein diacetate has already been used, for instance, to determine activity of microorganism or cells because they own, among others, active esterase, cleaving the quenching acetates.[19,26-29] In case of the FDA-containing VIPs, esterase should activate only the exposed FDA, because it cannot diffuse through silica matrix due to its size.

Esterase assay

In this work, esterase from porcine liver (PLE) was applied to activate exposed FDA. The activity of PLE was confirmed through a colorimetric activity assay based on the conversion of the artificial substrate p-nitrophenyl acetate (pNPA, at 0.2 mM) to acetate and 4-nitrophenol that absorb light at 405 nm in basic conditions. For optimal activity, the conversion was carried out at 37 °C in a phosphate buffer solution at 50 mM and pH 7.5, which was sufficient basic for measuring the product concentration continuously. The absorbance was converted to concentration values through a calibration curve of 4-nitrophenolate (ε: 14.3 $mM^{-1}cm^{-1}$, d: 0.45 cm, R^2: 0.999). The unit of the enzymatic activity (U) is defined as the amount of enzyme that hydrolyses 1 µmol of pNPA per minute at standard conditions. Activity assays were performed with different amounts of enzyme and stopped after different time intervals. The measurement results are shown in Fig. 4.57a:

a) The higher the enzyme concentration, the faster is the increase in the product concentration, *i.e.* the higher the production rate.

b) The production rate is constant up to 5 minutes for all enzyme concentrations.

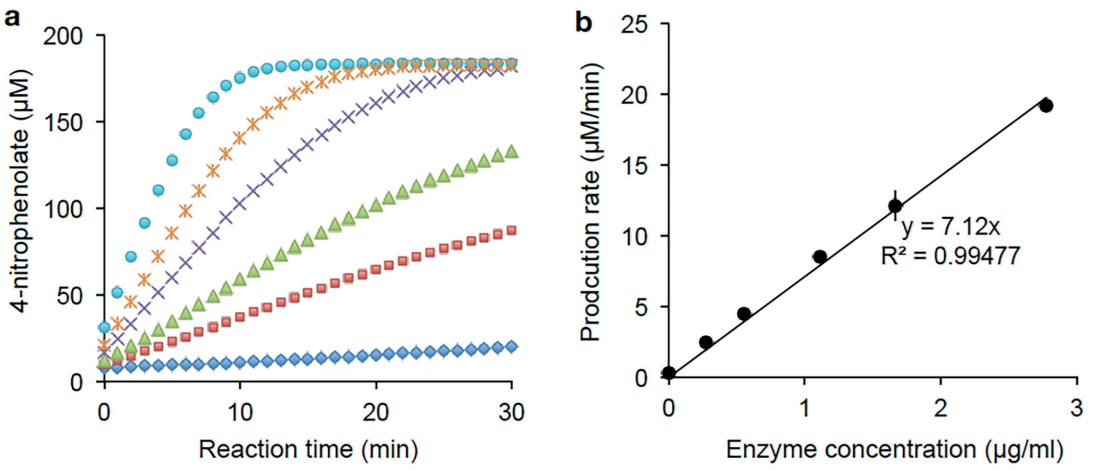

Figure 4.57: Esterase assay with varying enzyme concentrations - a) Increase of product concentration over time; b) Production concentration at 5 min plotted against the enzyme concentration; Enzyme concentration in use: 0, 0.3, 0.6, 1.2, 1.7 and 2.8 µg/ml.

Furthermore the production rate of the highest enzyme concentration decreased after 10 minutes, indicating that the concentration of the substrate is too low to sustain the reaction. Fig. 4.57b shows that the production rate obtained from a reaction time of 5 minutes correlates with the enzyme concentration linearly, allowing an enzyme concentration of up to 3 µg/ml to be quantified.

The ideal pH value for the esterase is pH 7.5. But to avoid auto-hydrolysis of the internal FDA, the pH value for the reaction was reduced to pH 6. The reduced pH value affected the activity of PLE significantly as it can be seen in Fig. 4.58; the reaction at pH 6 was almost twice slower than this at pH 7.5.

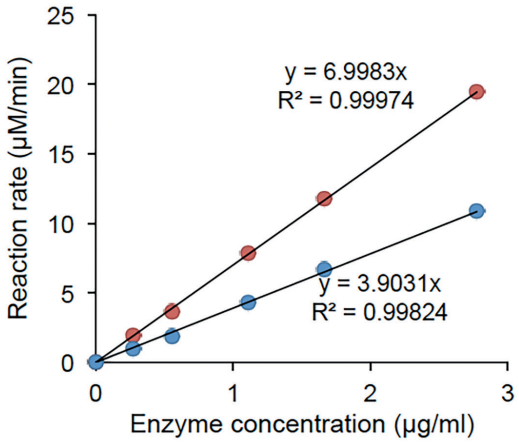

Figure 4.58: Esterase assay at pH 6 (blue) and pH 7.5 (red) - Product concentration at 5 min plotted against the enzyme concentrations: 0, 0.3, 0.6, 1.2, 1.7 and 2.8 µg/ml.

Free FDA and esterase

At first, the hydrolysis of the FDA by PLE was tested on the free FDA. For this purpose, PLE (at 30µg/ml) was incubated with varying concentration of FDA directly in a microtiterplate for reading the fluorescence. The on-going reaction process was monitored through continuous measurement of the fluorescence signal emitted by fluorescein (Fig 4.59).

Fig. 4.59a shows the measured curves of FDA at µM incubated with PLE (blue) and without PLE (red); these curves are representative also for the other FDA concentrations. The PLE-containing curve starts with a linear increase for approximately 15 minutes followed by the formation of a plateau. The signal increase indicates the cleavage of the quenching acetyl groups, while the plateau indicates the stop of ester cleavage. Since the final signal is lower than the signal by fluorescein at the same molar concentration, it was assumed that enzymatic reaction was blocked before all ester groups were hydrolysed. The blockage of the enzyme might be caused by rebinding of already hydrolysed products and, thus, for enzymes common observed product inhibition through competition.

Comparing the starting fluorescence signal (F_0) with the signal at the plateau (F_P), the degree of signal increase was determined for each applied FDA concentration (Fig. 4.59b). It can be seen that at low concentrations, the fluorescence signal increased by a factor of 5, while at higher concentrations, signal increased by a factor of 3.

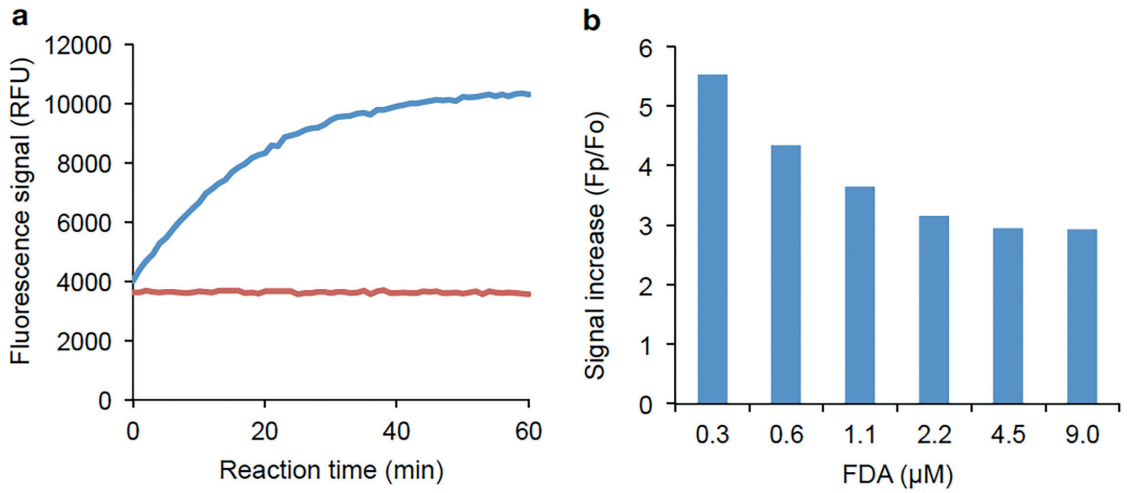

Figure 4.59: Effect of esterase on free FDA - a) Fluorescence signal during the incubation of FDA at 9µM with (blue) and without PLE at 30µg/ml (red); b) Signal increase defined as division of fluorescence signal at plateau (F_P) through signal at reaction begin (F_0) for each FDA concentration.

Silica particles and esterase

In order to hydrolyse the FDA that was exposed at the surface of silica particles, the PLE needed to come close to the surface. This required that the enzyme was not repulsed from the surface as in case of immobilization. To determine conditions with low electrostatic repulsion between PLE and silica particles, different pH values as well as additives were tested for the immobilization

yield of the PLE, as described in the previous section for AP and BSA.

In the first experiment in this context, the isoelectric point (IEP) was determined because the lowest repulsion is found at this pH value. PLE (at 6 µg/ml) was incubated with unmodified SNPs (at 3.2 µg/ml) in the following 50mM buffer solutions: MES buffer at pH 6 and 6.5, and HEPES at pH 7, 7.5 and 8. After 1h incubation, the unbound PLE molecules in solution were separated from the particles through centrifugation and determined via activity assay. The resulting concentrations of PLE in solution were used to calculate the immobilization yields (Fig. 4.60). The highest immobilization yield for PLE at 91 % was found at pH 6, which corresponds to the IEP of this PLE solution.

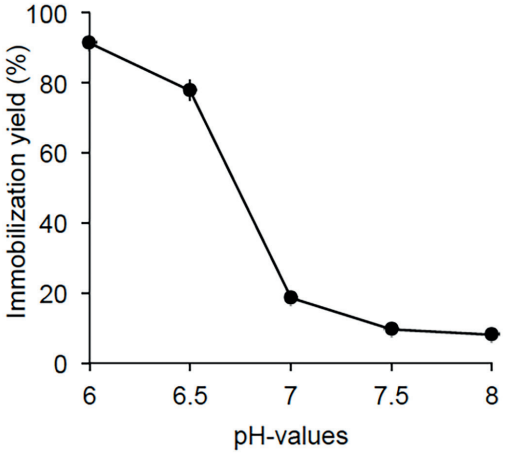

Figure 4.58: Immobilization yield of PLE on pure silica at different pH values – following buffer solutions (at 50 mM) in use: MES buffer at pH 6 and 6.5, and HEPES at pH 7, pH 7.5 and pH 8.

FDA-particles and esterase

To observe the effect on the fluorescence intensity by PLE, VIPs (at 0.2 mg/ml) were incubated with and without PLE (at 5 U/ml) at the same conditions (10 mM MES pH 6, 0.01 % Triton X-100, 7 mM citrate, room temperature, stirring at 400 rpm). Triton X-100 was added to stabilize PLE in solution without affecting the immobilization, while citrate was added to reduce particle aggregation. These conditions allowed the PLE to get close to the surface of the particles to reach the FDA for the ester cleavage. However, these conditions also led to immobilization of PLE on the silica surface. Using Bradford to determine the protein concentration in the supernatant, it was determined that up to 80 % of PLE was bound during the incubation.

After incubation for 36h at reaction conditions, VIPs were centrifuged and re-suspended in 100 mM citrate and 0.01 % Triton X-100 at pH 7 and incubated at 37 °C and 1000 rpm to remove bound PLE; interestingly, VIPs incubated without PLE showed visible aggregation, while VIPs with PLE that improves resolvability could be re-suspended easily at this state. After the removal of PLE, VIPs were centrifuged and re-suspended in 50 mM citrate and 0.01 % Triton X-100 at pH 6 for fluorescence measurement.; both VIPs showed visible aggregations, indicating the successful removal of PLE. VIPs were treated with ultrasonication until no aggregates were visible with the naked eye before measuring the fluorescence intensity per mg particles.

The fluorescence intensities were as follows:

- Esterase-treated VIP_FDA (VIPest): 1426 RFU per mg/ml particles (or 9.5 RFU/µg)
- Control VIP_FDA (VIPco): 1294 RFU per mg/ml particles (or 8.6 RFU/µg)
- Untreated VIP_FDA: 1931 RFU per mg/ml particles (or 12.9 RFU/µg)

The fluorescence intensity of VIPest was 10% higher than the intensity of the VIPco that was treated the same way, but without esterase. This result indicates that the esterase cleaved the quenching acetyl-groups, resulting in an increased fluorescence signal. However, both treated VIPs (VIPest and VIPco) show significantly lower fluorescence intensity as the untreated VIPs. The decrease in intensity might be attributed for instance to

a) The incubation conditions that degraded the fluorescein;

b) The particle aggregation during measurement that reduces the signal through scattering.

4.3.4. Quenching of fluorescence signal by NorVLP

The prepared fluorescent VIPs (VIP_F*, VIP_FDA and VIPest) were tested for their sensitivity to NorVLP. The binding of NorVLP on the imprints should result in quenching of the fluorescence signal emitted by fluorescein that was doped in the imprints. For this purpose, VIPs were incubated with increasing concentration of NorVLP in binding conditions, as described in the previous sections (see 4.1.2 and 4.2.5).

Besides NorVLP, a constant concentration of skim milk was added to reduce unspecific adsorption of NorVLP on non-imprinted surfaces. Both proteins - NorVLP and skim milk - were tested for their intrinsic fluorescence before performing the quenching tests.

An emission scan of NorVLP and skim milk, respectively, was determined with the excitation wavelength of 485 nm and both proteins at 1 mg/ml - scan of NorVLP in red and scan of skim milk in blue (Fig.4.61a). It can be seen that NorVLP did not show any fluorescence signal when excited at 485 nm, while skim milk, which presents a mixture of different proteins, showed strong intrinsic fluorescence, especially between 515 and 550 nm. Additionally, an excitation scan of skim milk was determined with λ_{EM} at 515 nm and at varying concentrations of skim milk.

The measured excitation spectra are shown in Fig. 4.61b:

a) The light absorbance correlates with the skim milk concentration, indicating the presence of intrinsic fluorophores.

b) At high skim milk concentration, there is a broad excitation band, ranging from 420 nm to 480 nm, overlapping with the absorbance maximum of fluorescein at 485 nm.

c) At 0.03 mg/ml skim milk, the excitation at 485 nm is very low because the excitation band is significantly small with maximal λ_{EX} at 440 nm.

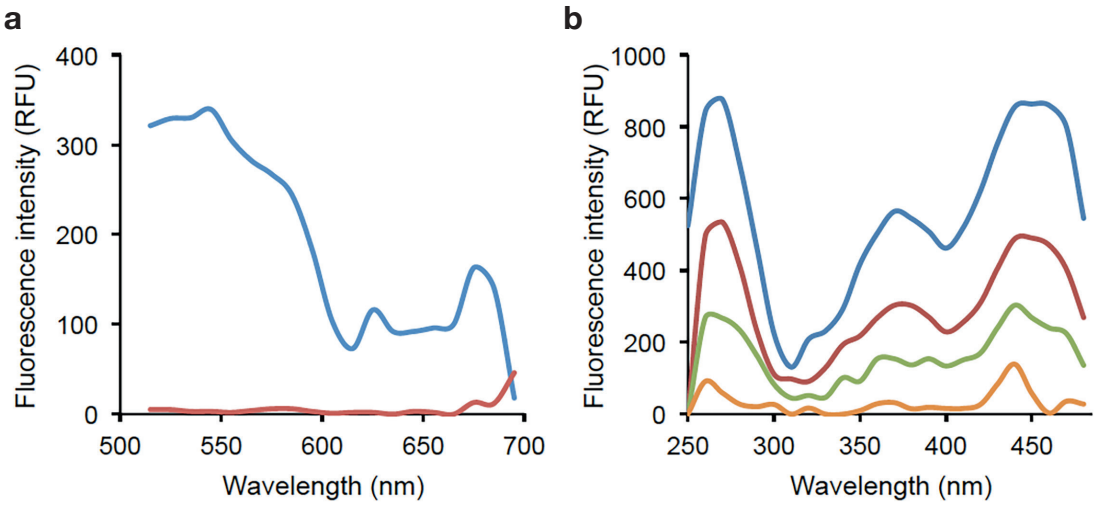

Figure 4.61: Fluorescence properties of NorVLP and skim milk – a) Emission spectra of skim milk (blue) and NorVLP (red), both at 1 mg/ml; b) Excitation spectra of varying skim milk concentrations: 1, 0.5, 0.25 and 0.03 mg/ml.

At binding conditions, the skim milk concentration of 0.025 mg/ml was used that does not affect the measurement of the fluorescence signal by fluorescein.

To determine the quenching of the fluorescein signal by NorVLP, fluorescent VIPs at 0.2 mg/ml were first incubated with varying concentrations of NorVLP (up to 25 µg/ml) for 20 min and then aliquoted in a black and flat microtiter plate. The untreated mixture of NorVLP and particles was measured for the fluorescence signal continuously for the duration of 30 min. The measurement of the emitted light overtime compensated for the light scattering by the particles, improving the precision of the signal. The average of the collected fluorescence intensities was then used to determine the quenching. The quenching was quantified in the form of the quenching quotient (QQ), which is the fluorescence intensity without quencher, divided by the intensity in the presence of the quencher. Here, the quencher is NorVLP, and the QQ-value was determined for each applied NorVLP concentration; the determined QQ-values for the prepared fluorescent VIPs (VIP_F*, VIP_FDA and VIPest) are shown in Fig. 4.62.

VIPs with fluorescein (VIP_F*, blue points in Fig. 4.57) showed no change in their fluorescence intensity by the presence of NorVLP, even the NorVLP-binding was confirmed by detecting the amount of unbound NorVLP via indirect ELISA, as described in previous sections. These results indicate that the presence of NorVLP quenched only a very low quantity of the available fluorescence dye. During imprinting, fluorescein-molecules were evenly integrated over the whole recognition layer, which is partly over 30 nm thick. Therefore, it can be expected that the majority of fluorescein was integrated at points of the recognition layer that are not part of the imprint and, thus, did not get in contact with NorVLP during binding.

VIP with fluorescein diacetate (VIP_FDA, red points in Fig. 4.57) showed a slight decrease in fluorescence intensity at increasing concentration of NorVLP. Even FDA is the quenched version of fluorescein due to the two acetyl-esters; the resulting VIPs still show a bit of fluorescence that

can be attributed to a few molecules of fluorescein that lost the acetyl-esters during integration or storage. The present NorVLP can quench some of these few fluorescein molecules that are by chance exposed in the imprints. However, the highest tested concentration of NorVLP quenched only 6 % of the total fluorescence.

Incubating VIP_FDA with esterase activated specifically the imprints-exposed FDA and, thus, increased the number of fluorescein in the imprints, which should thus increase the sensitivity to NorVLP. Indeed, VIPs with activated FD (VIPest, green points in Fig. 4.57) showed a decrease in fluorescence intensity at all concentrations of NorVLP. The highest quenching at 18 % was observed at 12.5 µg/ml NorVLP, while the next higher concentration did not significantly change the intensity, indicating saturation with NorVLP.

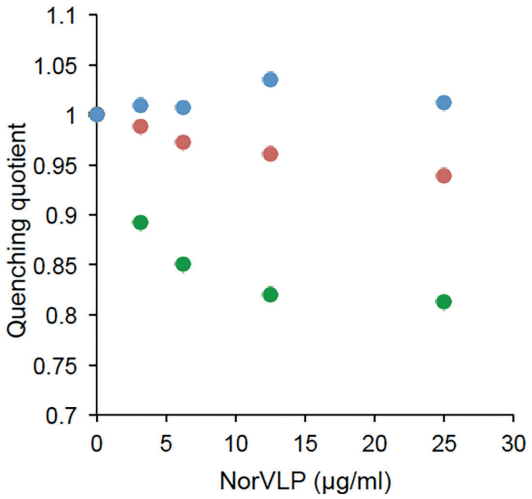

Figure 4.62: Effect of NorVLP-binding on fluorescence intensity - Quenching quotient of VIPs with fluorescein (blue), VIPs with FDA (red) and VIPs with esterase activated FDA (green).

It has to be mentioned that the showed data for quenching represent one measurement with the best outcome. Not all points could be reproduced, especially in case of the treated particles as aggregation affected the NorVLP-binding and the fluorescence measurement.

Nonetheless, the latest results demonstrate that a fluorescence dye can be locally activated in the imprints and that this improves the quenching sensitivity to the NorVLP-binding.

4.3.5. Suggestions for improvements

The outcome of this part of the thesis can be seen as preliminary test of a new synthesis protocol to provide virus recognition via fluorescence. During the development of this protocol some issues aroused that could not be solved in the frame of this work and give space for improvement. At this point some of the most crucial issues of the actual protocol as well as suggestions for improvement will be briefly explained here.

1 - Scaling up the synthesis of fluorescent dyes

One of the critical factors that affected the development of the synthesis protocol was the low quantity of APTES-conjugated fluorescein diacetate, limiting the numbers of synthesised particles and thus tests with the particles. That included some critical tests confirming the reaction such as the occurence of the deacetylation. Based on the current data it could be argued that the product obtained from the diacetylation might be an artifact and the remaining low fluorescence signal might come from little contamination with fluorescein. If scale and yield were higher, further analysis could be carried out to confirm the diacetylation.

In a first attempt to perform the acetylation reaction at high scale, there was found such high quantity of secondary products that could not be separated from the primary ones anymore. This observation suggests that the synthesis of acetylated APTES-conjuagated fluorescein requires further optimization to reduce the quantity of secondary products.

Alternatively, it could be performed the conjugation of APTES with the FDA, which is also commercially available. In that case the deacetylation during the conjugation have to be considerd and prevented through the use of hydrophobic or acidic conditions.

2 - Quantifying the content of fluorescence dyes in silica layer

It would be interesting to have a better understanding about the quantitiy of fluorescence dye inside the formed silica layer to explain a few feature of the fluorescent VIPs. For instance, the two APTES-conjugated fluorescence dyes – quenched and fully active – showed a relation of 1 to 10 in signal difference, while the particles with integrated dyes showed a relation of 1 to 30. This difference might be explained by the fact that the silica stabilizes the quenched dye better than the solvent. However random errors cannot be excluded with the currently applied method.

It was observed that two batches of the same particle (with fully acitve fluorescein) showed slightly different fluorescence intensities per µg of particles, indicating that a significant level of random errors affects the integration or the determination of the fluorescence signal. Furthmore the fluorscence signal depends on the degree of particle aggregation, which has to be considered for each fluorescence measurement.

The aim of future works on fluorescent particles should thus be to achieve a reliable correlation between dye concentration and fluorescence signal.

3 - Confirming the deacetylation reaction

Because the fluorescence signal depends on the degree of particle aggregation, it can be argued that the increase by 10 % after the treatment with esterase is due to the different degree of particle aggregation by remaining immobilized esterase on particle surface.

To prove that the reaction by the esterase is responsible for the fluorescence increase, the reaction by esterase might be followed additionally via the released acetate.

4.4 References

1 Phanasgaonkar, A. and Raja, V. S. (2009) Influence of curing temperature, silica nanoparticles- and cerium on surface morphology and corrosion behaviour of hybrid silane coatings on mild steel. *Surface and Coatings Technology* **203**, 2260-2271

2 Suegama, P. H., de Melo, H. G., Benedetti, A. V. and Aoki, I. V. (2009) Influence of cerium (IV) ions on the mechanism of organosilane polymerization and on the improvement of its barrier properties. *Electrochimica Acta* **54**, 2655-2662

3 Wang, D. and Bierwagen, G. P. (2009) Sol–gel coatings on metals for corrosion protection. *Progress in Organic Coatings* **64**, 327-338

4 Nichetti, D. (2004) Determination of mechanical properties of silica compounds using a curing kinetic model. *European Polymer Journal* **40**, 2401-2405

5 Correro, M. R. et al. (2016) Enzyme Shielding in an Enzyme-thin and Soft Organosilica Layer. *Angew Chem Int Ed* **55**, 6285-6289

6 Cao, S. et al. (2007) Structural basis for the recognition of blood group trisaccharides by norovirus. *J Virol* **81**, 5949-5957

7 Butler, R. T., Ferrell, N. J. and Hansford, D. J. (2006) Spatial and geometrical control of silicification using a patterned poly-l-lysine template. *Applied Surface Science* **252**, 7337-7342

8 Belton, D., Paine, G., Patwardhan, S. V. and Perry, C. C. (2004) Towards an understanding of (bio) silicification: the role of amino acids and lysine oligomers in silicification. *Journal of Materials Chemistry* **14**, 2231-2241

9 Dickerson, M. B., Sandhage, K. H. and Naik, R. R. (2008) Protein- and Peptide-Directed Syntheses of Inorganic Materials. *Chem. Rev.* **108**, 4935-4978

10 Groger, C., Lutz, K. and Brunner, E. (2008) Biomolecular self-assembly and its relevance in silica biomineralization. *Cell Biochem Biophys* **50**, 23-39

11 Patwardhan, S. V. (2011) Biomimetic and bioinspired silica: recent developments and applications. *Chem Commun* **47**, 7567-7582

12 Patwardhan, S. V. and Clarson, S. J. (2003) Silicification and biosilicification. *Materials Science and Engineering: C* **23**, 495-499

13 Patwardhan, S. V., Clarson, S. J. and Perry, C. C. (2005) On the role(s) of additives in bioinspired silicification. *Chem Commun*, 1113-1121

14 Patwardhan, S. V., Mukherjee, N. and Clarson, S. J. (2001) The Use of Poly-l-Lysine to Form Novel Silica Morphologies and the Role of Polypeptides in Biosilicification. *Journal of Inorganic and Organometallic Polymers* **11**, 193-199

15 Cuellar, J. L., Meinhoevel, F., Hoehne, M. and Donath, E. (2010) Size and mechanical stability of norovirus capsids depend on pH: a nanoindentation study. *J Gen Virol* **91**, 2449-2456

16 Sheldon, R. A. and van Pelt, S. (2013) Enzyme immobilisation in biocatalysis: why, what and how. *Chem Soc Rev* **42**, 6223-6235

17 Sträter, N., Klabunde, T., Tucker, P., Witzel, H. and Krebst, B. (1995) Crystal Structure of a Purple Acid Phosphatase Containing a Dinuclear Fe(II1)-Zn(II) Active Site. *Science* **268**, 1489-1492

18 Ferrer, M. L., Duchowicz, R., Carrasco, B., de la Torre, J. G. and Acuña, A. U. (2001) The Conformation of Serum Albumin in Solution: A Combined Phosphorescence Depolarization-Hydrodynamic Modeling Study. *Biophysical Journal* **80**, 2422–2430

19 Patel, B. C. M., Courtney, J. M., H., E. J. and P., P. J. (1991) Biocompatibility assessment: application of fluorescent probe response (FFR) technique. *Biomaterials* **12**, 722-726

20 Kramer, D. N. and Guilbault, G. G. A (1963) Substrate for the Fluorometric Determination of Lipase Activity. *Anal. Chem.* **35**, 588-589

21 Feng, H. et al. (2014) Surface molecular imprinting on dye–(NH2)–SiO2 NPs for specific recognition and direct fluorescent quantification of perfluorooctane sulfonate. *Sensors and Actuators B: Chemical* **195**, 266-273

22 Wan, W., Wagner, S. and Rurack, K. (2016) Fluorescent monomers: „bricks“ that make a molecularly imprinted polymer „bright“. *Anal Bioanal Chem* **408**, 1753-1771

23 Leung, M. K. P., Chow, C.-F. and Lam, M. H. W. (2001) A sol–gel derived molecular imprinted luminescent PET sensing material for 2,4-dichlorophenoxyacetic acid. *Journal of Materials Chemistry* **11**, 2985-2991

24 Lavis, L. D., Chao, T. Y. & Raines, R. T. (2011) Synthesis and utility of fluorogenic acetoxymethyl ethers. *Chem Sci* **2**, 521-530

25 Bornscheuer, U. W. and Kazlauskas, R. J. (2006) in *Hydrolases in Organic Synthesis. Regio- and Stereoselective Biotransformations. 2nd edition;* WILEY-VCH Verlag GmbH & Co. KGaA
26 Schnürer, J. and Rosswall, T. (1982) Fluorescein Diacetate Hydrolysis as a Measure of Total Microbial Activity in Soil and Litter. Appl. Environ. *Microbiol.* **43**, 1256-1261
27 Green, V. S., Stott, D. E. and Diack, M. (2006) Assay for fluorescein diacetate hydrolytic activity: Optimization for soil samples. *Soil Biology and Biochemistry* **38**, 693-701
28 Sánchez-Monedero, M. A. et al. (2008) Fluorescein diacetate hydrolysis, respiration and microbial biomass in freshly amended soils. *Biology and Fertility of Soils* **44**, 885-890
29 Rotman, B. and Papermaster, B. W. (1965) Membrane properties of living mammalien cells as studied by enzymatic hydrolysis of fluoregenic esters. *PNAS* **55**, 134-141

5 Conclusion and Outlook

5.1 Conclusion

Artificial antibodies represent very promising tools to prepare specific recognition elements for purification and detection in a broad field of applications. Consequently, a variety of different strategies have been developed to prepare artificial antibodies, above all, molecular imprinting. In terms of virus recognition, silica-based imprinting is the best choice due to the availability of silica-building organosilanes that mimic amino acids, and thus come closest to antibodies and their specific way of interactions with other biomolecules.

The possibility to generate specific surface recognition by collaboration of weak intermolecular interactions was demonstrated by Cumbo et al., whose imprinting protocol was the basis of the research work presented here. With the data collected in this work, the original virus-imprinting protocol was further extended in terms of:

1. Template virus;
2. Combination with other components, namely, enzymes and florescence dyes;
3. Construction of transduction systems at nanometer scale;

At the same time, further knowledge was gained, allowing better control of silica formation and improving the application of silica imprinting and encapsulation.

In the first part of my work, virus-like particles (VLP) were tested as safe replacement for imprinting of human pathogen viruses. Using a VLP of NorV, I successfully prepared imprinted particles (VIPs) with specific recognition properties and found the general standards for virus-imprinting.

Furthermore, greater insights regarding the formation of the silica layer were gained, such as:

- The effect of the reaction medium (ionic strength, pH) on silane polycondensation;
- Curing at ambient conditions as post-treatment after silica formation;

The findings about the silica formation at different tested conditions gave better understanding about the use of organosilanes in buffered media.

After the preparation of the recognition site for NorVLP binding, my work focussed on its combination with two different transduction systems, in which NorVLP binding modifies an optical signal for quantification of the virus-binding event. Both transducing systems developed here are based on the positioning of functionalized components (enzyme and fluorescence dye) to the virus inducing a signal change directly or indirectly.

In case of enzyme-based system, two differently functional silica layers were combined to form a correlation between a colorimetric enzymatic reaction and the concentration of a target mole-

cule. The signal is the absorbance by a product from an enzymatic reaction; the change is the production rate (or signal per time) and occurs indirectly via the substrate diffusion affected by the virus that is bound in the imprints.

In case of fluorescence-based system, in silica-integrated fluorescent dye, molecules were site-specifically activated. Because of this, most of the emitting dye was brought close to the virus for quenching. The signal was the fluorescence intensity of the in silica-integrated dye; the change was the quenching due to the presence of VLP that directly absorbed the emitted energy from the excited fluorescence dye.

Both transducing systems developed in this work represent new concepts for virus detection as well as imprinting. The outstanding feature of both detection systems is that recognition and transduction are done on the same nanoparticles. Because of this, virus detection is possible without preliminary separation of the bound and unbound virus or removal of reagents. As the detection assay consists of only one step, the time required for virus detection depends solely on the time required for virus binding and signal generation.

5.2 Outlook

The multi-functionalized particles presented here offer many beneficial features for future applications. Both recognition and transduction units are prepared at nanometer scale on one particle, allowing one-step detections. The quantification of virus-binding events occurs with easy applicable spectrophotometric systems. Considering the possibility of micro-sized optical detection, the size of the whole detection systems might be further reduced. Since an inorganic matrix carries the recognition unit, a high working time and high resistance against environmental stress can be expected. These features make the detection systems interesting for a broad application outside a laboratory, for instance, in the form of point-of-care diagnostics and mobile detection.

The problem of particle aggregation, which affects the surface modification and the virus detection, represents a drawback for an efficient industrial production. However, the advantage of silica is that it can be built on any surface. Therefore, a solution to reduce the degree of particle aggregation might be to use another carrier instead of SNP.

Magnetic nanoparticles are commonly used for analytical applications because the position of these particles can be controlled via a magnetic field. These particles can be easily adjusted with a silica layer to prepare one of the detection systems developed in the frame of this work.

Another idea of mine is to change from particles to solid-bound nanostructures with sufficient surface as carrier. I can imagine that these nanostructures are synthesized and functionalized directly on the surface of a microtiter plate. With the carrier static during the complete synthesis, no particle aggregation can occur, while the different functional silica layers are formed one by one on the carrier.

In conclusion, silica-based imprinting and encapsulation offers a broad range of possibilities in terms of functionality and applications, which can still be discovered.

6 Experimental details

6.1 Materials

Chemicals

Ammonium hydroxide (ACS grade, 28-30%), Ethanol (ACS grade, anhydrous), Glutaraldehyde (Grade I, 25 % in water), o-nitrophenyl-β-D-galactopyranoside (ONPG, Mr: 301.25), 4-methylumbelliferone β-D-galactopyranoside (MUG, Mr: 338.31), *p*-nitrophenyl acetate (pNPA, Mr: 181.15), 3,3´,5,5´-tetra-methylbenzidine (TMB), Fluorescein isothiocyanate (FITC, Mr: 389.38) and potassium tert-Butoxid (t-butoxid, Mr: 112.21) were purchased from Sigma-Aldrich (Switzerland).

Biotinylation kit containing EZ-Link™ Sulfo-NHS-LC-Biotin (21327) and NeutrAvidin™ Horseradish Peroxidase Conjugate (31001) were purchased from Thermo Scientific.

Organosilanes

Tetraethyl orthosilicate (TEOS, ≥ 99 %, Mr: 208.33) and (3-aminopropyl)-triethoxysilane (APTES, ≥ 98 %, Mr: 221.37) were purchased from ABCR (Germany).

Viruses

Norovirus-like particles (NorVLP, made of 180 copies of protein subunits with a mass of 58.96 kDa) and Turnip yellow mosaic virus (TYMV, made of 180 copies of protein subunits with a mass of 20 kDa) were provided by Dr. Lorber (University of Strasbourg) and were propagated and purified as described elsewhere.[1-3]

Proteins

Acid phosphatase from potato (AP, specific activity 6.6 U/mg protein), skim milk, monoclonal peroxidase-conjugated horse anti-mouse IgG and porcine liver esterase (PLE, specific activity 18 Umg^{-1} protein) were purchased from Sigma-Aldrich (Switzerland). Bovine serum albumin (BSA) was purchased from Roth (Germany). Monoclonal mouse anti recombinant viral protein 1 (VP1) of Norovirus genogroup II genotype 4 (GII.4) by Fitzgerald was purchased from LuBioScience (Switzerland). 2.8 g of this antibody were modified with the Biotinylation Kit by Thermo Scientific yielding 0.3mg/ml biotinylated antibody. Monoclonal mouse anti-Norovirus genogroup II genotype 4 (anti-NoV GII.4) antibodies purified from mouse ascites were provided by Dr. Lorber (University of Strasbourg).

APTES-modified fluorescein

APTES-conjugated fluorescein isothiocyanate (fluorescein-APTES, Mr: 610.75) and APTES-conjugated fluorescein diacetate (FDA-APTES, Mr: 694.82) were provided by El Idrissi from our research group (FHNW). Details about the synthesis are further described in appendix, while details about the purification and analysis (H-NMR, C-NMR) will be published somewhere else.

All chemicals and proteins were used without further purification. Nanopure water (resistivity ≥ 18 MΩ.cm) was freshly produced with a Millipore Synergy® water purification system.

6.2 Synthesis of particles

6.2.1 Synthesis of silica nanoparticles (SNPs)

Silica nanoparticles (SNPs) were prepared by adapting the procedures described elsewhere.[4-6] TEOS, ammonium hydroxide and ethanol were equilibrated at 20 °C for one hour in a water bath before use. 40 ml of ammonium hydroxide and 345 ml of ethanol were mixed in a 1liter round-bottom flask under magnetic stirring (600 rpm). 15ml of TEOS was added and the solution kept under stirring at 20 °C for 24 h. The resulting milky suspension was centrifuged (3220 x g for 10 to 20 min). The resulting supernatant was removed, while the pelleted SNPs were re-suspended in ethanol. The particles were repeatedly washed – a washing step included: centrifugation at 3220 x g for 10 min, removal of supernatant and re-suspension of particles. As solvent for re-suspension, first ethanol and then nanopure water were used each twice. After the last centrifugation step the particles were suspended in 40 ml water and stored at 4 °C until use.

6.2.2 Synthesis of virus-imprinted particles (VIPs)

The VIPs were prepared by adapting the procedure described previously by Cumbo et al.[6] as follows. All modifications of the SNPs as well as the imprinting were performed in 20 ml glass vials, in a final volume of 6ml, under stirring conditions (400 rpm), in a water bath at 20 °C unless otherwise described.

Surface modification of SNPs

In a typical synthesis experiment, 6 ml SNPs (3.2 mg/ml) were reacted with 4 µl (0.017 mmol) of APTES for 30 min in water. The so-modified particles were washed twice with nanopure water – a washing step included: centrifugation at 3220 x g for 5 min, removal of supernatant and re-suspension of the pelleted particles in nanopure water by ultrasonic treatment for 2 min using an Elmasonic S30H ultrasonic bath. Afterwards, the particles were incubated for 30 min in 6 ml of 1 % (v/v) aqueous glutaraldehyde solution. The so-modified particles were washed twice with nanopure water as described before.

Imprinting of NorVLP

For the imprinting, washed particles were re-suspended in a desired solution (*e.g.*: 25 mM citrate at pH 7 for standard conditions). Particles were then incubated with the NorVLP (at 0.03 mg/ml) for 1 h. Subsequently, 12 µl (0.054 mmol) of TEOS were added to the reaction mixture and allowed to react for 2 h. Temperature was then decreased to 10 °C before 6 µl (0.026 mmol) of APTES were added. Samples (0.2 to 1 ml) were collected at increasing reaction times and washed twice with nanopure water - a washing step with ≤ 1 ml included: centrifugation at 16,100 x g for 1 min, removal of supernatant and re-suspension of the pelleted particles in nanopure water. The organosilane polycondensation reaction was stopped after 18 h by washing the particles in nanopure water. To stabilize the organosilica layer, the resulting particles were kept at room temperature for 24 h for the curing and were then stored at 4 °C until use.

Non-imprinted reference particles were produced in a similar fashion by omitting the VLP addition step.

The pH value of the reaction suspension was measured with an indicator paper before and after initiating

the organosilane polycondensation, *i.e.* after adding TEOS and after adding APTES. Note: The pH-meter was not used because the organosilanes in suspension might react with the glass electrode).

Removal of template NorVLP

In a typical removal process (in 20 ml glass vials, in a final volume of 18 ml), VIPs were suspended to an end concentration of ca. 1 mg/ml in the removal solution (0.1 M HCl and 0.01% v/v Triton-X 100) and submitted to an initial ultrasonic treatment of 10 min at 30 °C. Subsequently, the VIP suspension was incubated for 30 min at 40 °C under stirring conditions (600 rpm). Afterwards, the so-treated VIPs were submitted to an additional ultrasonic treatment for 30 min, washed twice in nanopure water (centrifugation at 3220 x g for 5 min) and were stored at 4 °C.

6.2.3 Synthesis of biocatalytic VIPs (VIPcat)

Preparation of biocatalytic layer on SNPs

All reactions were performed in 20 ml glass vials, in a final volume of 18 ml, under stirring conditions (400 rpm), in a water bath at 20 °C unless otherwise described.

In a typical synthesis experiment, 18 ml SNPs (3.2 mg/ml) were reacted with 12 µl (0.051 mmol) of APTES for 30 min in water. The so-modified particles were washed twice with nanopure water – a washing step included: centrifugation at 3220 x g for 5 min, removal of supernatant and re-suspension of the pelleted particles in nanopure water by ultrasonic treatment for 2 min using an ultrasonic bath. Afterwards, the particles were incubated for 30 min in 18 ml of 0.1 % (v/v) aqueous glutaraldehyde solution and washed twice with nanopure water as described before.

The resulting pellet was suspended in 18 ml of MES buffer (10 mM, pH 6) and incubated with BSA (at 0.027 mg/ml) and acid phosphatase (at 0.044 mg/ml, corresponding to 290 U/l) for 1 h. Subsequently, a 1 ml aliquot of reaction suspension was taken and centrifuged at 16,1000 x g for 1 min. The resulting supernatant was tested for the enzymatic activity and total protein concentration via the commercial Bio-Rad® Protein assay based on Bradford. The remaining suspension was incubated with 60 µl (0.270 mmol) of TEOS for 1 h. Subsequently, 27 µl APTES (0.115 mmol) were added to the reaction suspension. Samples of reaction suspension were collected at increasing reaction times: aliquots of 0.05 ml were tested for the enzymatic activity in duplicate, while aliquots of 0.2 ml were washed twice and re-suspended in nanopure water for FESEM analysis. The organosilane polycondensation reaction was stopped after 5 h by washing the particles in nanopure water. The biocatalytic particles (SNPcat) were then re-suspended in 50 mM citrate buffer (pH 6), kept at room temperature for 24 h and stored at 4 °C until use.

Imprinting of NorVLP on biocatalytic particles

All reactions were performed in 20 ml glass vials, in a final volume of 6 ml, under stirring conditions (400 rpm), in a water bath at 20 °C unless otherwise described. For imprinting, 6 ml SNPcat (3.2 mg/ml) were reacted with 12 µl (0.054mmol) of TEOS for 1 h re-suspended in a desired solution (*e.g.:* 10 mM citrate at pH 6 for standard conditions). The so-modified particles were washed twice with nanopure water – a washing step

included: centrifugation at 3220 x g for 5 min, removal of supernatant and re-suspension of the pelleted particles in a desired solution (*e.g.*:10 mM citrate at pH 6 for standard conditions) by ultrasonic treatment for 2 min. Afterwards, the particles were reacted with 4 µl (0.017 mmol) of APTES for 30 min. The so-modified particles were washed twice as described before. Afterwards, the particles were incubated for 30 min in 6 ml of 0.1 % (v/v) aqueous glutaraldehyde solution. The so-modified particles were washed twice as described before.

For the imprinting, washed particles were re-suspended in 25 mM citrate at pH 7. Particles were then incubated with the NorVLP (at 0.03 mg/ml) for 1 h. Subsequently, 20 µl (0.090 mmol) of TEOS were added to the reaction mixture and allowed to react for 1 h. Temperature was then decreased to 10 °C before 10 µL (0.043 mmol) of APTES were added. Samples of reaction suspension were collected at increasing reaction times (24, 48 and 72 h after the addition of APTES): aliquots of 0.05ml were tested for the enzymatic activity in duplicate, while aliquots of 0.2 ml were washed twice and re-suspended in nanopure water for FESEM analysis. The organosilane polycondensation reaction was stopped after 72 h by washing the particles in nanopure water. The imprinted SNPcat (VIPcat) were then suspended in 50 mM citrate buffer (pH 6), kept at room temperature for 24 h and stored at 4 °C until use.

Non-imprinted reference particles were produced in a similar fashion by omitting the VLP addition step.

Removal of template NorVLP

In a typical removal process (in 2 ml reaction tube, in a final volume of 1.8 ml), VIPcat were suspended to an end concentration of 1.5 mg/ml in the removal solution (0.1 M sodium acetate and 0.01 % v/v Triton-X 100, pH 3) and submitted to ultrasonic treatment for 30 min. Subsequently, the so-treated particles washed twice in nanopure water (centrifugation at 16,100 x g for 1 min) and were stored in 10 mM citrate (at pH 6) at 4 °C or directly used in binding assays.

6.2.4 Synthesis of fluorescent VIPs

The fluorescent VIPs were prepared by adapting the procedure described previously for VIPs as follows. All modifications of the SNPs as well as the imprinting were performed in 20 ml glass vials, in a final volume of 6ml, under stirring conditions (400 rpm), in a water bath at 20 °C unless otherwise described.

Surface modification of SNPs

In a typical synthesis experiment, 6 ml SNPs (3.2 mg/ml) were reacted with 4 µl (0.017 mmol) of APTES for 30 min in water. The so-modified particles were washed twice with nanopure water – a washing step included: centrifugation at 3220 x g for 5 min, removal of supernatant and re-suspension of the pelleted particles in nanopure water by ultrasonic treatment for 2 min. Afterwards, the particles were incubated for 30 min in 6 ml of 0.1 % (v/v) aqueous glutaraldehyde solution. The so-modified particles were washed twice with nanopure water as described before.

Imprinting of NorVLP

For the imprinting, washed particles were re-suspended in 25 mM citrate at pH 7 and incubated with NorVLP (at 0.03 mg/ml) for 1 h. Subsequently, 12 µl (0.054 mmol) of TEOS were added to the reaction mixture and allowed to react for 1 h. Then 5.3 µl (0.086 µmol) of fluorescein-APTES and 6 µl (0.086 µmol) of FDA-APTES respectively, were added and allowed to react for 30 min. Afterwards, temperature was decreased to 10 °C before 6 µL (0.026 mmol) of APTES were added. Samples of reaction suspension were collected at increasing reaction times: aliquots of 0.2 ml were taken and centrifuged at 16,100 x g for 30 sec. The resulting supernatants were diluted 1 to 100 and tested for the fluorescence intensity with λ_{EX} at 490 nm and λ_{EM} at 520 nm using a Synergy H1 plate reader. The pellet was washed with nanopure water and then re-suspended in 50 mM citrate solution at pH 6. The organosilane polycondensation reaction was stopped after 6 h in case of NIPs and after 8 h in case of VIPs by washing the particles in nanopure water. The resulting particles were re-suspended in 5 ml of 25 mM citrate solution at pH 7 and kept at stirring condition at 10 °C until the synthesis of the second silica layer was induced.

Non-imprinted reference particles were produced in a similar fashion by omitting the VLP addition step.

Covering fluorescent silica layer

The previously synthesized fluorescent silica layer was further covered with an additional layer without fluorescein derivatives as follows. To the 5 ml suspension of imprinted particles, 12 µl (0.054 mmol) of TEOS were added and allowed to react for 1 h at 10 °C. Subsequently, 5 µL APTES (0.021 mmol) were added to the reaction suspension. Samples (0.1 ml) were collected at increasing reaction times and washed twice with nanopure water for FESEM analysis. The organosilane polycondensation reaction was stopped after 4 h by washing the particles in nanopure water. The resulting particles were re-suspended in 10 mM citrate solution at pH 6.

For curing, these particles were kept at room temperature for 24 h and were then stored light protected at 4 °C until use.

Removal of template NorVLP

In a typical removal process (in 1.5 ml reaction tube, in a final volume of 1 ml), VIPs were suspended to an end concentration of 1 mg/ml in the removal solution (0.1 M HCl and 0.01 % v/v Triton-X 100) and submitted to ultrasonic treatment for 30 min. Subsequently, the so-treated particles washed twice in nanopure water (centrifugation at 16,100 x g for 1 min) and were stored in 10 mM citrate (at pH 6) at 4 °C.

6.3 Characterization of particles

6.3.1 Determination of particles concentration

A 0.5 to 1 ml aliquot of particle suspension was freeze-dried and weighed in a 1.5 ml tube. The weight of the freeze-dried particles was determined through subtraction of the weight of the empty tube from the total weight (= tube with dried particles).

6.3.2 Scanning electron microscopy and Particle size measurement

Particles were imaged using a Zeiss SUPRA® 40VP scanning electron microscope. Two µl of sample were spread on freshly cleaved mica sheets, dried at ambient temperature and sputter-coated with a gold–platinum alloy for 15 sec at 10 mA (SC7620 Sputter coater). Micrographs were acquired using the InLens mode with an accelerating voltage of 20 kV.

Particle sizes were measured on micrographs acquired at a magnification of x 150,000 using the Olympus Analysis® software package. More than 100 measurements were performed per type of particles.

6.3.3 Zeta (ζ)-potential measurements

Particle suspension at 1 mg/ml in nanopure water were subjected to ultrasonication for 2 min and then transferred into a clear disposable zeta cell. Then zeta-potential measurements were performed using Zetasizer Nano series (Malvern instruments, UK) at 25 °C. In case of SNPcat and modified SNPcat, measurements were also carried out in 10 mM citrate buffer at pH 6 to avoid aggregation.

6.3.4 Enzyme assays and kinetic studies

Colorimetric β-galactosidase activity assay

The β-galactosidase activity of particle suspensions (= βgal-SNPs after incubation in different buffer solutions, after chemical modifications and NorVLP immobilization) was determined by measuring the hydrolysis of o-nitrophenyl-β-D-galactopyranoside (ONPG at 20 mM) in activity buffer (100 mM potassium phosphate, 5 mM $MgCl_2$, pH 6.5) under stirring at 650 rpm at 40 °C for 30 min. Total volume of reaction was 0.2 ml including the 0.05 ml of particle suspension. The reaction was stopped by adding 0.2 ml of 1M Na_2CO_3, and then centrifuged at 16,200 x g for 1 min. The concentration of produced o-nitro-phenolate was determined by measuring the absorbance at 420 nm of 0.2 ml supernatant in a 96-well plate using a Synergy H1 plate reader (BioTek).

Fluorescent-based β-galactosidase activity assay

The β-galactosidase activity of particle suspensions (= βgal-SNPs after chemical modifications, NorVLP immobilization and imprinting) was determined by measuring the hydrolysis of 4-methylumbelliferone-β-D-galactopyranoside (MUG at 0.7 mM) in activity buffer (100 mM potassium phosphate, 5 mM $MgCl_2$, pH 6.5). The reaction suspension (0.2 ml including the 0.05 ml of particle suspension) maintained under stirring at 650 rpm at 40 °C for 30 min and was stopped by adding 0.2 ml of 1M Na_2CO_3 and centrifugation at 16,200 x g for 1 min. The concentration of produced fluorescent molecule 4-methylumbelliferone (MUB) was determined by measuring the fluorescence intensity of 0.2 ml supernatant with λ_{EX} at 360 nm and λ_{EM} at 460 nm in a 96-well plate (black) using a Synergy H1 plate reader.

Phosphatase activity assay

The phosphatase activity of free enzyme and particle suspensions (= particles during enzyme encapsu-

lation and SNPcat) was determined by measuring the hydrolysis of p-nitrophenyl phosphate (pNPP, at 6 mM) in activity buffer (sodium acetate 40 mM, citrate 10 mM, pH 5.2) under stirring at 650 rpm at 37 °C for 10 min. Total volume of reaction was 0.2 ml including the 0.05 ml of particle suspension. The reaction was stopped by adding 0.2 ml of 1 M NaOH, and then centrifuged at 16,200 x g for 1 min. The concentration of produced 4-nitrophenolate was determined by measuring the absorbance at 405 nm of 0.2 ml supernatant in a 96-well plate using a Synergy H1 plate reader (BioTek). The reaction rate in U/l was determined through a calibration curve of 4-nitrophenolate.

For kinetic analysis, the activity assay for free enzyme was additionally performed at different reaction times (up to 30 min), varying enzyme concentrations (up to 11 µg/ml) and increasing substrate concentrations (up to 8 mM), respectively.

In case of VIPcat and NIPcat, the reaction time was elongated to 20 min.

6.3.5 Determination of fluorescence per mg particles

Particle suspensions at 3.2 mg/ml in nanopure water were subjected to ultrasonication for 2 min. Then a serial dilution of these suspensions was carried out using phosphate buffer (at 50 mM, pH 6) as diluent, a dilution factor of 2 and a final volume of 150 µl on a microtiter plate (black). The fluorescence intensity of the diluted particles suspensions was measured with λ_{EX} at 490 nm and λ_{EM} at 520 nm using a Synergy H1 plate reader.

For high precision fluorescent measurements, the fluorescence intensity was measured continuously for 10 min (detecting the signal every minute) to observe signal fluctuations. Only data point with a stable fluorescence intensity for 5 min (standard deviation lower than 5%) were used to determine the quenching quotient.

6.3.6 Efficiency in binding of NorVLP

When not otherwise described, the particles (at 834 µg/ml) were mixed with a solution containing 700 ng/ml of NorVLP (65 pM), 10 mM phosphate, 50 mM NaCl and 75 µg/ml of skim milk (pH adjusted to 6.2) in a final volume of 120 µl, in 0.5 ml test tube to allow the interaction. For each binding assay, a reference solution containing the same composition, including the NoVLP, was prepared by omitting the particle addition step. The binding assay and reference solutions were then incubated at 25 °C under stirring at 650 rpm in a thermomixer (Eppendorf Thermomixer® Comfort). After reaching the desired contact time (typically 30 min), the tube was centrifuged (16,200 x g for 1 min). The resulting supernatant containing unbound NorVLP were diluted (1:8) with carbonate-bicarbonate buffer (0.2 M, pH 9.6) and then immediately coated on a 96-well microplate (Nunc Maxisorp, ThermoScientific) at 4 °C overnight, in duplicate, for virus quantification by an indirect ELISA assay (see next section).

The measured values from the binding assay were compared with the values obtained from reference solutions, which were prepared and treated in the same way as the binding assay.

In case of biocatalytic particles with phosphatase active the binding buffer contained 10 mM MES, 10 mM

citrate, 50 mM NaCl, pH 6), 25 µg/ml of skim milk and determined concentration of NorVLP was mixed with the VIPcat at a concentration of 0.4 mg/ml in a final volume of 200 µl.

6.3.7 Determination of efficiency of NorVLP removal

Removal conditions were tested for their efficiency in removing remaining template NorVLP from the VIPs by washing the particles and subsequently determination of released NorVLP as follows.

The 0.2ml VIPcat (at 3mg/ml) were mixed with 0.2 ml of the desired removal solution in 1.5 ml test tube and treated with sonication for 30 min. Subsequently, the particle suspensions were washed (centrifugation at 16,200 x g for 30 sec, removal of supernatant and re-suspension of the pelleted particles in nanopure water) and re-suspended in 0.1 ml nanopure water. The treated particles were mixed with a solution containing 10 mM phosphate, 50 mM NaCl and 75 µg/ml of skim milk (pH adjusted to 6.2) in a final volume of 60 µl and then incubated at 25 °C under stirring at 650 rpm in a thermomixer (Eppendorf Thermomixer® Comfort). After 1h, the suspensions were centrifuged (16,200 x g for 1 min). The resulting supernatant containing released NorVLP were diluted (1:8) with carbonate-bicarbonate buffer (0.2 M, pH 9.6) and then immediately coated on a 96-well microplate (Nunc Maxisorp, ThermoScientific) at 4 °C overnight, in duplicate, for virus quantification by an indirect ELISA assay (see next section). The remaining particles were re-suspended in 120 µl nanopure water for measuring the phosphatase activity.

6.4 Characterization and detection of proteins and fluorescein-derivatives

6.4.1 Determination of isoelectric point of proteins

The isoelectric point (IEP) of each protein was determined via the immobilization on silica particles at different pH values as the pH value with the highest immobilization yield indicates the IEP. To determine the yield at different pH values, protein solutions of AP, BSA or esterase, respectively, at 6 µg/ml were incubated with unmodified silica particles (at 3.2 mg/ml) at 650 rpm for 1 h at 25 °C in buffer solutions with varying pH values. Following buffer solutions at 50 mM were applied: Acetate buffer at pH 5 and 5.5, MES buffer at pH 6 and 6.5, and HEPES at pH 7 and pH8. The immobilization yield of AP and esterase was determined via the respective enzymatic assay, while the yield of BSA was determined via commercial Bio-Rad® Protein assay based on Bradford.

6.4.2 Immunological detection of NorVLP via ELISA

Indirect ELISA

Buffered solutions containing NorVLP were diluted (1:8) with carbonate-bicarbonate buffer (0.2 M, pH 9.6) and then immediately coated on a 96-well microplate (Nunc Maxisorp, ThermoScientific) at 4 °C overnight, in duplicate. The microplate wells were washed three times with phosphate-buffered saline (PBS) containing 0.05 % (v/v) Tween-20 using a BioTek plate-washer ELx50 (USA). After 200 µl of skim milk (4 %

in PBS) were added to wells, the plate was incubated for 2 h at 37 °C and then washed as described before. Norovirus VP1 antibody was diluted 1:10,000 in PBS and added to the wells (100 µl per well). After incubation at 37 °C for 1 h, wells were washed as described above. Peroxidase conjugated antibody was diluted 1:10,000 with skim milk (4 % in PBS) and added to the wells (100 µl per well). After incubation at 37 °C for 30 min, wells were washed as described above. After adding 100 µl TMB substrate into each well, the plate was incubated at room temperature and in the dark for 15 min. Reaction was stopped through the addition of 50 µl per well of stop solution (1 M HCl). The optical density was measured at 450 nm using a Synergy H1 plate reader (BioTek). Negative controls were skim-milk-blocked wells without NorVLP and NorVLP-coated wells without the addition of Norovirus VP1 antibody. The average optical density from all negative controls was subtracted from the optical density from experimental wells.

PBS contained 0.2 g/l of potassium chloride, 0.2 g/l of potassium phosphate monobasic anhydrous, 8 g/l of sodium chloride and 1.15 g/l of sodium phosphate dibasic in nanopure water (final pH 7.5).

Sandwich ELISA

Norovirus GII4 antibodies were diluted 1:200 with carbonate-bicarbonate buffer (0.2 M, pH 9.6) and then immediately coated on a 96-well microplate (Nunc Maxisorp, ThermoScientific) at 4 °C overnight, in duplicate. The microplate wells were washed three times with phosphate-buffered saline (PBS) containing 0.05 % (v/v) Tween-20 using a BioTek plate-washer ELx50 (USA). After 200 µl of skim milk (4 % in PBS) were added to wells, the plate was incubated for 2 h at 37 °C and then washed as described before. Solutions containing increasing concentration of NorVLP in PBS were added to the microplate in duplicate (100 µl per well). After incubation at 37 °C for 1 h, wells were washed as described above. Biotinylated Norovirus VP1 antibody was diluted 1:1,000 in PBS and added to the wells (100 µl per well). After incubation at 37 °C for 1 h, wells were washed as described above. Peroxidase conjugated avidin was diluted 1:10,000 in PBS and added to the wells (100 µl per well). After incubation at 37 °C for 30 min, wells were washed as described above. After adding 100 µl TMB substrate into each well, the plate was incubated at room temperature and in the dark for 15 min. Reaction was stopped through the addition of 50 µl per well of stop solution (1 M HCl). The optical density was measured at 450 nm using a Synergy H1 plate reader.

Negative controls were skim-milk-blocked wells without NorVLP and antibody-coated wells without the addition of NorVLP. The average optical density from all negative controls was subtracted from the optical density from experimental wells.

PBS contained 0.2 g/l of potassium chloride, 0.2 g/l of potassium phosphate monobasic anhydrous, 8 g/l of sodium chloride and 1.15 g/l of sodium phosphate dibasic in nanopure water (final pH 7.5).

6.4.3 Absorbance, Emission and Excitation scan

In case of fluorescein-derivatives (fluorescein-APTES and FDA-APTES), a stock solution at 10 mg/ml was used to measure the absorbance, emission and excitation spectra, respectively, using a Synergy H1 plate reader. An absorbance scan was determined between 300 nm and 700 nm in a transparent 96-well plate. An emission scan was determined between 510 nm and 700 nm with the excitation wavelength at 480 nm,

while an excitation scan was determined between 300 nm and 490 nm with the emission wavelength at 520 nm. Both fluorescence scans were determined in a black 96-well plate.

An emission scan of NorVLP and skim milk, respectively, was determined between 515 nm and 700 nm with the excitation wavelength at 485 nm and both proteins at 1 mg/ml. In case of skim milk, additionally an excitation scan was determined between 250 nm and 485 nm with the emission wavelength at 515 nm and the protein concentration at 1 mg/ml. Both fluorescence scans were determined in a black 96-well plate using a Synergy H1 plate reader.

6.5 Activation of fluorescein diacetate

6.5.1 Hydrolyse in buffered solutions

Experiment 1

In a total volume of 0.7 ml, FDA-containing NIPs - NIP_{EX} and NIP_{IN} - at a concentration of 0.4 mg/ml were incubated with 10 mM citrate in a 50 mM Trizma buffer solutions at pH 7, 8 and 9, respectively, at 25 °C under stirring at 650 rpm for 14 h. After 2 min and 14 h, the fluorescence intensity of the particles suspensions was measured with λ_{EX} at 490 nm and λ_{EM} at 520 nm using a Synergy H1 plate reader.

Experiment 2

In a total volume of 1.8 ml, FDA-containing NIPs - NIP_{EX} and NIP_{IN} - at a concentration of 0.2 mg/ml were incubated in a 50 mM Trizma buffer solutions at pH 9 at 37 °C for 4 h in a 96-well plate (black). Each hour, the fluorescence intensity of 150 µl of the particles suspensions was measured with λ_{EX} at 490 nm and λ_{EM} at 520 nm using a Synergy H1 plate reader.

6.5.2 Hydrolysis via butoxid

Free FDA and Butoxid

In a total volume of 150 µl, FDA-APTES at a concentration of 3 µM was incubated with t-butoxid at different concentrations (0, 3 µM, 6 µM and 30 µM) in 1-butanol in 96-well plate (black). The fluorescence intensity of active fluorescein was continuously measured for 20 min at 25 °C with λ_{EX} at 490 nm and λ_{EM} at 520 nm using a Synergy H1 plate reader.

Particles and Butoxid

Fluorescein and FDA-containing particles (NIP_F*, NIP_{EX}, NIP_{IN} and VIP_FD) at 1 mg/ml were washed with nanopure water – the washing included: centrifugation at 16,100 x g for 1 min, removal of supernatant and re-suspension of the pelleted particles in nanopure water by ultrasonic treatment for 2 min. Afterwards, the water of the suspension was removed through centrifugation (16,100 x g for 30 sec) to re-suspend the pelleted particles in 1-butanol by ultrasonic treatment for 2 min.

In a final volume of 2.6 ml, the particles at 1 mg/ml were incubated with and without with 50 mM *t*-butoxid in 1-butanol at room temperature under stirring at 400 rpm. Aliquots of 0.8 ml were taken after immediately, 24 h and 48 h after mixing. The aliquots were washed first with 1-butanol and then with 100 mM citrate solution at pH 6 containing 0.01 % v/v Triton X-100 – the washing included: centrifugation at 16,100 x g for 1 min, removal of supernatant and re-suspension of the pelleted particles by ultrasonic treatment for 10 min. For complete re-suspension of the particles, pelleted particles were further treated with ultrasonication for 30 min and stirred at 1000 rpm for 1 h.

A 650 µl aliquot of the so-treated suspension was withdrawn for determination of particle concentration, while the remaining suspension was stored in 50 mM citrate solution at pH 6 containing 0.01 % v/v Triton X-100 protected from light at 4 °C until use.

6.5.3 Hydrolysis via esterase reaction

Esterase activity assay

The activity of esterase from porcine liver (PLE) was determined by measuring the hydrolysis of p-nitrophenyl acetate (pNPA, at 0.2 mM) in a 50 mM phosphate buffer solution at pH 6 or 7.5 in a total volume of 150 µl. The reaction was observed at 25 °C overtime via the concentration of produced 4-nitrophenolate by measuring continuously (one read per minute) the absorbance at 405 nm in a 96-well plate using a Synergy H1 plate reader. The reaction rate in U/l was determined through a calibration curve of 4-nitrophenolate.

Free FDA and esterase

In a total volume of 150 µl, increasing concentrations (up to 9 µM) of FDA-APTES and fluorescein-APTES, respectively, were incubated with and without PLE at a concentration of 30 µg/ml (corresponding to 0.5 U/ml) in a phosphate buffer solution (at 50 mM, pH 6) in 96-well plate (black). The fluorescence intensity of active fluorescein was continuously measured for 2 h at 37 °C with λ_{EX} at 490 nm and λ_{EM} at 520 nm using a Synergy H1 plate reader.

FDA-particles and esterase

In a total volume of 2.6 ml, FDA-containing VIPs at a concentration of 1 mg/ml were incubated with and without PLE at 5 U/ml in 10 mM MES pH 6, 0.01 % v/v Triton X-100, 7 mM citrate at room temperature under stirring at 400 rpm. Aliquots of 0.8 ml were taken after immediately, 18 h and 36 h after mixing. The aliquots were washed with 100 mM citrate solution at pH 7 containing 0.01 % v/v Triton X-100 – the washing included: centrifugation at 16,100 x g for 1 min, removal of supernatant and re-suspension of the by stirring at 1000 rpm and at 37 °C for 1 h. Afterwards, the particle suspension was centrifuged at 16,100 x g for 1 min. The resulting supernatant was tested for the total protein concentration via the commercial Bio-Rad® Protein assay based on Bradford. The pelleted particles were re-suspended in 100 mM citrate solution at pH 6 containing 0.01 % v/v Triton X-100 by stirring at 1000 rpm and at 25 °C for 1h and sonication for 1 h. A 650 µl aliquot of the so-treated suspension was withdrawn for determination of particle concentration, while the remaining suspension was stored in 50 mM citrate solution at pH 6 containing 0.01 % v/v Triton X-100 protected from light at 4 °C until use.

6.6 Detection of NorVLP via functionalized particles

6.6.1 NorVLP detection by imprinted βgal-SNP

In a total volume of 100µl, βgal-SNP at a concentration of 1.4mg/ml, interacted with a determined concentration of NorVLP in binding buffer (10mM MES, 10mM citrate, 50mM NaCl, pH 6.2), The interaction assays were incubated at 25°C under stirring at 650rpm for 30min. Subsequently, 100µl aliquots of the interaction assays were transferred in duplicate on a 96-well plate (black) and mixed with 100µl of MUG (1.5mM in binding buffer). The fluorescence intensity of the released MUB was measured continuously for 2h at 40°C with λ_{EX} at 360nm and λ_{EM} at 460nm using a Synergy H1 plate reader.

6.6.2 NorVLP detection by imprinted phosphatase particles

Separate mode

In a total volume of 120µl, VIPcat at a concentration of 791µg/ml interacted with a determined concentration of NorVLP and 58µg/ml of skim milk in binding buffer (10mM phosphate, 10mM citrate, 50mM NaCl, at pH 6.2). The interaction assays were incubated at 25°C under stirring at 650rpm for 30min and stopped through centrifugation at 16,100xg for 30sec. The resulting supernatant was withdrawn for the quantification of unbound NorVLP via indirect ELISA (see 6.3.3), while the pelleted particles were re-suspended in 60µl of solution containing 58µg/ml skim milk and activity buffer (10mM phosphate, 10mM citrate, 50mM NaCl, pH 5). These suspensions were mixed with 60µl substrate (pNPP at 6mM) and incubated at 37°C under stirring at 650rpm for 1h. The enzymatic reaction was stopped through centrifugation at 16,100xg for 1min. The 75µl of the resulting supernatant was mixed with 1N NaOH in a 96-well plate and tested for the concentration of produced 4-nitrophenolate by measuring the absorbance at 405nm using a Synergy H1 plate reader. The remaining supernatant was withdrawn for the determination of NorVLP, which was released during the incubation, via indirect ELISA (see 6.3.3).

Continuous mode

In a total volume of 200µl, the particles (VIPcat, NIPcat or SNPcat) at a concentration of 0.4mg/ml with 0.01% v/v Triton X-100 interacted with a determined concentration of NorVLP and 25µg/ml of skim milk in binding buffer (10mM phosphate, 10mM citrate, 50mM NaCl, pH 6.2. The interaction assays were incubated at 25°C under stirring at 650rpm for 20min. Subsequently, 75µl aliquots of the interaction assay were transferred in duplicate on a 96-well plate and mixed with 75µl of pNPP (12mM in binding buffer). The concentration of produced 4-nitrophenolate was determined over a time frame of 750min at 25°C by measuring the absorbance at 405nm using a Synergy H1 plate reader. The reaction rate in U/g was determined through a calibration curve of 4-nitrophenolate and subsequent division by the particles concentration. To avoid evaporation, samples were put in the middle of the plate, while the remaining empty wells were filled with water.

The effect of TYMV on the phosphatase activity of VIPcat was determined through performing the same assay as described before by using TYMV instead of NorVLP.

6.6.3 NorVLP detection with fluorescent particles

The interaction assay had a total volume of 160 µl and contained the fluorescent VIPs (VIP_F*, VIP_FDA and VIPest) at a concentration of 0.2 mg/ml, 0.01 % v/v Triton X-100, 25 µg/ml of skim milk and a determined concentration of NorVLP in binding buffer (10 mM MES, 10 mM citrate, 50 mM NaCl, pH 6.2). Before adding the proteins, particle suspensions were treated with sonication for 10 min. The interaction assays were incubated at 25 °C under stirring at 750 rpm for 20 min. Subsequently, the fluorescence intensity of a 150 µl aliquot of the interaction assays was measured continuously for 30 min at 25 °C with λ_{EX} at 490 nm and λ_{EM} at 520 nm in 96-well plate (black) using a Synergy H1 plate reader.

6.7 Appendix - Prepartation of fluorescein modified APTES

Fluorescein-APTES was synthesized following the protocol reported by Feng[7]. First, 600 mg of FITC (**1**) was dissolved in 30 ml anhydrous ethanol and allowed to react with 396 µl of APTES **(2**) for 6 h under stirring in a dried flask under a dry nitrogen atmosphere and protected from light. In this reaction, the amino group of the silane coupling agent APTES reacts with the isothiocyanate group of FITC to form N-1-(3-triethoxysilylpropyl)-N′-fluoresceylthiourea, here called fluorescein-APTES (**3**), see equation 1. The resulting mixture was then precipitated into 300 ml heptane. Ethanol was evaporated under vacuum and the remaining suspension was centrifuged at 4000 rpm for 15 min. The resulting supernatant was removed and the pellet washed with heptane to remove remaining APTES. After re-suspending the pellet in heptane again, suspension was dried under vacuum.

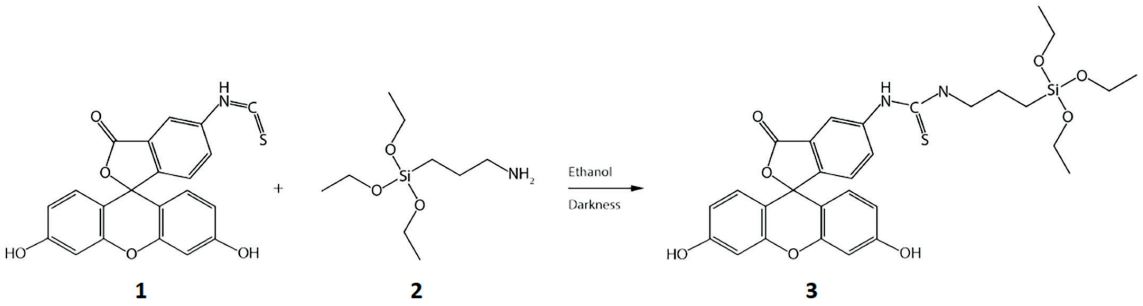

Equation 1: APTES-conjugation on FITC

The dried fluorescein was converted to the diacetate via an adjusted protocol commonly used for esterification. First, 56 µl acetyl chloride, 120 mg of FITC-APTES and 1 mg of 4-(dimethylamino)pyridine (DMAP) were mixed in 4 ml of DMF and stirred overnight at room temperature. In this reaction, acetyl chloride reacts with carbonyl group of the ester in the fluorescein part of fluorescein-APTES (**3**) to form the acetylated fluorescein-APTES (**4**), see equation 2. This process was followed via TLC (DCM/methanol 8/2). A saturated solution of $NaHCO_3$ (3 ml) was slowly added to the mixture to quench the reaction. The product was extracted with chloroform (2 x 2 ml) into the organic phase. After separating the layers, the organic phase was washed with slightly acidic water (at pH 6) (3 x 2 ml), dried over anhydrous Na_2SO_4 and concentrated under reduced pressure to obtain the final product.

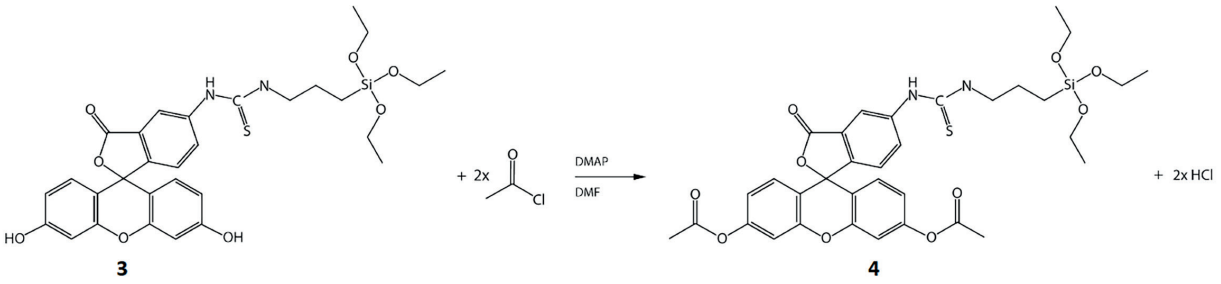

Equation 2: Synthesis of FDA-FITC-APTES conjugate out of fluorescein-APTES

6.8 References

1 de Rougemont, A. *et al.* (2011) Qualitative and quantitative analysis of the binding of GII.4 norovirus variants onto human blood group antigens. *J Virol* **85**, 4057-4070

2 Belliot, G. *et al.* (2001) Characterization of capsid genes, expressed in the baculovirus system, of three new genetically distinct strains of „Norwalk-like viruses". *J Clin Microbiol* **39**, 4288-4295

3 Lorber, B., Adrian, M., Witz, J., Erhardt, M. and Harris, J. R. (2008) Formation of two-dimensional crystals of icosahedral RNA viruses. *Micron* **39**, 431-446

4 Blaaderen, A. V., Geest, J. V. and Vrij, A. (1992) Monodisperse Colloidal Silica Spheres from Tetraalkoxysilanes: Particle Formation and Growth Mechanism. *Journal of Colloid and Interface Science* **154**, 481-501

5 Stöber, W. & Fink, A. (1968) Controlles Growth of Monodisperse Silica Spheres in the Micron Size Range. *Journal of Colloid and Interface Science* **26**, 62-69

6 Cumbo, A., Lorber, B., Corvini, P. F., Meier, W. and Shahgaldian, P. (2013) A synthetic nanomaterial for virus recognition produced by surface imprinting. *Nat Commun* **4**, 1503-1509

7 Feng, H. et al. (2014) Surface molecular imprinting on dye–(NH2)–SiO2 NPs for specific recognition and direct fluorescent quantification of perfluorooctane sulfonate. *Sensors and Actuators B: Chemical* **195**, 266-273

Name:	Sabine Sykora
Adresse:	Krottendorfer Straße 8b/7, A-8052 Graz
Email:	sabine.sykora@gmail.com
Telefon:	+43 (0) 664 46 799 34
Nationalität:	Österreich
Geburtsdatum:	28.05.1984

Ausbildung

06/2013 – Heute

Doktorat in Biochemie – Universität Basel, Basel (CH),

Vertiefung in:

- Proteinanalytik
- Nanotechnologie
- Fluoreszenzmessung und -mikroskopie
- Wissenschaftliches Schreiben
- Schreiben von Projektanträgen
- Patentwesen

09/2005 – 11/2011

Diplomstudium in Chemie, Karl-Franzens-Universität, Graz;
Abschluss mit „Magistra Rerum Naturae“;
Schwerpunkt: Biochemie und Molekularbiologie;

09/2005 - 06/2009

Bachelorstudium in Molekularbiologie, Karl-Franzens-Universität, Graz;
Abschluss mit “Bachelor of Science”;
Schwerpunkt: Molekularbiologie, Bioinformatik und Biotechnologie;

10/2002 - 09/2005

Akademie für den medizinisch-technischen Laboratoriumsdienst des Landes Steiermark, Graz;
„Diplomierte Biomedizinische Analytikerin“ mit Auszeichnung;
- Standardisierte Durchführung von Diagnoseverfahren;
- Behandlung und Analyse von humanen Proben;

09/1998 - 06/2002

Matura, Oberstufenrealgymnasium, Hartberg
Schwerpunkt: Biologie, Physik und Chemie;

Berufliche Erfahrung

06/2013 – 11/2016

Wissenschaftliche Mitarbeiterin

Hochschule für Life Sciences, Fachhochschule Nordwestschweiz, Muttenz (CH);

- selbständige Forschungsaktivitäten
- Präsentationen von Forschungsergebnissen bei Meetings und Konferenzen
- Laborорganisation und Betreuung von Laborgeräten
- Betreuung von Studenten im Praktikum

11/2009 – 06/2011	*Wissenschaftliche Mitarbeiterin im Zuge der Diplomarbeit* Institut für Biotechnologie und Bioprozesstechnik, Technische Universität, Graz; - Selbständige Durchführung von Messungen - Genexpression und Proteinreinigung - Vertiefung in Enzymologie
06/2009	*Ferialarbeit* Institut für Strukturbiologie, Karl-Franzens-Universität, Graz; - Proteinreinigung und -kristallisierung
10/2002 - 09/2005	*Praktikantin im Zuge der Ausbildung* im Labor für Rheumatologie der Universitätsklinik Graz, im Hygieneinstitut und im Zellkulturlabor des Instituts für Pathophysiologie der Karl-Franzens-Universität; - Durchführung von biomedizinischen Diagnoseverfahren - Instandhaltung des Labors und der Laborinfrastrukturen

Publikationen

Sykora S, Correro MR, Moridi N, Belliot G, Pothier,P, Arnal C, Dudal Y, Corvini PFX and Shahgaldian P: A Biocatalytic Nanomaterial for the Label-Free Detection of Virus-Like Particles; ChemBioChem 18, 996 (2017)

Correro MR, Takacs M, **Sykora S**, Corvini PFX and Shahgaldian P: Supramolecular enzyme engineering in complex nanometer-thin biomimetic organosilica layers; RSC Adv, 6, 89966 (2016)

Correro MR, Moridi N, Schützinger HJ, **Sykora S**, Ammann E, Peters H, Dudal Y, Corvini PFX and Shahgaldian P: Enzyme Shielding in an Enzyme-thin and Soft Organosilica Layer; Angew Chem Int Ed 55, 6285-6289 (2016)

Sykora S, Cumbo A, Belliot G, Pothier,P, Arnal C, Dudal Y, Corvini PFX and Shahgaldian P: Virus-like particles as virus substitutes to design artificial virus-recognition nanomaterials; Chem Commun 51, 2256 (2015)

Eixelsberger T, **Sykora S**, Egger S, Brunsteiner M, Kavanagh KL, Oppermann U, Brecker L, Nidetzky B.: Structure and mechanism of human UDP-xylose synthase: evidence for a promoting role of sugar ring distortion in a three-step catalytic conversion of UDP-glucuronic acid; J Biol Chem 3, 229-238 (2012).

Konferenzen

09/2015	10th International Conference on Surfaces, Coatings and Nanostructured Materials (Nanosmat), Manchester (UK): **Winner** of 3rd Prize at "Young Scientist Lecture Competition" für einen **Vortrag**
05/2014	Swiss NanoConvention, Brugg/Windisch (CH): **Poster**
04/2014	Clariant Chemistry Day, University of Basel, Basel (CH): **Poster**